THE UNIVERSITY OF CALGARY

Harmonic Upconversion in Radio-on-Fiber Systems

by

John-Peter van Zelm

A THESIS

SUBMITTED TO THE FACULTY OF GRADUATE STUDIES

IN PARTIAL FULFILLMENT OF THE REQUIREMENTS FOR THE

DEGREE OF MASTER OF SCIENCE

DEPARTMENT OF ELECTRICAL AND COMPUTER

ENGINEERING

CALGARY, ALBERTA

December, 2003

THE UNIVERSITY OF CALGARY

FACULTY OF GRADUATE STUDIES

The undersigned certify that they have read, and recommend to the Faculty of Graduate Studies for acceptance, a thesis entitled "Harmonic Upconversion in Radio-on-Fiber Systems" submitted by John-Peter van Zelm in partial fulfillment of the requirements for the degree of Master of Science.

Supervisor, Dr. Abu B. Sesay
Department of Electrical and Computer Engineering

Co-Supervisor, Dr. Robert J. Davies
Department of Electrical and Computer Engineering

Dr. G. McGibney
Telecommunications Research Laboratories

David J.I. Fry

Dr. David J.I. Fry
Department of Physics

Jan 16, 2004

Date

Abstract

Pure harmonic upconversion exploits a system nonlinearity to translate a passband radio signal to a higher frequency. Radio-on-fiber (RoF) systems are particularly well suited for the application of pure harmonic upconversion as they are inherently nonlinear in nature. They also stand to benefit enormously from the system simplification and bandwidth relaxation offered by pure harmonic upconversion.

In this thesis study, the concept of pure harmonic upconversion is presented and associated theory developed with a focus on application in RoF systems. Distortion mechanisms relating to the harmonic upconversion process and the RoF link are characterized, and predistortion presented as a mitigation scheme. The effects of fiber nonlinearity on RoF link operation and harmonic generation are also investigated.

As part of this work, simulations are performed to test and demonstrate the effectiveness of predistortion in various scenarios. An experimental harmonically upconverting RoF link employing dispersive fiber is described in detail, and used to demonstrate the application of pure harmonic upconversion in a realistic scenario. Experimental results are presented validating pure harmonic upconversion as a feasible method of signal upconversion in RoF systems.

Acknowledgements

There are many people who deserve thanks for helping me arrive at this point. I thank my supervisors, Bob Davies and Abu Sesay, for taking me as their student and allowing me to pursue my ideas in my own way. I thank my fellow students, Sean Hum, Rob Randall, Mike Weldon, Glenn Watson, Rob Sizeland, Oscar Gaitan, and others for stimulating conversation, technical help, and friendship. Simon Arseneault, I am particularly grateful for your patient help. My loving parents I thank for instilling in me the necessary motivation and discipline. I especially thank Jennifer Hartwell for her constant support and encouragement. Finally, I gratefully acknowledge the financial support of the National Sciences and Engineering Research Council of Canada (NSERC), the University of Calgary, and *TRL*abs.

Table of Contents

List of Tables

List of Figures

List of Symbols and Abbreviations

Symbol	Definition
α	Fiber loss coefficient
β	Wave propagation constant
β_2	GVD parameter
η	Optical material intrinsic impedance
η_{LD}	Laser diode efficiency
γ	Fiber nonlinearity coefficient
λ_o	Optical carrier wavelength
ϕ	Dispersion phase shift
ϕ_{NL}	SPM induced phase shift
$\mathcal{R}$	Photodiode responsivity
τ_{grp}	Group delay
A_{eff}	Effective area
ADSL	Asymmetric Digital Subscriber Line
APD	Avalanche Photodiode
AWG	Arbitrary Waveform Generator
BER	Bit Error Rate
BPF	Band Pass Filter
c	Free space speed of light (23)
CATV	Community Antenna Television Network
CDMA	Code Division Multiple Access
D	Dispersion parameter
DC	DC
D_M	Material dispersion parameter
D_W	Waveguide dispersion parameter
DD	Direct Detection
DSL	Digital Subscriber Line
E_{PD}	Incident photodiode optical electric field
$E_{in,MZM}$	Electric field input to MZM
$E_{out,MZM}$	Electric field output of MZM
E/O	Electro-Optic
EAM	Electro-Absorption Modulator
EDFA	Erbium Doped Fiber Amplifier
f	Frequency
f_c	Radio subcarrier frequency
f_o	Optical carrier frequency

j	$\sqrt{-1}$
FFP	Fiber Fabry-Perot device
FTTC	Fiber To The Curb
FTTH	Fiber To The Home
GVD	Group Velocity Dispersion
$H_D(f)$	Optical dispersion frequency transfer function
$H_T[.]$	Hilbert transform operator
HFC	Hybrid Fiber Coaxial
I	In-phase signal component
I_{PD}	Photodiode current
I_b	LD bias current
I_d	Laser diode drive current
I_{th}	Laser diode lasing threshold current
IEEE	Institute of Electrical and Electronics Engineers
IF	Intermediate Frequency
IM	Intensity Modulation
J_x	x^{th} order Bessel function of the first kind
k_o	Wave number
L	Fiber length
L_{NL}	Nonlinear length
LD	Laser Diode
LED	Light Emitting Diode
LMCS	Local Multipoint Communications System
LMDS	Local Multipoint Distribution System
LO	Local Oscillator
LO	Low Pass Filter
m	Modulation index
m_{pred}	Predistored signal amplitude/modulation index
$m_{\text{lin,max}}$	Maximum modulation index of linear region
$m_{\text{lin,min}}$	Minimum modulation index of linear region
MATB	Maximum Transmission Bias
MITB	Minimum Transmission Bias
MZM	Mach-Zehnder Modulator
n_2	Nonlinear index coefficient
n_o	Linear refractive index
NLS	Nonlinear Schrödinger (equation)
O/E	Opto-Electric
ODSB	Optical Double Side Band
OFDM	Orthogonal Frequency Division Multiplexing
OQPSK	Offset Quadrature Phase Shift Keying

OSSB	Optical Single Side Band
P_o	Optical power
$P_{o,LD}$	Laser diode output power
$P_{o,PD}$	Incident photodiode optical power
PD	Photodiode
PM-IM	Phase Modulation to Intensity Modulation
POTS	Plain Old Telephone System
PRBS	Pseudo Random Binary Sequence
Q	Quadrature-phase signal component
QoS	Quality of Service
QAM	Quadrature Amplitude Modulation
QB	Quadrature Bias
QPSK	Quadrature Phase Shift Keying
R_{LD}	LD series resistance
RoF	Radio on Fiber
RF	Radio Frequency
SAC	Subscriber Access Cabinet
SNR	Signal to Noise Ratio
SPM	Self Phase Modulation
SSF	Split-Step Fourier
SSSF	Symmetrized Split-Step Fourier
t	Time
Tx	Transmitter
v_a	MZM upper arm input voltage
v_b	MZM lower arm input voltage
v_{in}	MZM input voltage
$v(t)$	Voltage information signal
V_π	MZM switching voltage
V_{bias}	MZM DC bias voltage
VDSL	Very high data rate Digital Subscriber Line
VSA	Vector Signal Analyzer
VSG	Vector Signal Generator
w_o	Optical angular frequency
WAN	Wide Area Network
WISP	Wireless Internet Service Provider
WLAN	Wireless Local Area Network
WMAN	Wireless Metropolitan Area Network
XPM	Cross-Phase Modulation

Chapter 1

Introduction

Consumer appetite for bandwidth has been steadily developing since the advent of the Internet in the early 1990s. This trend will only continue to accelerate with the offering of new applications and services such as streaming video, video conferencing, video/music on demand, interactive gaming, on-line shopping, etcetera. Consequently, there is fierce competition in the growing market of broadband delivery services. This battle is largely taking place in the "last-mile" link.

The "last-mile" describes the problem of economically connecting the fringes of the Internet backbone to the end consumer. Any company that desires a piece of the broadband delivery market must develop a feasible solution to the last mile problem, and pit it against those of others. The competitive environment leads to increased broadband connectivity for the consumer at a lower cost. As more and more consumers subscribe to broadband services, content providers respond by developing yet more bandwidth intensive services. More services and content spurs on the demand for bandwidth, and the cycle continues.

1.1 Broadband Access Solutions

There are currently several broadband solutions offered to general public, and a few emerging solutions.

1.1.1 Digital Subscriber Lines

Telephone companies entered the broadband delivery market with digital subscriber lines (DSL). This technology allows telephone companies to leverage their existing plain old telephone system (POTS) twisted pair network to provide broadband directly into the home of their clients, without impairing normal telephone service. Since each user has a direct connection to their local central office through their telephone line, there is no bandwidth sharing between users, and data rates remain relatively consistent.

Leveraging the existing twisted pair infrastructure is highly desirable, but unfortunately, also presents significant challenges; the twisted pair channel has limited bandwidth and high loss. This translates into a reach problem, where data throughput is limited by the length and quality of the twisted pair loop connecting the user and the central office. The most commonly deployed DSL is ADSL (Asymmetric DSL), promising data rates of 6Mb/s downstream over 3.2km of high quality twisted pair line[1]. In reality however, the twisted pair loop in many neighborhoods has degraded with age, resulting in limited availability and downstream rates of only 1.5Mb/s. It has been estimated that 60% of North American homes are beyond the reach of DSL service[2]. Although this is continually being improved through network upgrades, the reach problem is still a major hindrance for phone companies trying to secure a significant share of the broadband delivery market.

Other higher speed varieties of DSL have been developed, such as HDSL (High data rate DSL), and VDSL (Very high data rate DSL), but these are even more vulnerable to the reach problem and so are not widely deployed.

1.1.2 Cable Modems

North American cable companies, trying to get a piece of the broadband delivery market, have invested US$75 billion since 1996 in upgrading their extensive CATV (Community Antenna Television Network) and HFC (Hybrid Fiber Coaxial) networks[3]. They now offer broadband services to residential markets through a cable modem connection allowing peak downstream data rates of 10Mb/s to 20Mb/s[4], regardless of separation distance from the central office. However, the cable network employs a Wide Area Network (WAN) topology, which requires bandwidth be shared among users. Downstream rates are therefore heavily dependent on system load. Users typically see data rates between 300kb/s and 600kb/s[4]. This is expected to improve as cable companies continue to upgrade and reorganize their networks.

Unlike telephone companies, cable companies are mostly limited to residential markets, as the CATV network is not well developed outside of residential areas. This leaves the small and medium sized business markets inaccessible via a cable connection. To remedy this, cable companies have recently begun experimenting with wireless links as a way of accessing this potentially lucrative market.

1.1.3 Optical Fiber

The ultimate in broadband connectivity offering virtually unlimited bandwidth is Fiber-To-The-Home (FTTH). This solution proposes an all optical connection directly into a home or business. Unfortunately, such schemes are only feasible in developing neighborhoods, where fiber can be installed along with other utilities. Installing fiber into existing homes and businesses is intrusive and labour intensive making it exorbitantly expensive, and therefore infeasible.

A compromise is found in Fiber To The Curb (FTTC) topologies where the fiber link is made only to a location within a neighborhood, such as a subscriber access cabinet (SAC), and not directly into the home or business. From there, the last length (<1500 meters) is bridged through a high speed DSL technology or a wireless link.

In a bid to overcome the reach limitations of DSL and secure a larger portion of an exploding market, several large US telcos, including Verizon Communications, Inc., Bell South, and SBC have recently declared plans to provide their customers with FTTC or FTTH service within the next 10–15 years, at an estimated total cost of US $40 billion per carrier[3]. Users can expect data rates of 20Mb/s; 40 times the rate of cable modems.

1.1.4 Wireless Last Mile

To date, telephone and cable companies have enjoyed exclusive access to the broadband delivery market as they alone posses existing infrastructure to leverage. This represents a significant barrier to entry for other parties wishing to compete for market share. The only feasible way to circumvent the telephone and cable companies is to enter the market through a wireless last mile solution.

A wireless broadband delivery scheme, where the last-mile is bridged by the radio channel, is attractive due to its low infrastructure costs and non-intrusive nature [5]. A provider need only place a basestation in a neighborhood and provide subscribers with a radio unit. The potential of such schemes has been recognized and the first wireless internet service providers (WISPs) are beginning to emerge.

The recently established standard, IEEE 802.16, clears the way for wireless metropolitan area networks (WMANs), much as the IEEE 802.11 standards did for wireless local area networks (WLANs). As WMAN technology develops, WISPs will be able to provide broadband services at a cost on par with or cheaper than DSL or cable. Although WMANs are still in their infancy, they already represent a US$250 million a year market[6] that is growing quickly. Undoubtably, WISPs will become a significant contender for the broadband delivery market.

Telephone companies have taken notice, and themselves are pursuing wireless links coupled with FTTC solutions to overcome their DSL reach problems and to service rural, low density areas. Similarly, cable companies have been investigating wireless as a means of providing service to small and medium businesses.

One of the major issues facing a wireless last mile solution is bandwidth. The nature of a broadband delivery system demands large blocks of radio spectrum, necessitating operation in the less congested microwave or millimeter wave frequency range. In anticipation of wireless broadband services, the Canadian and American governments have allocated spectrum in the 25–32GHz bands, known as the LMCS (Local Multipoint Communications System)[7] and LMDS (Local Multipoint Distribution System)[8] bands respectively.

Unfortunately, the high cost associated with operation at high radio frequencies is slowing the roll out of LMCS/LMDS systems. The expense stems from the dense basestation deployment required to compensate for the rapid attenuation of high frequency signals. While rapid signal attenuation and dense basestation deployment are favorable from a frequency reuse or system capacity perspective, a large number of basestations will incur significant infrastructure costs. This is further exacerbated by the high cost of LMCS/LMDS band radio equipment. For a wireless broadband delivery system, such as LMCS/LMDS, to be commercially feasible, basestations will have to be made as cheap as possible. Fortunately, radio-on-fiber (RoF) architecture can be employed to reduce infrastructure costs of an LMCS/LMDS system.

1.2 Radio-on-Fiber Architecture

Any feasible wireless last mile system would likely employ RoF technology. This technology exploits the massive bandwidth and low loss characteristics of optical fiber to deliver high frequency radio signals to remote locations. In the case of a wireless broadband delivery system such as LMCS/LMDS, RoF would be employed to distribute high frequency radio signals from a central office to remote basestations within service areas. Figure 1.1 shows the basic RoF architecture for such a system.

RoF cellular systems have many advantages over traditional cellular systems. In RoF systems, high frequency radio signals, not baseband data, are delivered to remote basestations. Basestations then, only need be comprised of an optical-electrical conversion device, an amplifier and an antenna; there is no need for expensive modulating or high frequency upconverting hardware. This greatly reduces basestation costs, and ultimately translates into significant infrastructure cost savings.

Further cost savings can be had through the inherent centralization that RoF provides. In RoF architecture, all the modulating and high frequency upconverting equipment have been brought back from the network edges and placed in the central office. This allows component sharing (e.g. high frequency local oscillators, filters, etc.) among basestations, easy accessibility for maintenance and upgrading, and increased reliability (easy to strictly control the operating environment, reducing

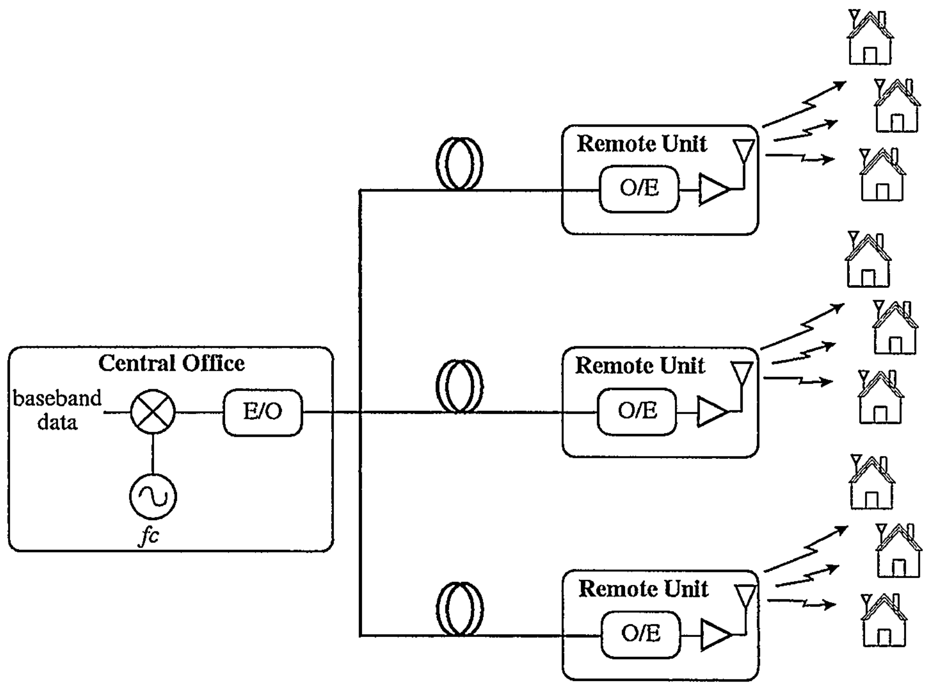

Figure 1.1: Radio-on-fiber system architecture

component failures).

RoF based networks also have the added advantage of generic remote units that are transparent to channel frequency and modulation format. This gives the central office the ability to employ dynamic frequency allocation, variable bit rates, and the choice of modulation format to maximize system capacity and regulate quality of service (QoS). This transparency also reduces the cost of system upgrades, as only the central office need be altered.

To date, only a one third of the broadband delivery market is serviced by telephone companies, with the other two thirds belonging to the cable companies[9]. With the imminent arrival of WISPs, telcos must solve their DSL reach problems if they are to maintain or increase their market share. As mentioned previously, many telecom companies have begun pursuing FTTC schemes as a solution. RoF becomes particularly attractive then, as it allows these companies to leverage these optical links, with the added benefits of wireless and RoF.

RoF is however, not without challenges. The high operating frequency and bandwidth requirements of LMCS systems require the use of high frequency oscillators, filters, and optical modulators. These components present serious design challenges, and can be extremely expensive.

These challenges have been the subject of much research, and various techniques have been proposed for the generation of high frequency radio signals —even beyond the electrical bandwidth of the optical modulator— without the use of high frequency oscillators and mixers. These techniques include, but are not limited to, the use of the phase modulation to intensity modulation (PM-IM) conversion characteristic of dispersive fiber[10], optical combining of an IF (Intermediate Frequency) and LO (Local Oscillator) signal[11], opto-electric mixing in an optical modulator[12], laser nonlinearities[13], external modulator nonlinearity[14] and nonlinear photodetection[15].

These schemes all generate a modulation-bearing millimeter or microwave radio carrier at the remote unit, but at the cost of added complexity or additional required electrical or optical equipment. This limits their cost reduction potential.

In this study, pure harmonic upconversion is presented as a new method of frequency translation. First proposed by Davies[16], this technique relies on the nonlinearity inherent in an analog optical link. Essentially, an information bearing IF signal is applied to a non-linear link, and a harmonic of choice is captured at the output with a bandpass electrical filter. The optical link then not only provides signal transport, but also provides frequency translation, replacing the final RF (Radio Frequency) upconversion stage in a typical transmitter.

Pure harmonic upconversion has many advantages; it provides frequency translation without additional hardware, is compatible with existing optical infrastructures and all types of digital RF and optical modulation schemes, and extends the bandwidth of the system while reducing the bandwidth of the transmitter components. Ultimately harmonic upconversion promises significant cost reductions in RoF systems.

Unfortunately, pure harmonic upconversion is not without challenges. Severe phase and amplitude distortion results from the harmonic upconversion process and is further compounded by fiber chromatic dispersion. Predistortion algorithms are thus required for distortionless upconversion of modulation bearing signals.

1.3 State of the Art and Contribution to the Art

The idea of frequency translating an information bearing signal solely through a nonlinearity was first introduced by Davies[16]. In the context of radio-on-fiber systems, he performed a theoretical analysis of the harmonic mechanism, characterized the associated distortion process and proposed a mitigating predistortion scheme for digital radio modulation. Preliminary proof-of-concept experiments were completed with QPSK (quadrature phase shift keying) radio modulation.

Davis[24] later demonstrated the harmonic upconversion of a multi-level modulation scheme in a non-dispersive RoF system, by employing a rough scaling type amplitude predistortion scheme. The author is not aware of any other advances in harmonic upconversion, and considers the work of Davis as state of the art.

The purpose of this study is to solidify and expand upon the state of the art in harmonic upconversion research, with the ultimate goal of validation. To satisfy this purpose, this study will:

Formalize the concept of pure harmonic upconversion in RoF systems. A concise and thorough development of the concept of pure harmonic upconversion and the associated theory in the context of radio-on-fiber systems would be a valuable contribution to the current state of literature. Such a resource would facilitate further research and bring pure harmonic upconversion closer to implementation.

Account for chromatic dispersion in predistortion. To date, harmonic upconversion demonstrations have only been implemented with non-dispersive fiber links. The effects of chromatic dispersion must be considered before a practical harmonically upconverting link can be demonstrated.

Demonstrate precise amplitude predistortion. In previous demonstrations, amplitude predistortion has only approximately linearized the amplitude characteristic of RoF links through scaling. This scheme, while simple, is insufficient for distortion sensitive signals, and limits signal power. Improving the amplitude predistortion scheme brings harmonic upconversion to its full potential.

Investigate the effects of fiber nonlinearity. The effects of fiber nonlinearity on RoF link operation and the harmonic upconversion process have not been investigated. A preliminary investigation of such effects would identify possible benefits or detriments.

Perform a practical demonstration. A harmonically upconverting radio-on-fiber system employing dispersive fiber has never been demonstrated. The demonstration of such a system would validate harmonic upconversion as a viable upconversion scheme for real world applications.

1.4 Outline of Thesis

Four chapters follow this Introduction. Each is briefly outlined below.

1.4.1 Chapter 2: The Radio-on-Fiber Link

A basic understanding of the RoF link is necessary to fully comprehend the study undertaken. This chapter provides an overview of the fundamental RoF link components with an emphasis on those suitable for LMCS/LMDS application. This is followed by a detailed discussion of the characteristics and modes of operation of a Mach-Zehnder based RoF link with direct detection. The impacts of chromatic dispersion are also covered, and optical single sideband modulation presented as a mitigation scheme.

1.4.2 Chapter 3: Pure Harmonic Upconversion

This chapter presents the general concept of pure harmonic upconversion with an emphasis on application in RoF systems. The RoF link harmonic response is characterized under various operating conditions. Distortion resulting from the harmonic upconversion process is discussed and predistortion presented as a mitigation scheme.

Fiber nonlinearity is also discussed and the effects on RoF link operation and harmonic generation detailed.

1.4.3 Chapter 4: Simulation and Experimentation

In this chapter, a RoF simulator is used to verify and compare the performance of the predistortion schemes presented in Chapter 3. Simulations are also performed to illustrate harmonic upconversion in bandwidth limited systems, dispersive systems, and various link configurations. As proof of concept and viability, an experimental harmonically upconverting, dispersive RoF link is described in detail and experimental results presented and discussed.

1.4.4 Chapter 5: Conclusion

In this final chapter, the accomplishments and conclusions of this study are summarized. Recommendations for future work are also discussed.

Chapter 2

Radio-on-Fiber

Before pure harmonic upconversion can be discussed, it is necessary to have a basic understanding of RoF technology. In this chapter, an overview of the fundamental RoF link components is given followed by a discussion of the link transfer characteristics and operation. The impacts of fiber chromatic dispersion in RoF links is also presented along with mitigation schemes.

2.1 Radio-on-Fiber Link Components

A basic RoF link is comprised of a light source, an electro-optic conversion device (E/O), a length of optical fiber, and an optical-electric conversion device (O/E). Figure 2.1 shows the basic RoF link components.

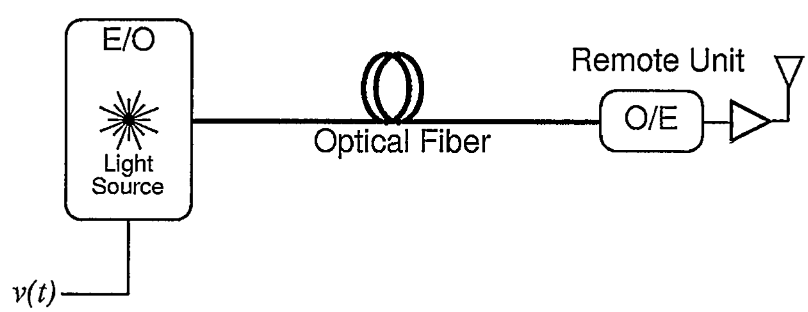

Figure 2.1: Radio-on-fiber link components

2.1.1 Light Sources

All optical systems require a fiber compatible light source. Currently, there are two main light sources suitable for optical communications.

Light-Emitting Diodes

Light-emitting diodes (LEDs) are inexpensive light sources that do not require complex drive circuitry. However, their low modulation bandwidth (<200MHz), wide spectral line width and low optical power output precludes them from use in RoF applications[18]. For this reason LEDs are not considered further in this study.

Laser Diodes

Semiconductor laser diodes (LDs) are common in high performance optical links as they produce high intensity coherent light that can be efficiently coupled into small core optical fiber, such as single mode fiber. They also offer light with a narrow, near monochromatic spectral linewidth, which allows transmission through fiber with less dispersion effects.

Figure 2.2 shows the optical output power characteristic of a laser diode. Clearly, optical output power in a laser diode is related to the diode drive current. At low drive currents ($I_d < I_{th}$), the device acts as a LED, emitting a spectrally broad, incoherent light. Optical output intensity increases only marginally with increasing drive current. As the drive current approaches the lasing threshold I_{th}, emitted light becomes more coherent and the spectral width narrows. A sharp increase in the optical power output occurs once the lasing threshold is passed, and the device enters the lasing region ($I_d > I_{th}$). In this region of operation, optical power increases rapidly with drive current, until saturation eventually occurs and maximum output power is asymptotically reached.

When operating in the lasing region, the output optical power $P_{o,LD}$, is directly proportional to diode drive current I_d, as in

$$P_{o,LD} = \eta_{LD} \left(I_d - I_{th} \right), \qquad I_d > I_{th} \tag{2.1}$$

where η_{LD} is the drive current to optical power efficiency.

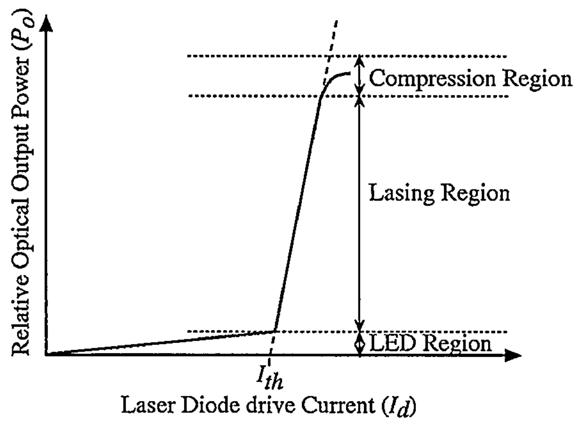

Figure 2.2: Laser diode characteristic

2.1.2 Optical Modulators

Like radio communications systems, optical systems require a carrier to transmit information. Radio systems employ tone radio carriers, and optical systems employ monochromatic light carriers. Although carriers in both systems can be both amplitude and phase modulated, the methods of effecting the modulation differ.

In electrical communications systems, modulation is easily achieved through a mixer device. A mixer essentially performs a multiplication function, making amplitude modulation a trivial operation. Phase modulation is more complicated, but still is easily accomplished through a structure incorporating two mixers known as a quadrature modulator.

Optical modulation is more difficult as there is no optical mixer equivalent. Instead, optical modulation is achieved either through the direct modulation of a light source drive current, or through the application of external devices that exploit electro-optic materials to alter either the amplitude or phase of an optical carrier.

Direct Modulation

Imposing an information process on a light stream by directly varying the drive current of a LD (or LED) so as to vary the optical output power, is known as direct modulation. The optical output power P_o, in a directly modulated LD is then

$$\begin{aligned} P_{o,LD} &= \eta_{LD}\left(I_d - I_{th}\right) \\ &= \eta_{LD}\left(I_b + \frac{v(t)}{R_{LD}} - I_{th}\right), \qquad I_d > I_{th} \end{aligned} \tag{2.2}$$

where I_b is the laser diode bias current, $v(t)$ is an information voltage signal, and R_{LD} is the series resistance of the LD.

The linear relationship between laser drive current and optical output power makes direct modulation one of the simplest methods of optical intensity modulation. However, care must be taken to ensure distortion free modulation; the laser diode must be biased and the information signal scaled such that LD operation remains within the lasing region (see Figure 2.2). Should at any time the overall drive current (bias current plus modulation current) push the laser into compression, signal distortion will result. Similarly, should I_d drop below the lasing threshold I_{th}, clipping distortion will occur. In higher frequency signals, additional distortion may result from the finite time required for a laser diode to make the transition back into the lasing region. Also, damage may occur to the LD if it is reverse biased at any time.

Under proper bias and drive current modulation, the modulation bandwidth of a typical LD is limited. The most advanced of semiconductor lasers have recently been reported to attain modulation bandwidths in excess of 25GHz[20]. However, these are limited by relative intensity noise (RIN), frequency chirp and other distortions. Practical directly modulated optical links are therefore limited to less than 20GHz[21].

The bandwidth and distortion limitations of direct modulation discourage its use in RoF LMCS/LMDS systems. External modulation is a more favorable method for such systems.

External Optical Modulation

Using an electro-optic device, external to a luminescent source, to modulate a constant intensity light stream is known as external modulation. There are several varieties of external modulators suitable for optical fiber communications. These include semiconductor electro-absorption modulators (EAMs), Mach-Zehnder electro-optic interferometer modulators (MZMs), and polymer modulators. Of these, only the MZM will be considered in this study.

The Mach-Zehnder electro-optic interferometer is an external optical modulator commonly used in high bandwidth digital and high frequency analog optical fiber networks. A diagram of a travelling wave MZM is shown in Figure 2.3.

The MZM is essentially comprised of two parallel optical phase modulators. An optical signal entering the modulator structure is split into two parallel waveguides

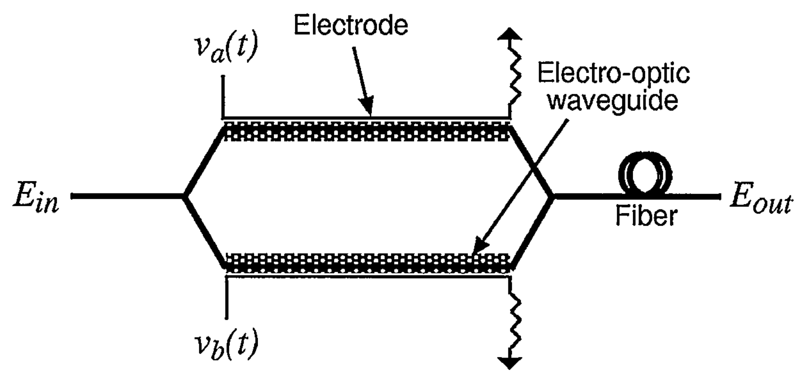

Figure 2.3: Travelling wave Mach-Zehnder electro-optical modulator structure

that each run alongside an embedded electrode. Each waveguide is constructed from an electro-optic material whose dielectric constant changes when exposed to an electric field. A voltage that is applied to the embedded electrode then causes a change in dielectric constant, changing the electrical length of the optical path, and inducing a phase shift in the optical signal passing through. Upon recombination, the two optical waves combine with a varying degree of destructive or constructive interference. An optical signal passing through the structure can be modulated through careful application of voltage signals to the MZM electrodes.

Typical MZMs employ either $LiNbO_3$ (lithium niobate) crystal or III-V compound semiconductors for an electro-optic material. $LiNbO_3$ is most commonly used as it exhibits a strong linear electro-optic effect, and thus is amenable to device modeling and construction. Type III-V semiconductors on the other hand, exhibit a weaker nonlinear electro-optic effect. However, the benefits of semiconductor crystal growth and fabrication techniques raise modulation efficiencies on par with $LiNbO_3$, and allow for easy integration with other components such as lasers, photodiodes, and amplifiers. The mathematical model of a MZM device depends on the type of electro-optic material employed. For the purposes of this study, only the $LiNbO_3$ based MZM will be considered due to its extremely well defined characteristic, and common use. All references to MZMs herein will be assumed to be $LiNbO_3$ based.

The MZM is highly versatile as it has the ability to act as a phase and amplitude modulator, in both optical single sideband (OSSB) and optical double sideband (ODSB) formats. The MZM has a larger modulation bandwidth, and is more robust than direct modulators, making it a favorable choice for RoF links.

The electrical bandwidth of a MZM is limited by the electrical bandwidth and transmission characteristics of the embedded electrodes. To improve bandwidth, these electrodes are usually constructed as transmission lines, and resistively terminated to ensure a broadband impedance match. In addition, the electrodes are designed such that the electrical wave travelling along the electrode is velocity matched to the optical wave travelling in the optical waveguide, thus maximizing phase modulation depth and modulation bandwidth. This configuration is known as a travelling wave MZM, and is shown in Figure 2.3.

Before the MZM model can be presented, it is necessary to briefly review the concept of complex envelope.

Complex Envelope

Consider a bandpass signal $x(t)$. The associated analytic signal is

$$x_p(t) = x(t) + j\hat{x}(t), \tag{2.3}$$

where $\hat{x}(t)$ is the Hilbert transform of $x(t)$, and j is equal to $\sqrt{-1}$. The analytic signal represented by Equation 2.3, is single sideband in nature, containing only the positive frequency components of $x(t)$. It can therefore can be represented as a frequency translated baseband signal as in

$$x_p(t) = x(t) + j\hat{x}(t) \equiv \tilde{x}(t)e^{j2\pi f_o t}. \tag{2.4}$$

In Equation 2.4, $\tilde{x}(t)$ is known as the complex envelope, or baseband equivalent signal, and is generally complex with both real and imaginary components.

The bandpass signal can be acquired by taking the real portion of the bandpass analytic signal as in

$$\begin{aligned} x(t) &= \Re\left[x_p(t)\right] && (2.5)\\ &= \Re\left[\tilde{x}(t)e^{j2\pi f_o t}\right] && (2.6)\\ &= \Re\left[x(t) + j\hat{x}(t)\right] && (2.7) \end{aligned}$$

By using the complex envelope, the frequency translation aspect of a bandpass signal or system can be ignored. Analysis of the interaction of bandpass signals with a bandpass system can thus be greatly simplified through the complex envelope.

Complex envelope notation is of particular use in optical systems, where the carrier frequency is in the order of THz. Therefore the optical complex envelope will be used herein, unless otherwise stated.

Mach-Zehnder Modulator Model

Recognizing that the MZM is comprised of two parallel phase modulators, the output optical electric field can be easily derived using the optical complex envelope as

$$E_{out,MZM} = \frac{E_{in,MZM}}{2}\left[\underbrace{e^{j\pi\left(\frac{v_a(t)}{V_\pi}\right)}}_{\text{upper phase mod.}} + \underbrace{e^{j\pi\left(\frac{v_b(t)}{V_\pi}\right)}}_{\text{lower phase mod.}}\right], \tag{2.8}$$

where $E_{in,MZM}$ and $E_{out,MZM}$ are the MZM input and output optical electric fields respectively, v_a and v_b are the real electrical voltages applied to the upper and lower electrodes respectively, and V_π is the voltage required to induce a 180° phase shift in one of the arms of the MZM. V_π is also known as the extinction or switching voltage of the modulator, as a voltage of V_π applied across the modulator electrodes will extinguish the output.

Equation 2.8 assumes an ideal MZM where input optical power is split equally between two identical modulator arms. In reality, MZMs may have imperfect power splitting, slightly asymmetric modulator arms, and undesirable polarization effects, that all contribute to imperfect extinction. In practice, a well designed and carefully configured MZM combined with a polarization controller can minimize the aforementioned non-idealities, and obtain extinction ratios in excess of 25dB. Equation 2.8 can therefore be assumed to accurately model the operation of a high quality MZM.

Mach-Zehnder Phase Modulator

The MZM can be configured as a phase modulator by setting $v_a = v_b = v_{in}$. Equation 2.8 then reduces to

$$E_{out,MZM} = E_{in,MZM} e^{\left(j\pi \frac{v_{in}(t)}{V_\pi}\right)}. \tag{2.9}$$

As shown in Equation 2.9, the phase of the optical signal is proportional to the input voltage. Although not common, this configuration can be used with a coherent optical detector to recover the phase modulated signal, or with other optical components to translate the phase modulation to intensity modulation for recovery with a standard photodetector[10]. The high cost of coherent optical detectors, and the added complexity of phase to intensity converters however, limits the use of the MZM as a phase modulator.

Mach-Zehnder Amplitude Modulator

The MZM is most commonly configured as an amplitude only modulator (equivalently an optical intensity modulator). In this case, the two MZM arms are driven differentially with $v_a = -v_b = v_{in}$.

The MZM characteristic is then

$$\begin{aligned} E_{out,MZM} &= \frac{E_{in,MZM}}{2}\left[e^{j\pi\left(\frac{v_{in}}{V_\pi}\right)} + e^{j\pi\left(\frac{-v_{in}}{V_\pi}\right)}\right] \\ &= E_{in,MZM}\cos\left(\pi\frac{v_{in}}{V_\pi}\right). \end{aligned} \tag{2.10}$$

Equation 2.10 shows that the output optical electric field has a constant phase, and an amplitude related to the MZM input voltage through the cosine function. Examination of a plot of output optical electrical field versus input voltage, shown in Figure 2.4, indicates that linear regions suitable for amplitude modulation do exist. Distortionless amplitude modulation of the optical electrical field can therefore be achieved through careful biasing and scaling of the driving voltage signals so as to restrict operation to the linear region of the characteristic. This will be discussed further in Section 2.2.

2.1.3 Optical Fiber

Silica fiber is the transport medium in optical communications systems, carrying modulated light from a light source to a remote receiver. Optical fiber is attractive as a communications medium as it is extremely broadband in nature. It is also however, a lossy and dispersive medium.

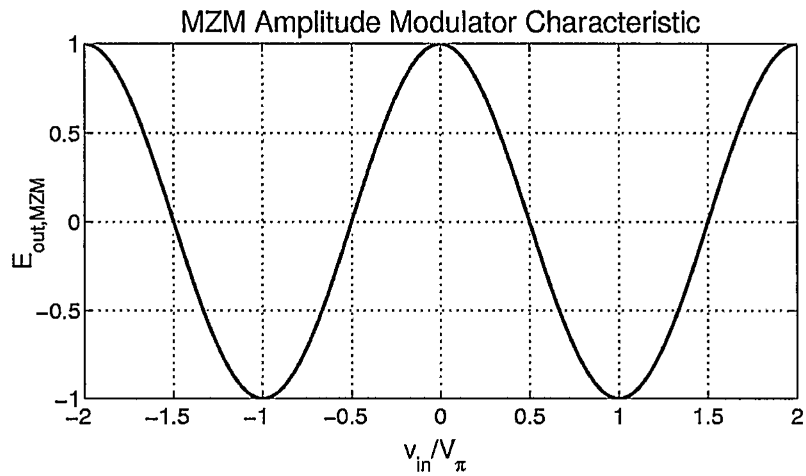

Figure 2.4: Mach-Zehnder amplitude modulator characteristic

Fiber Attenuation

As light propagates through fiber, it experiences losses stemming from a varying degree of scattering, waveguide imperfections, absorption, and radiative losses[18]. These losses are wavelength dependent, with a local minimum of 0.34dB/km at a wavelength of 1310nm, and a global minimum of 0.2dB/km at 1550nm (Corning SMF-28 fiber). To minimize losses, this study concerns only 1550nm optical carriers.

Optical Dispersion

Light propagating through silica glass fiber becomes increasingly distorted by optical dispersion. There are three main mechanisms that give rise to optical dispersion: intermodal delay, material dispersion and waveguide dispersion.

Depending on the fiber characteristics, light can travel along a fiber in several different modes of propagation simultaneously. As each mode can travel with a different group velocity, an optical pulse comprised of multiple modes will spread in time. This is called intermodal delay. To avoid this form of dispersion, most optical systems employ single mode fiber, where propagation is limited to only one mode. For the purposes of this study, only single mode fiber will be considered, and intermodal delay will not be considered further.

Material dispersion stems from the wavelength dependence of refractive index in silica glass; different wavelengths in the spectrum of an optical signal will travel at different speeds, leading to pulse spreading.

Waveguide dispersion occurs because optical power in single mode fibers is contained in both the fiber core and cladding. The difference in light velocity between the core and the cladding gives rise to spreading.

Material and waveguide dispersion can be characterized by dispersion parameters D_M and D_W respectively, both with units ps/nm·km. The combined effect of the two dispersions is called chromatic dispersion, and is characterized as $D = D_M + D_W$.

D_M and D_W have opposing slopes over frequency, creating a zero-dispersion point at a wavelength of ~1300nm. Unfortunately, operation at 1300nm has the disadvantage of increased optical loss, and precludes the use of erbium doped fiber amplifiers (EDFAs) which operate exclusively at 1550nm. Dispersion shifted, or dispersion flattened fibers, where the zero-dispersion point has been shifted to 1550nm, have been made through careful tailoring of the core refractive index profile so as to alter the degree of waveguide dispersion present. However, these fibers are not widely deployed as they incur higher losses and are more expensive.

The effects of chromatic dispersion can be modeled as the frequency domain transfer function

$$H_D(f) = e^{\frac{j\pi D\lambda_o^2(f-f_o)^2 L}{c}}, \tag{2.11}$$

where λ_o and f_o are the optical carrier wavelength and frequency respectively, D is the dispersion parameter, L is the fiber length, and c is the free-space speed of light[16]. It is apparent that dispersion induces a phase shift proportional to the square of the frequency offset from the optical carrier. Dispersion induced group delay is then

$$\begin{aligned} \tau_{grp}(f) &= \frac{-1}{2\pi}\frac{d}{df}\left(\angle H_D(f)\right) \\ &= \frac{-1}{2\pi}\frac{d}{df}\left(\frac{\pi D\lambda_o^2(f-f_o)^2 L}{c}\right) \\ &= -\frac{D\lambda_o^2(f-f_o)L}{c}. \end{aligned} \tag{2.12}$$

Figure 2.5 shows the dispersion transfer function and group delay over frequency offset. The group delay over frequency is non-flat, indicating that different signal frequency components will travel with different group velocities. This variation in group velocity gives rise to pulse spreading and is known as group velocity dispersion (GVD).

If the bandwidth of an optical signal is significant with respect to the optical carrier frequency, the non-flat group delay characteristic of dispersive fiber will cause distortion in the form of inter-symbol interference (ISI) and equalization may be necessary. In typical RoF applications, signal bandwidths are usually narrowband with respect to the optical carrier frequency (<1GHz). Assuming typical fiber lengths of $L < 100$km and a dispersion parameter of $D \approx 18$ps/nm·km, the group delay variation across the signal bandwidth will be negligible, and the signal will remain distortion free[16]. However, the difference in group delay between the optical sidebands can be significant, especially with high frequency radio subcarriers. This has serious implications in the photodetection process and will be discussed further in

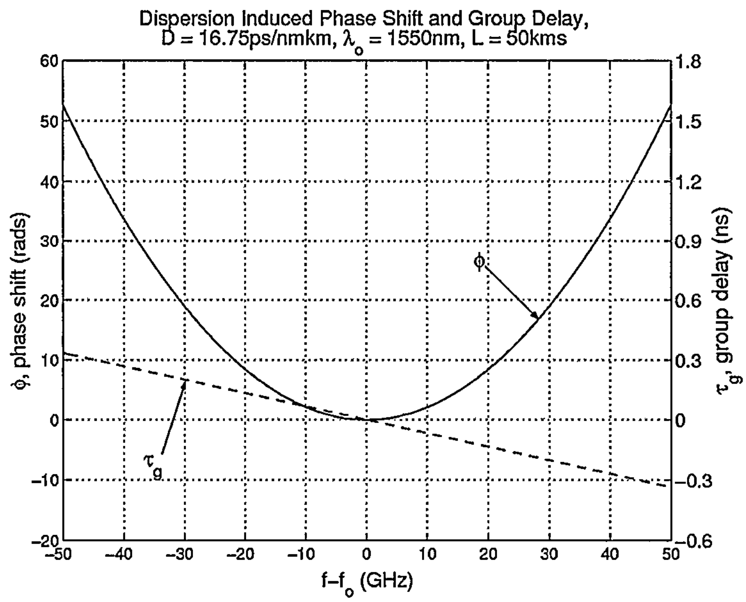

Figure 2.5: Dispersion phase and group delay transfer function

Section 2.2.2.

2.1.4 Photodiodes

At the receiving end of a RoF link, there is an opto-electric conversion device, called a photodetector, to recover the original information signal from the optical carrier. The most common photodetector in fiber optic systems are avalanche semiconductor photodiodes (APDs).

An APD generates an electrical current that is proportional to incident optical power, or the square of the input optical electric field. This type of conversion is called square-law detection, or envelope detection or direct detection (DD). The output current of a photodiode I_{PD}, is then

$$I_{PD} = \mathcal{R}P_{o,PD}$$

$$= \mathcal{R}\frac{|E_{PD}|^2}{\eta}, \tag{2.13}$$

where $\mathcal{R}$ is the detector responsivity, $P_{o,PD}$ is the incident optical power, E_{PD} is the incident optical electric field, and η is the intrinsic impedance of the optical material. Responsivity relates to the opto-electric conversion efficiency of the diode.

A consequence of direct detection is the loss of phase information in the optical electric field due to the square-law nature of a photodiode. For this reason, envelope compatible modulation schemes must be used.

2.2 The Radio-on-Fiber Transfer Characteristic

The typical components of a RoF link have been presented in the previous section. Next, the RoF link as a whole is considered, and the transfer characteristic derived for both non-dispersive and dispersive fiber. The system considered in this study is based on a laser diode light source with an external Mach-Zehnder modulator, connected through a length of single mode fiber to an APD for photo detection.

Revisiting the general MZM transfer function (Equation 2.8), but now incorporating a DC biasing voltage V_{bias}, to the lower modulator electrode arm gives the general equation for the optical electric field launched into a fiber from a MZM,

$$E_{out,MZM} = \frac{E_{in,MZM}}{2}\left[e^{j\pi\left(\frac{v_a}{V_\pi}\right)} + e^{j\pi\left(\frac{v_b}{V_\pi}+\frac{V_{\text{bias}}}{V_\pi}\right)}\right] \tag{2.14}$$

$$= E_{in,MZM}\cos\left(\pi\frac{v_a - v_b}{2V_\pi} - \pi\frac{V_{\text{bias}}}{2V_\pi}\right)e^{\left(j\pi\frac{v_a+v_b+V_{\text{bias}}}{2V_\pi}\right)}. \tag{2.15}$$

2.2.1 MZM/DD Non-Dispersive Fiber Link Characteristic

In a direct detection link, optical power is converted to an electrical current at the receiver by a photodiode. The transfer characteristic of a MZM/DD optical link employing non-dispersive optical fiber (zero length fiber or dispersion shifted/flattened fiber), neglecting fiber losses, is then

$$\begin{aligned} I_{PD} &= \mathcal{R}P_{o,PD} \\ &= \mathcal{R}\frac{|E_{out,MZM}|^2}{\eta} \\ &= \mathcal{R}\frac{\left|E_{in,MZM}\cos\left(\pi\frac{v_a-v_b}{2V_\pi}-\pi\frac{V_{\text{bias}}}{2V_\pi}\right)e^{\left(j\pi\frac{v_a+v_b+V_{\text{bias}}}{2V_\pi}\right)}\right|^2}{\eta} \\ &= \mathcal{R}\frac{|E_{in,MZM}|^2}{\eta}\cos^2\left(\pi\frac{v_a-v_b}{2V_\pi}-\pi\frac{V_{\text{bias}}}{2V_\pi}\right) \\ &= \frac{k}{2}+\frac{k}{2}\cos\left(\pi\frac{v_a-v_b}{V_\pi}-\pi\frac{V_{\text{bias}}}{V_\pi}\right), \end{aligned} \tag{2.16}$$

where $P_{o,PD}$ is the input optical power to the photodiode, $E_{in,MZM}$ and $E_{out,MZM}$ are the input and output optical electric fields of the MZM respectively, k is a constant equal to $\mathcal{R}\frac{|E_{in,MZM}|^2}{\eta}$, where $\mathcal{R}$ is the detector responsivity, and η is the intrinsic impedance of the optical material. The transfer characteristics of both the MZM and the overall MZM/DD link are shown in Figure 2.6, with the MZM configured for amplitude modulation ($v_{in} = v_a = -v_b$) and $V_{\text{bias}} = 0$.

Clearly the overall optical link characteristic is highly nonlinear in nature. To minimize distortion, the MZM is biased at the center of the most linear region of the link characteristic, and the modulating signal appropriately scaled to remain within the linear region. This bias point is known as the quadrature bias (QB) point, and is achieved by setting $V_{\text{bias}} = \frac{nV_\pi}{2}$, where n is odd. For $n = \ldots, -5, -1, 3, 7, \ldots$, the

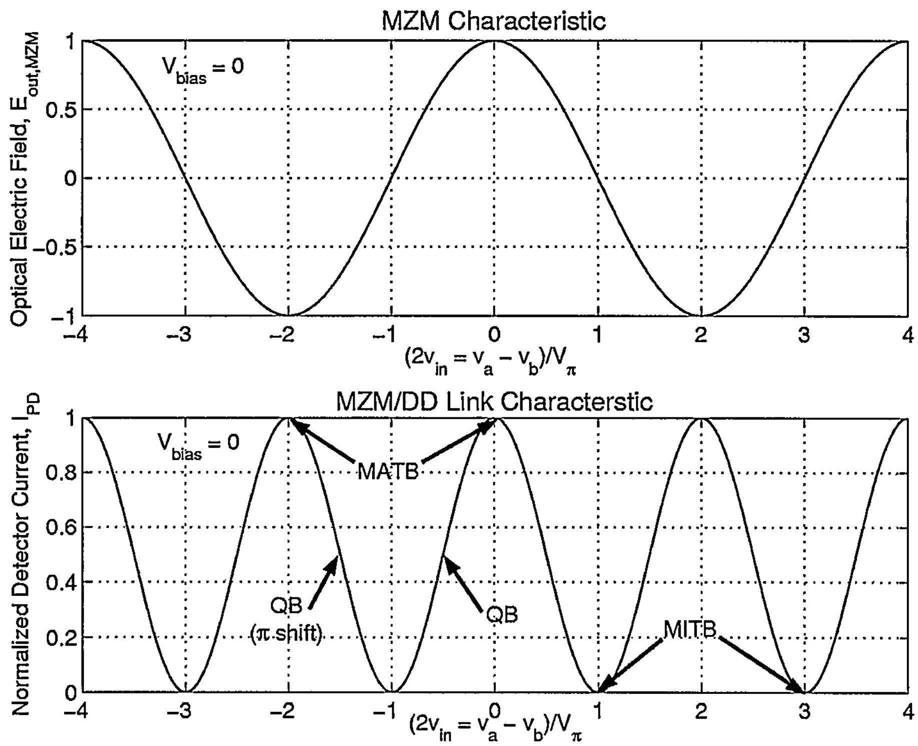

Figure 2.6: MZM/DD link characteristic

characteristic has a negative slope, resulting in a 180° phase shift in the transmitted signal.

Consider a subcarrier signal of the form $v_{in} = A\cos(2\pi f_c t)$, where A is the peak magnitude of the input signal, f_c is the subcarrier frequency, and t is time. Note that $m = \frac{A}{V_\pi}$ represents a modulation index. Differential application of this signal to a MZM biased at quadrature yields optical double sideband intensity modulation (ODSB-IM). Figure 2.7 shows the simulated spectrum for this scenario.

Clearly the optical spectrum is double sideband in nature, and contains both even and odd harmonics. The square-law detection process is seen to eliminate all

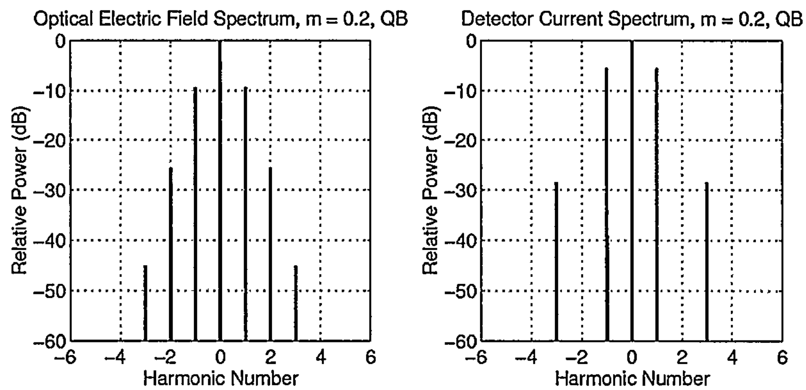

Figure 2.7: QB MZM electric field and detector current spectra

even harmonics, leaving only odd harmonics in the detector output spectrum. This harmonic behavior is attributed to the odd symmetry of the MZM/DD link transfer characteristic about the bias point ($V_{\text{bias}} = \frac{V_\pi}{2}$); odd symmetry will give rise only to odd harmonics, and even symmetry gives rise only to even harmonics[23]. However, the transfer characteristic of the MZM alone has neither even nor odd symmetry about the bias point, and so generates both even and odd harmonics.

Biasing the MZM at the link characteristic peaks, by setting $V_{\text{bias}} = \pm nV_\pi$ for n even, results in maximum transmitted optical carrier power. These bias points are accordingly named the Maximum Transmission Bias (MATB) points (see Figure 2.6).

At the MATB point, both the MZM and the overall link characteristics have even symmetry, and so only even harmonics are present in both the optical and detector current spectrums, as shown in Figure 2.8. A further consequence of even symmetry is the absence of the fundamental term. This restricts the use of the MATB point in RoF systems to harmonic upconversion applications.

The complement of the MATB point is the Minimum Transmission Bias (MITB)

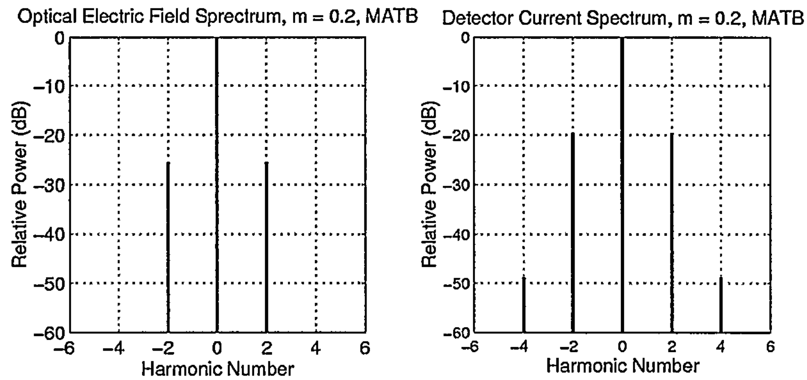

Figure 2.8: MATB MZM electric field and detector current spectra

point and is achieved by setting $V_{\text{bias}} = nV_{\pi}$, for n odd. In this case, the minimum optical carrier power is transmitted, as shown in Figure 2.9. The MZM transfer characteristic has odd symmetry being centered around the zero electric field point, and so generates only odd harmonics in the optical spectrum. The square-law process is seen to generate only even harmonics in the detector current. Like MATB, MITB lacks a fundamental term in the detector current, and is also limited to harmonic upconversion applications in RoF systems.

In the aforementioned bias scenarios, the harmonic content of the optical and detector spectrums is directly related to the modulation index, m. Increasing the modulation index, will incur more distortion, and increase the harmonic content of the signals. This will be discussed in depth in Chapter 3.

2.2.2 Direct Detection and Chromatic Dispersion

In trying to minimize infrastructure costs, RoF systems will likely leverage existing fiber infrastructure wherever possible. Since the majority of installed fiber today is

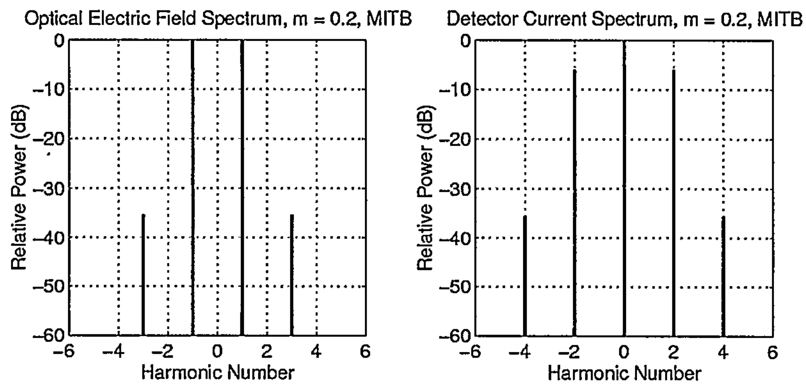

Figure 2.9: MITB MZM electric field and detector current spectra

dispersive, the effects of chromatic dispersion in RoF links must be investigated.

As discussed earlier in Section 2.1.3, typical RoF signals are narrowband with respect to the optical carrier, and so experience negligible GVD related distortion. However, the variation in group delay between the subcarrier sidebands can be significant at higher subcarrier frequencies. This variation causes the sidebands to rotate in phase with respect to one another. At the receiver, the sidebands will interact in the square-law photodetection process with a varying degree of constructive or destructive interference, depending on the dispersion induced phase shift. The overall effect of dispersion in a narrowband RoF link is a power fading pattern over fiber length and subcarrier frequency that reduces usable fiber length and bandwidth. For an ODSB-DD link, the fundamental tone fading is described by [19]

$$P(f_c) \propto \cos^2\left(\frac{\pi D \lambda_o^2 f_c^2 L}{c}\right) \tag{2.17}$$

where D is the dispersion parameter, λ_o is the optical wavelength, f_c is the subcarrier frequency, L is the fiber length, and c is the speed of light in free space.

The fading pattern over dispersive fiber length for an ODSB-DD link with $\lambda_o =$ 1550nm, and D = 17 ps/(nm·km), is shown in 2.10(a) for a LMCS/LMDS suitable subcarrier frequency of f_c = 31GHz, and in 2.10(b) over subcarrier frequency for a fiber length of 30km. Clearly the fading profile over fiber length is severe with 3dB of power lost after only 1.95km. Similarly, the fading profile over subcarrier frequency shows a 3dB fiber bandwidth of only 7.8GHz. Even a shorter fiber length of 3km, more typical of an urban RoF system, still only has a bandwidth of 24.7GHz.

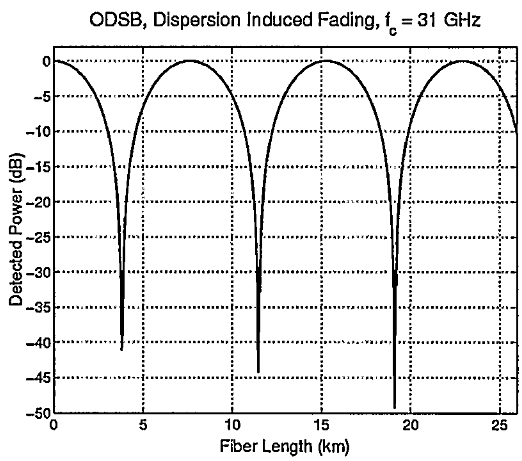

(a) Power fading over fiber length

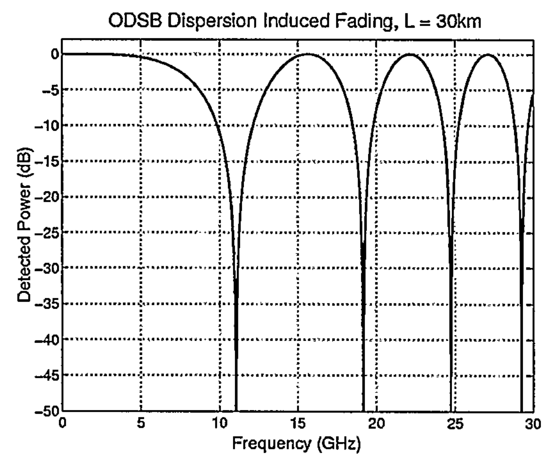

(b) Power fading over subcarrier frequency

Figure 2.10: Dispersion induced power fading patterns

Chromatic dispersion severely affects both fiber bandwidth and signal reach to the extent of preventing LMCS/LMDS RoF applications. Fortunately there are several methods of mitigating dispersion related fading. The simplest is to ensure that the receiver does not reside within a power null by adding dispersive fiber length to the system[17]. Adding fiber however is not always practical or cost effective and requires customization.

Another method of chromatic dispersion compensation incorporates fiber Bragg gratings into the fiber link to flatten the group delay of dispersive fiber, reducing the severity of the fading mechanism. These gratings must be tailored specifically for each optical link.

Dispersion shifted/flattened fibers exhibit zero dispersion at the optical carrier wavelength and can be used in new fiber installations to prevent subcarrier fading. However, these fibers are more expensive, and typically are more lossy than standard fiber.

A new method aimed specifically at reducing dispersion related fading is optical single sideband (OSSB) modulation[16, 22]. In this method, one of the subcarrier sidebands is removed, eliminating the interference mechanism and the associated power penalty. OSSB is fiber length independent, and relatively easy to implement in a MZM based system, making it the method of choice for RoF systems. For this reason, this study will only consider OSSB modulation for subcarrier fading mitigation.

Figure 2.11 shows dispersion related fading patterns for ODSB and OSSB modulation schemes at a low subcarrier modulation index ($m = 0.1$). ODSB modulation is subject to severe power fading over both frequency and fiber length, while OSSB has a flat power characteristic, with a uniform 3dB power penalty resulting from the loss of one sideband. At higher modulation indexes however, the OSSB characteristic begins to exhibit a slight ripple due to the interaction of higher order harmonics in the detector as shown in Figure 2.11(c). Despite the increased ripple, OSSB modulation still prevents the deep fades exhibited by ODSB modulation.

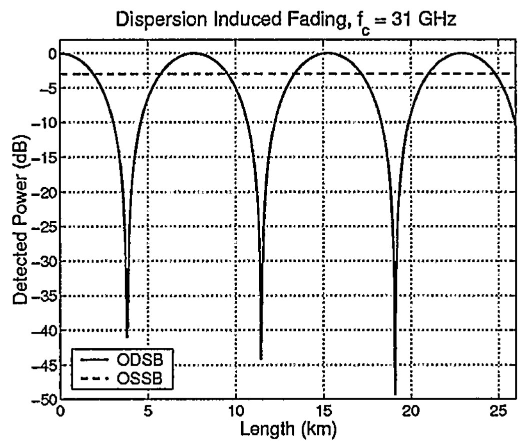

(a) Fading over fiber length $m = 0.1$

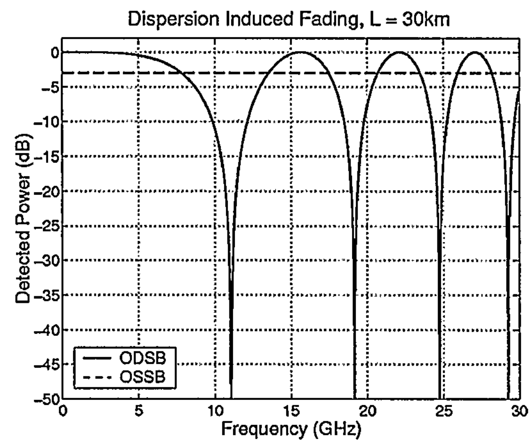

(b) Fading over frequency $m = 0.1$

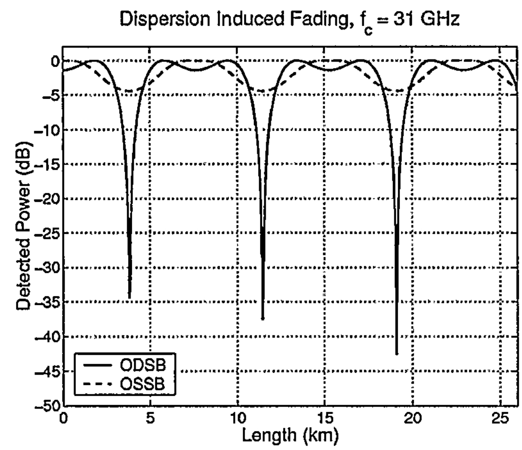

(c) Fading over fiber length, $m = 0.4$

Figure 2.11: Dispersion induced power fading patterns, OSSB and ODSB

Optical Single Sideband Generation in RoF Systems

It has been shown that OSSB modulation can be achieved through a Hartley configured MZM[22]. In this configuration the MZM is biased at quadrature and the arms are driven with a Hilbert transform pair ($v_b = H_T[v_a]$, where $H_T[v_a]$ is the Hilbert transform of v_a).

For subcarrier systems, the Hilbert transform is easily accomplished through

Bedrosian's theorem

$$H_T\left[a(t)b(t)\right] = a(t)H_T\left[b(t)\right], \tag{2.18}$$

so long as $b(t)$ and $a(t)$ do not overlap in frequency and $b(t)$ is higher in frequency than $a(t)$. Applying the theorem to a subcarrier signal,

$$\begin{aligned} H_T\left[a(t)\cos(2\pi f_c t)\right] &= a(t)H_T\left[\cos(2\pi f_c t)\right] \\ &= a(t)\sin(2\pi f_c t) \\ &= a(t)\cos(2\pi f_c t - \frac{\pi}{2}), \end{aligned} \tag{2.19}$$

shows that the Hilbert transform of a subcarrier can be achieved by multiplying (mixing) the data signal with a carrier shifted by $-\frac{\pi}{2}$ radians.

Setting $v_a = A\cos(2\pi f_c t)$, $v_b = A\sin(2\pi f_c t)$, and $V_{\text{bias}} = \frac{V_\pi}{2}$ in Equation 2.14, gives

$$E_{out,MZM} = \frac{E_{in,MZM}}{2}\left[e^{j\left(\pi\frac{A\cos(2\pi f_c t)}{V_\pi}\right)} + e^{j\left(\pi\frac{A\sin(2\pi f_c t)}{V_\pi}+\frac{\pi}{2}\right)}\right] \tag{2.20}$$

$$\begin{aligned} &= E_{in}\cos\left(\pi\frac{m\cos(2\pi f_c t) - m\sin(2\pi f_c t)}{2} - \frac{\pi}{4}\right)e^{j\left(\pi\frac{m\cos(2\pi f_c t)+m\sin(2\pi f_c t)}{2}+\frac{\pi}{4}\right)} \\ &= E_{in}\cos\left(\frac{\sqrt{2}m\pi\cos(2\pi f_c t + \frac{\pi}{4})}{2} - \frac{\pi}{4}\right)e^{j\left(\frac{\sqrt{2}m\pi\cos(2\pi f_c t - \frac{\pi}{4})}{2}+\frac{\pi}{4}\right)}, \end{aligned} \tag{2.21}$$

where, m is a modulation index and is defined as

$$\begin{aligned} m &= \frac{v_{in,peak}}{V_\pi} \\ &= \frac{A}{V_\pi}. \end{aligned} \tag{2.22}$$

The Hartley configured MZM optical electric field and detector current spectrums are shown in Figure 2.12 for $m = 0.2$. This configuration generates optical single sideband modulation with the alternating elimination of upper and lower harmonic sidebands, beginning with the lower fundamental sideband. Changing the bias point to a 180° shifting QB point will reverse the order of alternation. Square-law detection recovers DSB modulation with only odd harmonics in the detector spectrum. Square-law detection also removes the residual phase modulation (frequency chirp) term shown in Equation 2.21.

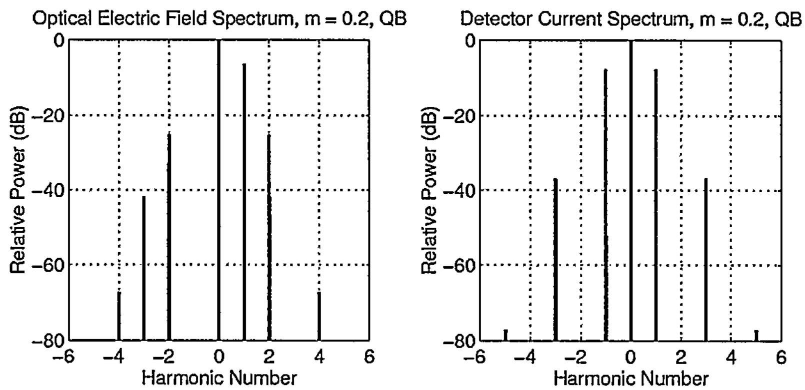

Figure 2.12: Hartley MZM electric field and detector current spectra

2.3 Summary

In this chapter, the basic components of a RoF link were presented and mathematical models developed. The transfer characteristic of MZM/DD based RoF link was derived, and various modes of operation characterized and demonstrated. Fiber chromatic dispersion and associated effects were also discussed with an emphasis on subcarrier fading. OSSB modulation, shown to be easily achieved with a Hartley configured MZM, was demonstrated as an effective subcarrier fading mitigation scheme.

Chapter 3

Pure Harmonic Upconversion

Pure harmonic upconversion is a new method of frequency translation that holds much potential. Although the concept itself is relatively straight forward, application is not. This chapter serves to formalize the concept of pure harmonic upconversion, with a focus on application in RoF systems.

The general theory behind pure harmonic upconversion is presented in Section 3.1. Section 3.2 outlines the many benefits of application in RoF links. As pure harmonic upconversion is entirely dependent on the harmonic characteristics of a nonlinearity, an in depth study of the RoF link harmonic response is performed in Section 3.3 for both non-dispersive and dispersive links. Section 3.4 addresses the issue of distortion stemming from the harmonic upconversion process and presents predistortion as a mitigation scheme. Predistortion implementation is also discussed. A preliminary investigation into fiber nonlinearity is performed in Section 3.5, with the goal of identifying possible benefits or detriments to RoF systems in general and those implementing harmonic upconversion.

3.1 Concept

When a signal passes through a nonlinear system, distortion is incurred. As illustrated in Figure 3.1, this distortion takes the form of a series of added harmonic and intermodulation (not shown) products. In transmission systems, these added frequency components are considered undesirable as they represent lost power and distortion.

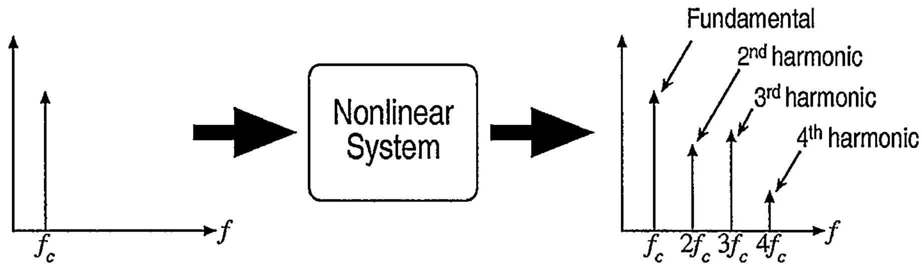

Figure 3.1: Nonlinear distortion (single tone input)

The individual distortion terms arising from a nonlinear system can be useful when isolated. The harmonic terms are particularly useful as frequency multipliers, even in the context of distortion sensitive communication systems.

Consider a transmission system with a nonlinear transfer characteristic generating harmonics. If a bandpass filter is placed at the system output to isolate one of the generated harmonics, the system as a whole then acts as an upconverter, in addition to providing signal transport. As opposed to typical upconversion schemes involving an oscillator and a mixer, or other harmonic upconversion techniques involving a combination of an oscillator harmonic tone and mixer, this upconversion was performed purely through the harmonic mechanism. Consequently, this upconversion scheme is coined “pure harmonic upconversion”. Note that the term “pure harmonic upconversion” will be referred to herein as simply “harmonic upconversion”, unless otherwise stated.

While theoretically any nonlinearity can be used to perform harmonic upconversion, in practice the harmonic generation ability of a nonlinearity must be reasonably efficient and well defined; inefficient harmonic generation increases drive power requirements, reducing the net benefits of harmonic upconversion, and a well defined harmonic behavior is essential for reliable, and distortionless upconversion.

3.2 Pure Harmonic Upconversion in Radio-on-Fiber Links

MZM based RoF links are extremely well suited for harmonic upconversion as they are inherently nonlinear in nature, efficiently generate harmonics, and have well defined characteristics. They also stand to gain enormously from the simplification and bandwidth relaxation offered by harmonic upconversion.

Consider as an example, the 30GHz LMCS/LMDS RoF system shown in Figure 3.2(a). The transmitter is comprised of a 30GHz linear RF upconversion stage, and a 30GHz broadband optical modulator. The high frequency requirements make these components expensive.

Figure 3.2(b) shows the same RoF system, but employing a fifth order harmonic upconversion scheme. In this scenario, the 30GHz RF upconversion stage is no longer required. Only a cheaper, lower frequency, 6GHz IF upconversion stage is necessary. Also, since the harmonic upconversion mechanism takes place in the optical domain, the electrical bandwidth requirements of the optical modulator are reduced to that of the IF stage. Harmonic upconversion has reduced the bandwidth requirements of the transmitter by a factor of the harmonic order used in the upconversion, without added components. This translates into a lower cost transmitter.

Harmonic upconversion and the RoF link however, incur severe distortion in

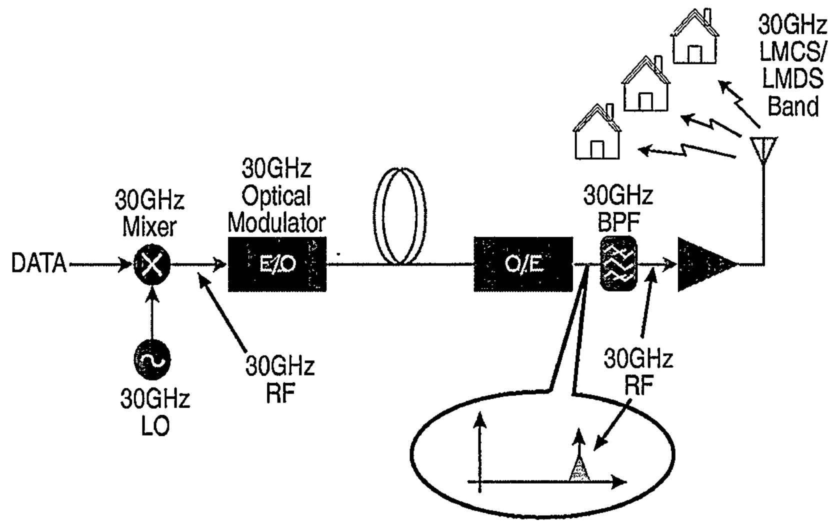

(a) Linear upconversion

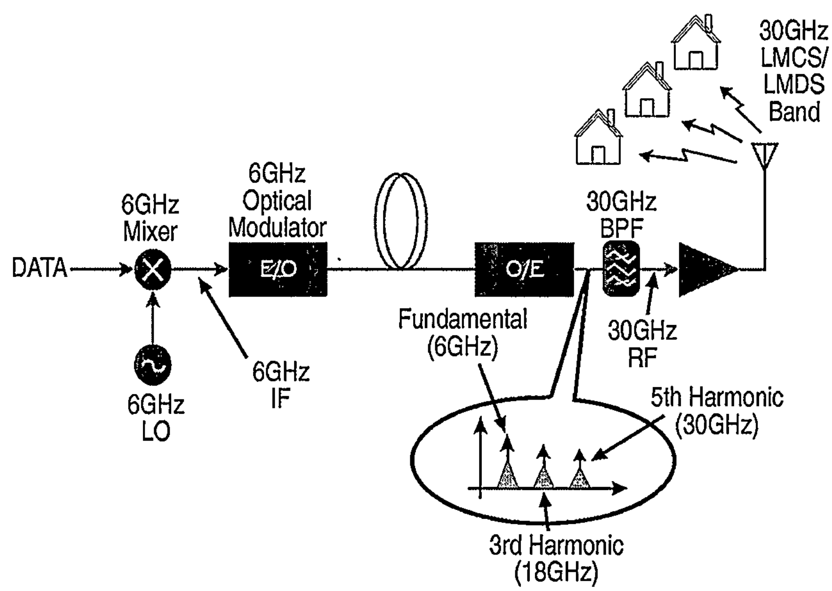

(b) Harmonic upconversion

Figure 3.2: Linear and harmonic upconversion in a 30GHz LMCS/LMDS RoF link

information signals. In an effort to find mitigation schemes, the nature of the RoF link nonlinearity must be analyzed in order to identify the distortion mechanisms of a specific harmonic response.

3.3 Radio-on-Fiber Harmonic Response

Recall the sinusoidal link characteristic from Section 2.2.1, shown again for convenience in Figure 3.3. Normally the link would be biased at quadrature and driven at a low modulation index (i.e. $m \ll 1$) to ensure that operation remains within the linear region. As the driving signal increases, the region of operation expands to include increasingly nonlinear portions of the characteristic, causing the harmonic content of the output signal to grow. Figure 3.3 shows the simulated detector output spectrum for a non-dispersive MZM/DD RoF link biased at quadrature and driven with a single tone of magnitude $0.7V_\pi$. Clearly the the nonlinearity in the link leads to significant harmonic content at the detector output.

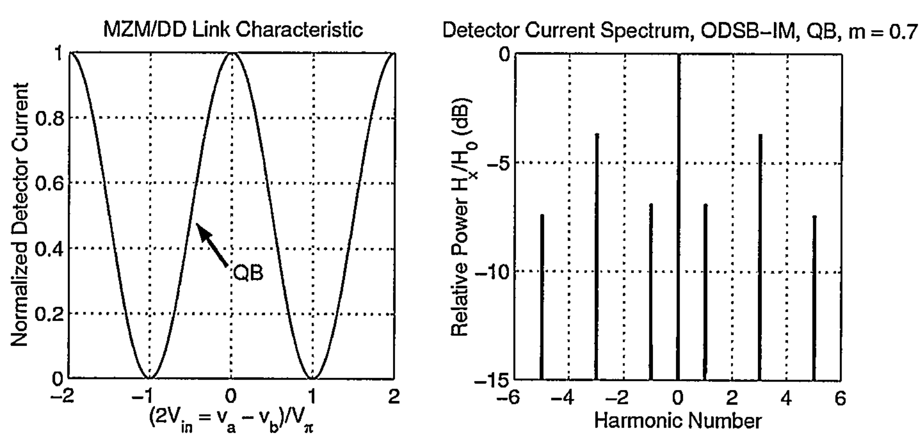

Figure 3.3: MZM/DD link characteristic and output harmonic content

In this study of harmonic upconversion, a MZM is driven with a radio carrier at a high modulation index so as to generate a series of harmonics in the optical domain. As the optical signal propagates through the fiber link it is distorted by chromatic dispersion and possibly fiber nonlinearity. At the receiver, it is further distorted by the square-law nature of APD photodetection. The resulting signal is filtered for the desired harmonic, leaving a signal translated in frequency by a factor of the harmonic number used.

The response of a specific harmonic at the link output is determined by the MZM, the fiber channel (chromatic dispersion and fiber nonlinearity), and the square-law detection process. It is necessary to characterize the harmonic response in order to identify and mitigate any distortion mechanisms. Fortunately, the MZM/DD link is extremely well characterized and reasonably amenable to mathematical analysis.

The following sections contain an analysis of the harmonic response of the MZM/DD link under various operating conditions, for both non-dispersive and dispersive links. The combined effects of fiber chromatic dispersion and nonlinearity will be considered in Section 3.5.

3.3.1 Non-Dispersive Links

RoF links that employ dispersion shifted or flattened fiber, or sufficiently short fiber lengths, will not be affected by chromatic dispersion and can be analyzed solely from the MZM/DD transfer function, previously described in Equation 2.16.

Setting the MZM drive signals as differential subcarrier signals, $v_a = -v_b = A\cos(2\pi f_c t)$, and setting $V_{\text{bias}} = \frac{nV_\pi}{2}$, where n is odd, achieves QB ODSB-IM. This scenario is described as

$$\begin{aligned} I_{PD} &= \frac{k}{2} + \frac{k}{2}\cos\left(\pi\frac{v_a - v_b}{V_\pi} - \pi\frac{V_{\text{bias}}}{V_\pi}\right) \\ &= \frac{k}{2} + \frac{k}{2}\cos\left(\pi\frac{2A\cos(2\pi f_c t)}{V_\pi} - \frac{n\pi}{2}\right) \\ &= \frac{k}{2} \pm \frac{k}{2}\sin\left(2m\pi\cos(2\pi f_c t)\right), \end{aligned} \tag{3.1}$$

where $m = \frac{A}{V_\pi}$ is a modulation index and $k = \mathcal{R}\frac{|E_{in,MZM}|^2}{\eta}$ is a constant, where $\mathcal{R}$ is the detector responsivity, $E_{in,MZM}$ is the input optical electric field of the MZM, and η is the intrinsic impedance of the optical material. Using the identity

$$\sin(u\cos x) = 2\sum_{n=1}^{\infty}(-1)^{n+1}J_{2n-1}(u)\cos\left((2n-1)x\right), \tag{3.2}$$

where J_x is a x^{th} order Bessel function of the first kind, Equation 3.1 can be expanded as

$$I_{PD} = \frac{k}{2} \pm \frac{k}{2}\left[2\sum_{n=1}^{\infty}(-1)^{n+1}J_{2n-1}\left(2\pi m\right)\cos\left(2\pi(2n-1)f_c t\right)\right]. \tag{3.3}$$

Equation 3.3 indicates that the output current is comprised of a series of odd harmonics, verifying the simulation results of Section 2.2.1. Note that if a π-shift QB point is selected (i.e. $V_{\text{bias}} = \frac{nV_\pi}{2}, n = \ldots, -5, -1, 3, 7, \ldots$), the second term will be negated.

The MATB expansion is performed in a similar manner, but with $V_{\text{bias}} = nV_\pi = 0$, where n is even;

$$\begin{aligned} I_{PD} &= \frac{k}{2} + \frac{k}{2}\cos\left(2\pi m\cos(2\pi f_c t)\right) \\ &= \frac{k}{2} + \frac{k}{2}\left[J_0\left(2\pi m\right) + 2\sum_{n=1}^{\infty}(-1)^n J_{2n}\left(2\pi m\right)\cos\left(2\pi(2n)f_c t\right)\right], \end{aligned} \tag{3.4}$$

with the following identity used to perform the expansion,

$$\cos(u\cos x) = J_0(u) + 2\sum_{n=1}^{\infty}(-1)^n J_{2n}(u)\cos(2nx). \tag{3.5}$$

Similarly, the MITB expansion can be found by setting $V_{\text{bias}} = nV_\pi$, where n is odd;

$$\begin{aligned} I_{PD} &= \frac{k}{2} + \frac{k}{2}\cos\left(2\pi m \cos(2\pi f_c t + \pi)\right) \\ &= \frac{k}{2} - \frac{k}{2}\left[J_0\left(2\pi m\right) + 2\sum_{n=1}^{\infty}(-1)^n J_{2n}\left(2\pi m\right)\cos\left(2\pi(2n)f_c t\right)\right]. \end{aligned} \tag{3.6}$$

The MATB and MITB expansions show detector currents composed only of even harmonics with identical behavior, with the exception of a 180° phase difference.

Although OSSB modulation is generally not employed for non-dispersive links, it is instructive to perform the expansion. For a Hartley OSSB modulator, $V_{\text{bias}} = \frac{\pi}{2}$, $v_a = A\cos(2\pi f_c t)$, and $v_b = A\sin(2\pi f_c t)$. The expansion follows as

$$\begin{aligned} I_{PD} &= \frac{k}{2} + \frac{k}{2}\cos\left(\pi\frac{A\cos(2\pi f_c t) - A\sin(2\pi f_c t)}{V_\pi} - \frac{\pi}{2}\right) \\ &= \frac{k}{2} + \frac{k}{2}\cos\left(\sqrt{2}\pi m\cos\left(2\pi f_c t + \frac{\pi}{4}\right) - \frac{\pi}{2}\right) \\ &= \frac{k}{2} + \frac{k}{2}\sin\left(\sqrt{2}\pi m\cos(2\pi f_c t + \frac{\pi}{4})\right) \\ &= \frac{k}{2} + \frac{k}{2}\left[2\sum_{n=1}^{\infty}(-1)^{n+1}J_{2n-1}(\sqrt{2}\pi m)\cos\left((2n-1)(2\pi f_c t + \frac{\pi}{4})\right)\right], \end{aligned} \tag{3.7}$$

where Equation 3.2 was used in the expansion.

Again, the harmonic amplitudes correspond to Bessel functions. However, the argument of the Bessel function in the OSSB scenario is reduced by a factor of $\sqrt{2}$ compared to that of ODSB. Consequently, for a given modulation index m, the output power of every harmonic component is lowered by 3dB, reducing generation efficiency. This is a tradeoff for dispersion related fading mitigation.

The simulated harmonic evolution with respect to the fundamental component over modulation index m, for both QB and MITB/MATB in a non-dispersive link is shown in Figure 3.4, where H_x refers to the x^{th} order harmonic component. These results have been experimentally verified by Davis [32].

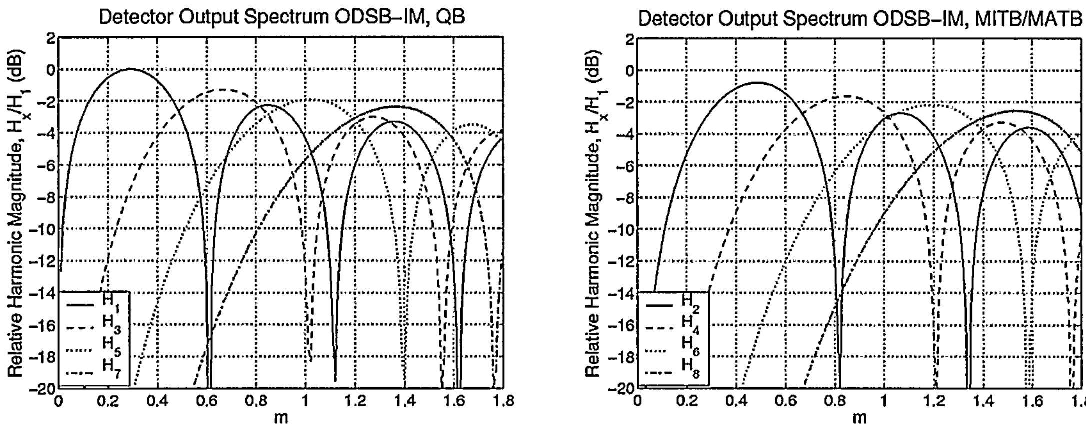

(a) Odd harmonic growth

(b) Even harmonic growth

Figure 3.4: Harmonic growth over modulation index, m

Several observations can be made in examining Figure 3.4. First, harmonic growth is clearly a nonlinear function of modulation index. This is not surprising as an examination of Equations 3.3, 3.4, and 3.6 indicate that regardless of biasing, the amplitudes of the generated harmonics are all related to nonlinear Bessel functions.

Secondly, the MZM/DD link is shown to be an excellent harmonic generator, with maximum harmonic magnitudes only a few dB below that of the fundamental, and obtained with relatively low modulation indexes.

Thirdly, a desired harmonic is easily maximized through appropriate selection of modulation index and MZM bias point.

Fourthly, in order to maximize a given harmonic, significantly more power is required than for the fundamental. This implies an increased link loss.

Looking from a harmonic upconversion perspective, the second and third observations are highly desirable; harmonic generation is very efficient, reducing the demands on drive circuitry in the transmitter such as amplifiers, and the ability to fine tune the harmonic behavior of the MZM/DD link allows maximum upconversion efficiency and flexibility. The first observation however, does present problems when harmonically upconverting information bearing signals. This will be discussed in detail later in this chapter. The fourth presents a significant drawback of harmonic upconversion and deserves further discussion.

To illustrate the problem, consider the harmonic characteristic shown in Figure 3.4(a). To maximize the fundamental component at the link output, the MZM must be driven at modulation index of 0.29, which corresponds to an average input signal power of 12.31dBm, assuming a V_π of 4.5V and system impedance of 50Ω. Similarly for the 5th harmonic, a modulation index of 1.0 is required, corresponding to 23.0dBm average signal power. Accounting for the 3.84dB difference in maximum output power between the two components, the 5th harmonic exhibits 14.59dB more link loss than the fundamental. As RoF systems are already plagued by link losses in excess of 30dB, this added loss is significant.

Fortunately, there is promising research directed at decreasing the V_π parameter of MZMs; a lower V_π voltage reduces the required power to achieve a given modulation index. Ridged Ti:$LiNbO_3$ MZMs for example, have been demonstrated with V_π values as low as 3.5V[25] and polymer based MZMs are promising even more reductions[26]. These modulators can be further improved with resonant enhancement[27, 28]. Such techniques have been shown to reduce link loss by more than 15dB for a 1% bandwidth[29].

A resonantly enhanced, low V_π MZM, would allow harmonic upconversion to be applied with little to no increase in required drive equipment. Even so, the significant advantages offered by harmonic upconversion (elimination of the high frequency RF upconversion stage, and reduced optical modulator electrical bandwidth requirements) can outweigh the disadvantage of increased link loss.

3.3.2 Dispersive Links

Many practical RoF systems employ fiber lengths sufficient to accumulate significant chromatic dispersion. Consequently, the effects of chromatic dispersion on harmonic evolution must be considered.

Chromatic dispersion complicates the optical field at the photodetector, making mathematical analysis of the link harmonic response considerably more difficult. Fortunately, the technique first introduced by Walker et al[10] and expanded upon by Davies[16], derives a general formula for the detector current harmonic content (equivalently the optical power harmonic content) in response to any periodic optical signal traveling through dispersive fiber.

Using this technique, Davies showed that for an ODSB link biased at quadrature, with a subcarrier input signal $A\cos(2\pi f_c t)$, the detector current can be expanded into the following exponential Fourier series,

$$\begin{aligned} I_{PD} &= \sum_{n=-\infty}^{\infty} I_n e^{j2\pi n f_c t} \\ &= \frac{k}{2}\left[J_0\left(2\pi m \sin(2n\phi)\right) + \sum_{n=-\infty,\ n\neq 0}^{\infty} J_{2n}\left(2\pi m \sin(2n\phi)\right) e^{j2\pi(2n)f_c t} \right. \\ &\quad \left. + \sum_{n=-\infty,\ n\neq 0}^{\infty} (-1)^{n+1} J_{2n-1}\left(2\pi m \cos\left((2n-1)\phi\right)\right) e^{j2\pi(2n-1)f_c t} \right], \end{aligned} \tag{3.8}$$

where

$$\begin{aligned}
J_n &= n^{\text{th}}\text{order Bessel function of the first kind,} \\
m &= \frac{A}{V_\pi}, \\
k &= \mathcal{R}\frac{|E_{in,MZM}|^2}{\eta}\ \text{(A)}, \\
\phi &= \frac{\pi D \lambda_o^2 f_c^2 L}{c}\text{(radians)}, \\
D &= \text{fiber dispersion parameter (s/m}^2\text{)}, \\
\lambda_o &= \text{optical wavelength (m)}, \\
f_c &= \text{fundemental subcarrier frequency (Hz)}, \\
L &= \text{fiber length (m)}, \\
c &= \text{speed of light in free space (m/s), and} \\
n &= \text{harmonic number.}
\end{aligned}$$

Equation 3.8 indicates that the detector current contains both even and odd harmonic terms whose amplitudes are governed by Bessel functions, as was the case for non-dispersive links. The Bessel function arguments however, are now dependent on a dispersion term which describes subcarrier fading over fiber length and frequency.

Similarly, for OSSB (Hartley configuration), it can be shown that the detector current is represented by the exponential Fourier series,

$$\begin{aligned}
I_{PD} &= \sum_{n=-\infty}^{\infty} I_n e^{j2\pi n f_c t} \\
&= \frac{k}{4}\sum_{n=-\infty}^{\infty} e^{j2\pi n f_c t}\left\{J_{-n}\left(2\pi m \sin(n\phi)\right) + j^n J_n\left(2\pi m \sin(n\phi)\right)\right. \\
&\quad \left. + je^{\frac{-n\pi}{4}}\left[J_{-n}\left(2\pi m \sin(n\phi - \frac{\pi}{4})\right) - J_{-n}\left(2\pi m \sin(n\phi + \frac{\pi}{4})\right)\right]\right\}.
\end{aligned} \tag{3.9}$$

Both Equations 3.8 and 3.9 simplify to their non-dispersive counterparts, Equations 3.3 and 3.7, if either the dispersion parameter D, or fiber length L, are set to zero and Fourier representations matched. Further analysis is generally difficult due to the mathematical complexity of Equations 3.8 and 3.9. A better understanding can be gained however, through the graphical representation of the magnitude and phase response of the complex Fourier coefficient of the harmonic of interest.

Figure 3.5, shows the 5^{th} harmonic magnitude and phase response over dispersive fiber length L, and modulation index m, for both ODSB and OSSB links with a fundamental subcarrier frequency f_c, of 6GHz. The chromatic dispersion induced subcarrier fading characteristic of intensity modulated, direct detection (IMDD) links is clearly visible in Figure 3.5(a). As indicated by Equation 3.8, the phase response is flat over modulation index, m. OSSB-IM is shown in Figure 3.5(b), to effectively mitigate dispersion induced fading. Unlike ODSB modulation, OSSB is shown to have a non-flat phase response over modulation index.

It is interesting to note that the effects of chromatic dispersion lead to the generation of even harmonics in the detector spectrum, of both OSSB-IMDD and ODSB-IMDD links, where otherwise there would be none. The efficiency at which these even harmonics are generated is dependent on the link configuration, subcarrier frequency and accumulated dispersion and can under certain conditions, rival that of odd harmonic generation. When considering harmonics in the design of a harmonically upconverting link, the characteristics of both even and odd harmonics should be examined to ensure the desired efficiency and dynamic range.

Another point of interest is the resistance of harmonically generated subcarriers to dispersion induced subcarrier fading. For example, Figure 3.6 compares signal power

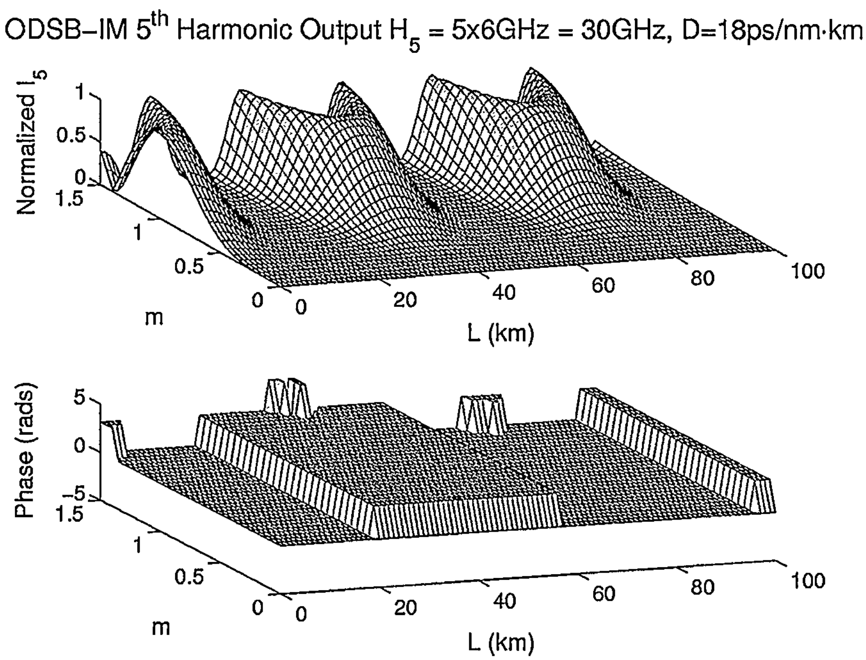

(a) ODSB-IMDD 5^{th} harmonic response

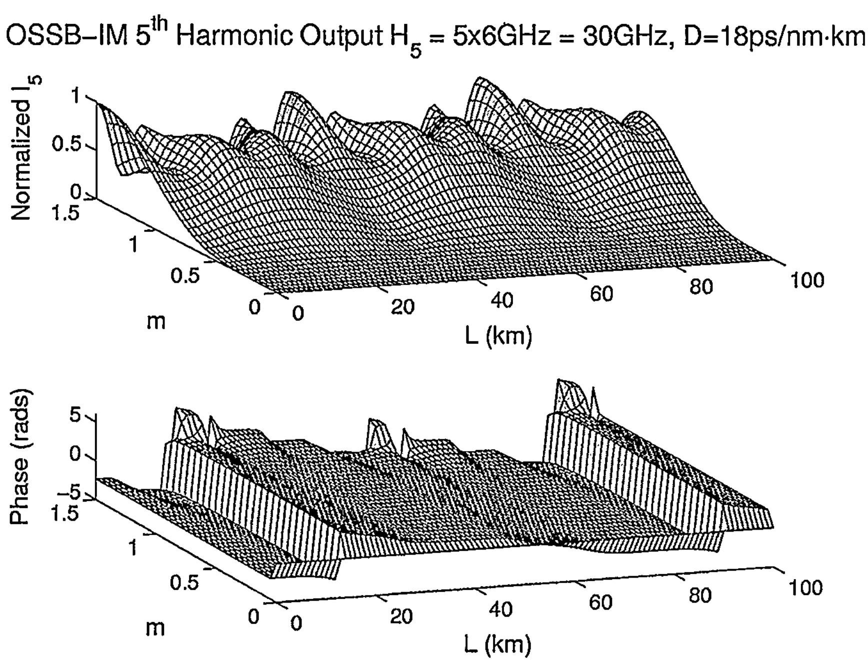

(b) OSSB-IM 5^{th} harmonic response

Figure 3.5: ODSB/OSSB-IMDD link 5^{th} harmonic magnitude and phase responses

over dispersive fiber length (D = 18ps/nm·km) for 17.35GHz ODSB-IM and OSSB-IM subcarriers generated through a 5^{th} order harmonic upconversion (m = 1.0), as well as an 17.35GHz ODSB-IM subcarrier obtained through a conventional linear upconversion (m = 0.2). Clearly OSSB-IM still offers significant fading mitigation in a harmonic upconversion scenario. The residual ripple in power over fiber length is a result of the interaction of higher order harmonics at the photodetector.

Comparing the ODSB-IM subcarriers, it is apparent that harmonic upconversion provides dispersion compensation; the harmonically unconverted subcarrier nulls are more widely spaced than those of the linearly unconverted subcarrier. Harmonic upconversion can therefore be used as a means of extending useable fiber lengths for ODSB-IMDD links, even when the desired subcarrier frequency is within range of feasible RF components.

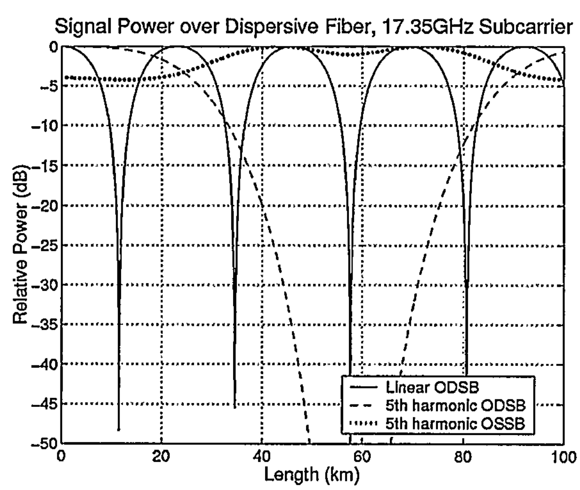

Figure 3.6: Detected 17.35GHz subcarrier power over dispersive fiber length

3.4 Harmonic Upconversion Distortion

The goal of upconversion in general is to translate an information bearing signal to a higher frequency without incurring distortion. In a harmonically upconverting RoF link however, severe distortion results from the harmonic upconversion process itself, chromatic dispersion introduced by the fiber, and square-law detection. These distortions, and their interactions, render most information bearing signals useless. To achieve the goal of distortionless harmonic upconversion, a distortion mitigation scheme must be found.

Consider again the response of a nonlinear system to an unmodulated carrier, $v(t) = Ae^{j2\pi f_c t}$, as initially illustrated in Figure 3.1. Since $v(t)$ is periodic in nature, the output will also be periodic and therefore can be represented by the complex exponential Fourier series,

$$r(t) = \sum_{n=-\infty}^{\infty} a_n(A)e^{j2\pi n f_c t}, \tag{3.10}$$

where the harmonic coefficients, a_n, are determined by the system characteristics.

Now consider a modulated carrier input, $A(t)e^{j(2\pi f_c t+\phi(t))}$, with a time varying amplitude information process $A(t)$, and a time varying phase information process $\phi(t)$. If the information processes are sufficiently narrowband with respect to the carrier frequency, a slowly varying envelope approximation can be made. The input signal is then considered as periodic and the nonlinear system can be modeled in the same manner as the unmodulated carrier case,

$$\begin{aligned} r(t) &= \sum_{n=-\infty}^{\infty} a_n\left(A(t)\right) e^{jn(2\pi f_c t+\phi(t))} \\ &= \sum_{n=-\infty}^{\infty} a_n\left(A(t)\right) e^{j(2\pi n f_c t+n\phi(t))}. \end{aligned} \tag{3.11}$$

In considering Equation 3.11 from the perspective of harmonic upconversion, there are two distortions immediately apparent. The phase information process of the n^{th} harmonic is multiplied by the harmonic number n, and the amplitude has been modified by some process $a_n()$, that is dependent on the nonlinearity.

Predistortion of the information processes can mitigate these distortions, permitting distortionless harmonic upconversion[16].

3.4.1 Phase Compression Predistortion

Equation 3.11 shows that in general, the phase of the n^{th} harmonic produced by a nonlinear system is multiplied by the harmonic number n. The previous harmonic expansions in Equations 3.3, 3.4, 3.6, 3.7, 3.8, and 3.9 all show agreement with this property.

This distortion can be easily mitigated by compressing the phase of the input signal by a factor of the harmonic number used in the harmonic upconversion. This operation is dubbed simple phase compression. The predistorted phase then expands in the harmonic upconversion process, restoring the original signal phase. Figure 3.7 illustrates the predistortion and recovery of a QPSK constellation for a n^{th} order harmonic upconversion.

There are certain modulation formats that do not require phase compression predistortion. If the constellation point in a constellation maps uniquely after phase expansion, no predistortion is necessary; only a remapping of the symbol bit representation is required. One such signal is QPSK. However, signal transition paths will be severely distorted resulting in spectral spreading. For this reason, phase compression predistortion must always be employed in harmonic upconversion.

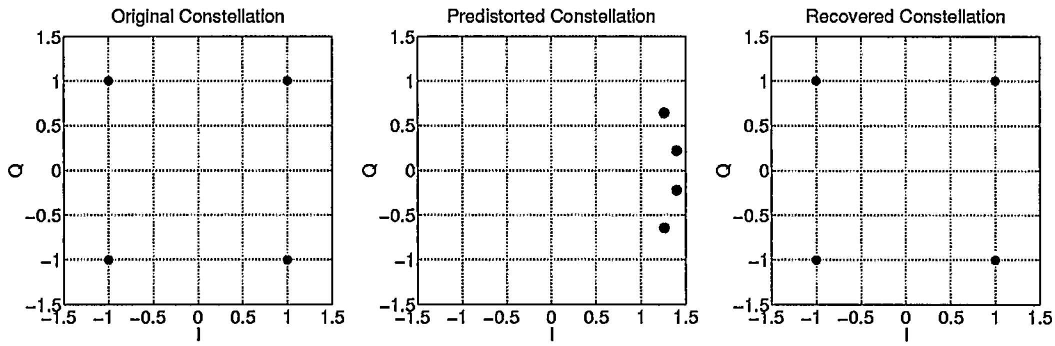

(a) Original QPSK constellation (b) Predistorted constellation for 5^{th} harmonic (c) Recovered 5^{th} harmonic constellation

Figure 3.7: 5^{th} harmonic predistorted and recovered QPSK constellations

Phase compression followed by harmonic expansion is trivial mathematically. Actual implementation however, presents unexpected complications, especially for multicarrier systems.

System Bandwidth Effects

The available spectral bandwidth of a communications system directly affects how a signal transitions between points in a signal constellation. In large bandwidth systems, sufficient high frequency components exist to create rapid signal changes leading to sharper, near ideal, constellations with straight transitions and minimal overshoot. Limited bandwidth systems on the other hand, cannot support high frequency components. Constellation transitions in these systems are slower, less direct, and exhibit overshoot or ringing effects. A signal constellation with distorted transitions can lead to an increased BER (Bit Error Rate) in noisy environments. In practical communication systems, perfect transitions are infeasible as spectral bandwidth is prohibitively expensive. Signals are therefore carefully bandlimited by specially designed filters. As these filters control the information pulse shape, they also control constellation transitions in such a manner so as to optimize performance parameters, such as inter-symbol interference (ISI) and jitter sensitivity. The raised cosine filter for example, creates pulses that minimize ISI at symbol sample points.

The limited bandwidth of practical communication systems has implications for phase compression predistortion that are not generally obvious. The following discussion uses a Matlab based simulation that models the baseband equivalent of the harmonic upconversion phase process to study the effects of successive phase compression and expansion on a phase modulated signal under various bandwidth limitations. Since both the simulation and real world systems must employ discrete time processing, the simulation results depict those of real systems.

The simulator block diagram is shown in Figure 3.8. A pseudo random binary sequence (PRBS) is used to create in-phase (I) and quadrature-phase (Q) QPSK signal components. QPSK was chosen as it contains only phase information. The I and Q components are pulse shaped (low pass filtered) before being phase predistorted (phase compressed) for the n^{th} harmonic. At this point, an adjustable filter is used to model the finite bandwidth of a practical system. To model the harmonic phase expansion property of a nonlinearity, the signal phase is simply multiplied by the desired harmonic number. Finally, a filter with a cut-off frequency tailored to signal bandwidth is applied to model the final stage transmitter filter of the communication system. A high sampling rate of 100 samples/symbol is used to ensure sampling of signal transitions.

Reconciling the simulator block diagram with a RoF system, the QPSK modulator, pulse shaping filter and system bandwidth filter collectively represent the

MZM electrical drive equipment. The phase expansion block represents the MZM nonlinearity. To model the enormous bandwidth of optical fiber, no system bandwidth filter has been applied after the phase expansion block, as might otherwise be expected. The final stage filter block then represents the harmonic selection filter and/or the final filter before the basestation antenna.

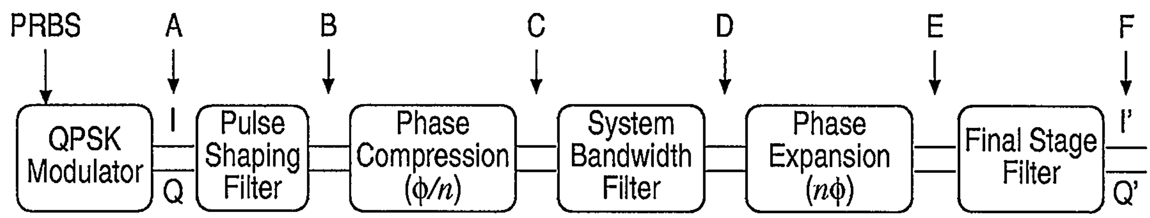

Figure 3.8: Harmonic upconversion phase process simulator block diagram

Phase Compression in a High Bandwidth System

It is instructive to first consider an ideal, high bandwidth, harmonically upconverting system with no pulse shaping. Figure 3.9 shows a quadrature phase shift keyed (QPSK) signal constellation and magnitude spectrum without bandlimiting pulse shaping (Point B), after phase compression predistortion for the 5^{th} harmonic (Point C), and after phase expansion (Point E).

In examining Figure 3.9, several observations can be made. Consistent with a high bandwidth system, transitions are shown to be extremely fast and beyond the sampling ability of the simulation, as indicated by the lack of transition sample points. Comparison of Figures 3.9(a) and 3.9(c) demonstrates that successive phase compression and expansion has no effect on the frequency spectrum, and incurs no distortion in the signal constellation. Phase compression however, does shift signal

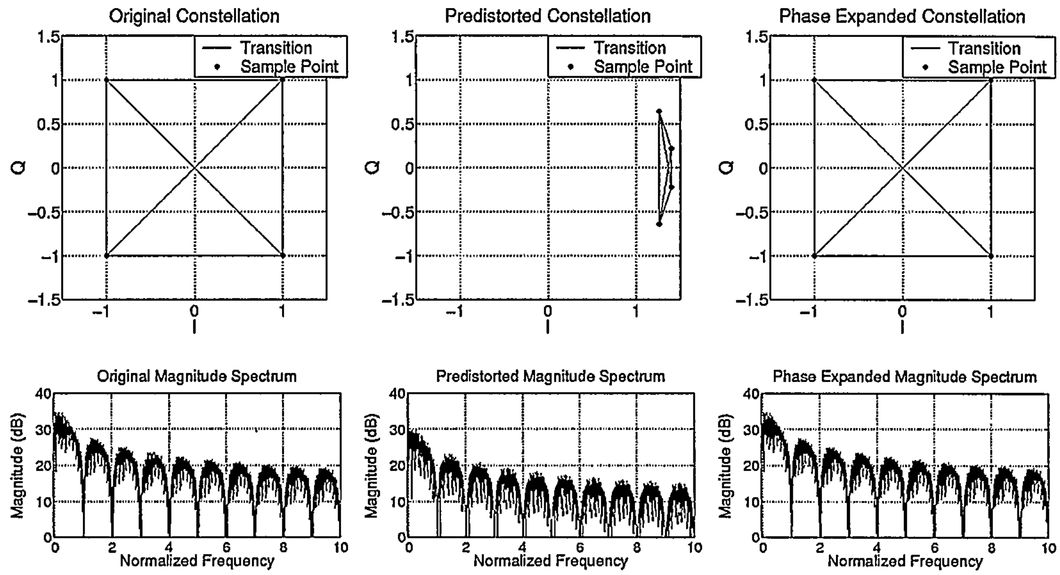

(a) Point A (b) Point C (c) Point E

Figure 3.9: Signal phase compression and expansion – No pulse shaping, high bandwidth system

power to a DC component, as seen in Figure 3.9(b). This is attributed to the non-zero average in the phase compressed constellation I signal component. Phase expansion completely reverses this effect.

Phase Compression in a Limited Bandwidth System

Consider now the same system, but with a bandwidth limitation of $5\times$ the symbol rate (implemented in simulation with a "brick wall" filter), and no pulse shaping. Figure 3.10 shows the signal constellation and magnitude spectrum at various points in the system.

The decreased system bandwidth causes the signal transitions to slow such that sample points begin to appear along the transition paths. Upon phase expansion, these transitions "unwrap", giving the circular constellation shown in Figure 3.10(b) at Point E, and not the original constellation. These circular transitions appear as a rapid ringing originating at the start of symbol transitions, as easily seen in the signal eyediagrams shown Figure 3.11(a), and are associated with the appearance of increased high frequency components in the signal spectrum after phase expansion. In the higher bandwidth system depicted in Figure 3.9, the circular transitions still exist, but occur at speeds well beyond the system sampling capability and so are not detected. Although error free at the symbol sample points, the phase expanded circular constellation can lead to an increased BER in a noisy environment. Tight filtering is required to remove the high frequency components and the associated ringing, as shown in Figures 3.10(c) and 3.11(b). The resulting signal is significantly improved, but still exhibits an asymmetry stemming from the transitions between points (-1,1) to (-1,-1). These distorted transitions can lead to increased error rates.

Phase Compression and Pulse Shaping in a Bandlimited System

The distortion in the phase expanded constellation shown in Figure 3.10(b), stems from the transition paths formed in the phase compressed signal. If these transitions were controlled such that upon phase expansion, the transition paths fall along a desired route between points, the distortion should be mitigated. This can be easily accomplished through pulse shaping of the original signal before phase compression. Pulse shaping also has the added benefit of bandlimiting the signal as would be required in any practical radio communication system. In a multicarrier system, pulse shaping of each individual subcarrier is especially necessary to limit spectral overlap.

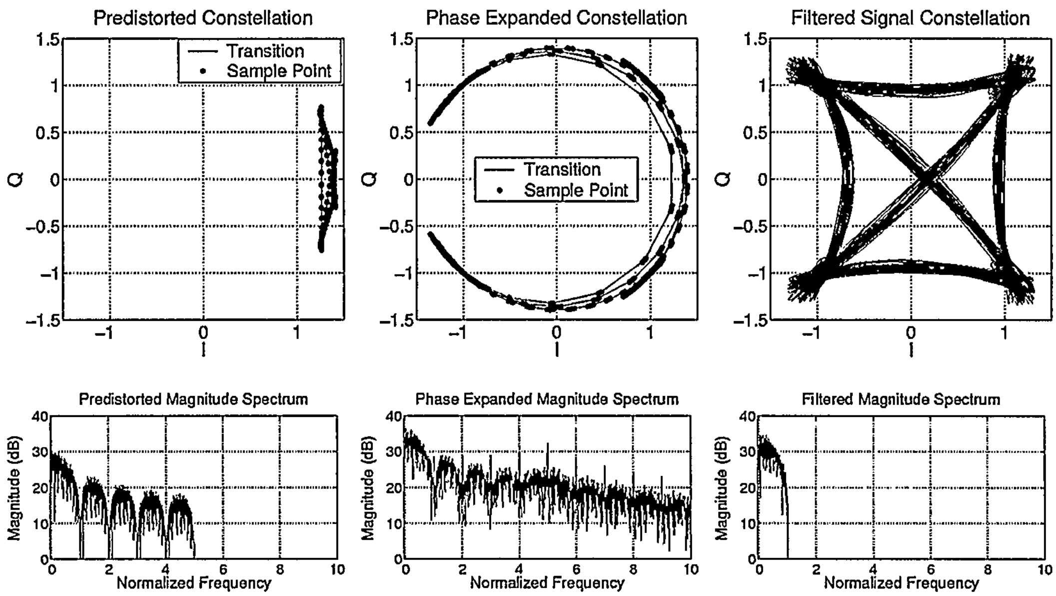

(a) Point D (b) Point E (c) Point F

Figure 3.10: Signal phase compression and expansion – No pulse shaping, 5×symbol rate bandwidth system

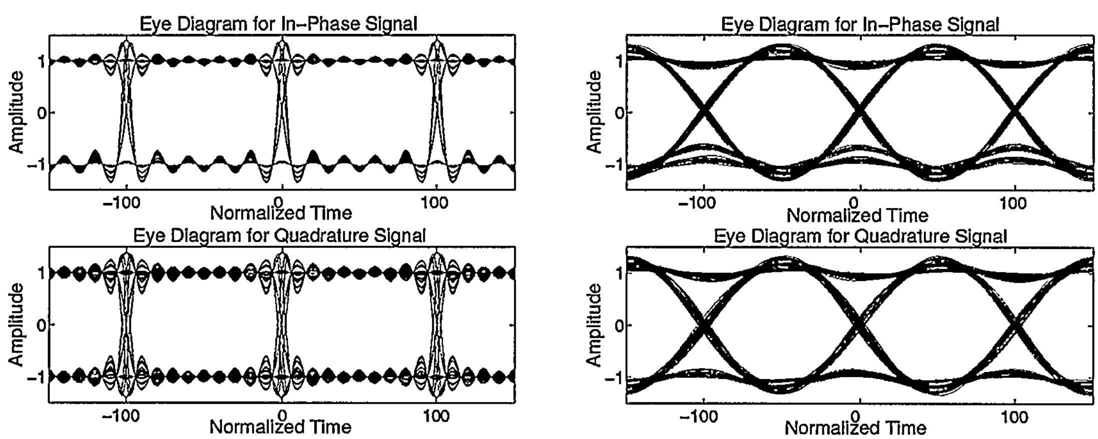

(a) Phase expanded signal – Point E (b) Filtered phase expanded signal – Point F

Figure 3.11: Phase expanded and filtered signal eyediagrams - 5×symbol rate bandwidth system

Figure 3.12 shows the evolution of a raised cosine pulse shaped signal through a harmonic upconversion system bandlimited at 5×symbol rate. The signal spectrum after pulse shaping shown in Figure 3.12(a), demonstrates the low pass characteristic of the raised cosine pulse shape. After bandlimited phase compression (Point D), the low pass characteristic of the raised cosine pulse is destroyed, and the signal spectrum spreads to the limits of the system bandwidth (5×symbol rate) as shown in Figure 3.12(c). When the predistorted signal undergoes phase expansion, the transition paths expand resulting in the constellation shown in Figure 3.12(d). While the phase expanded constellation resembles the original, there is significant distortion in the form of large circular transition paths. The low pass characteristic of the signal has also been impaired, with significantly frequency content beyond the signal information bandwidth, indicating spectral spreading.

Despite the distorted transitions, the constellation is error free at the symbol sample point. The distorted transition paths need to be corrected however, as they can lead to a higher link BER characteristic in nonideal conditions. Also of concern, is the degraded lowpass characteristic of the upconverted signal; as radio systems must strictly control radio emissions, any spectral spreading is unacceptable, and further filtering must be performed.

Figures 3.12(e) and 3.13(b) show that removal of all signal components higher than the information bandwidth through further filtering produces a significantly improved constellation that is nearly identical to the original, with the exception of the transitions between the two left most points, (-1,1) and (-1,-1). These transitions remain slightly distorted, and may yet affect the BER.

In a multicarrier system, where a block of carriers are harmonically upconverted,

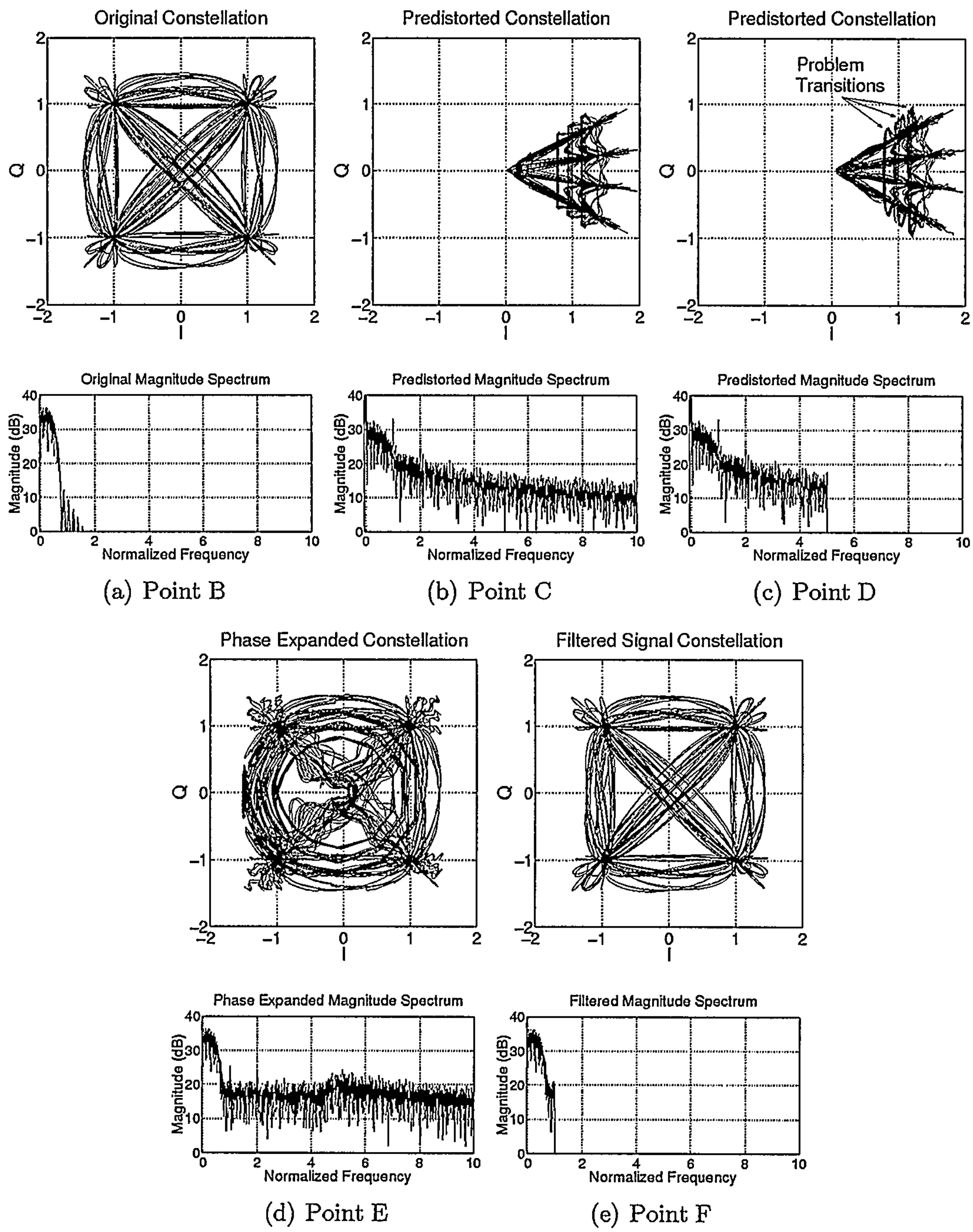

Figure 3.12: Signal phase compression and expansion – Raised cosine pulse shaping, 5×symbol rate bandwidth system

phase expansion and the associated spectral spreading, would cause individual carriers to spread energy into adjacent channels, inflicting distortion that cannot be corrected through filtering. To prevent this distortion, the spreading mechanism itself must be mitigated to produce a distortion free constellation after phase expansion.

The increased frequency content outside the signal bandwidth after phase expansion is associated with the distorted signal transitions. This is confirmed by the disappearance of distorted transitions after filtering. Preventing the formation of these inefficient transitions will therefore reduce the severity of spectral spreading, and alleviate filtering requirements.

Transition distortion is a direct result of limited bandwidth. For instance, comparing the non-bandlimited and bandlimited phase compressed constellations shown in Figures 3.12(b) and 3.12(c) respectively, demonstrates that bandlimiting rounds sharp corners. This causes distortion when the bandlimited predistorted constellation fails to reach the critical center point (0,0), creating upon phase expansion, diagonal transitions that deviate in a circular manner around the origin, as shown in Figure 3.12(d).

The larger circular transitions are also a result of bandwidth limitation. The problem transitions indicated in Figure 3.12(c) arise from the discontinuity created when the transitions between points (-1,1) and (-1,-1) are split along the I axis in phase compression. In a limited bandwidth system, these transitions cannot occur instantaneously, and so upon phase expansion, create large circular transitions that manifest as higher amplitude ringing visible in the phase expanded eyediagram in Figure 3.13(a). These transitions are responsible for the presence of much of the higher frequency components in the phase expanded signal.

In very high bandwidth systems, the large circular transitions are still present, but are extremely rapid and so occur over a very short time relative to the signal period. The associated high frequency signal components are consequently very low in power, and the impact of spectral spreading will be minimal. Transition distortion can therefore be avoided by allowing sufficient bandwidth in the predistortion circuit.

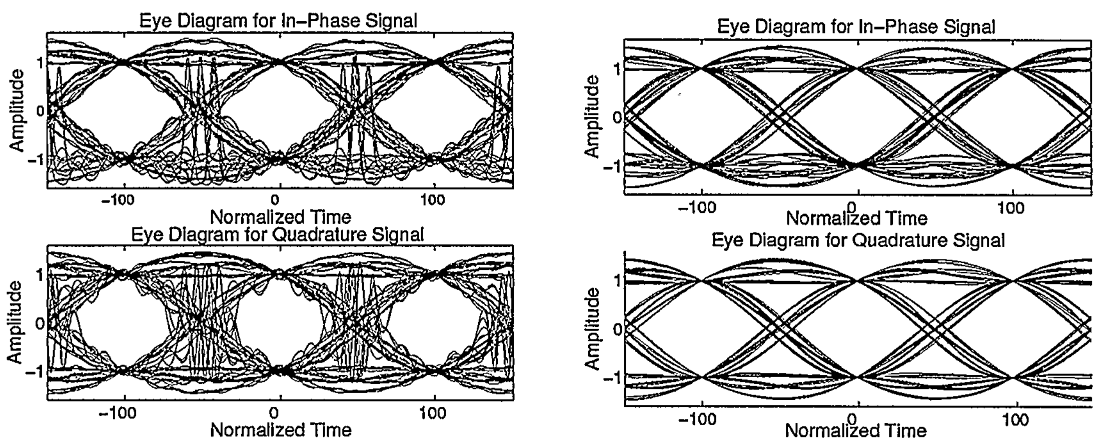

(a) Phase expanded signal – Point E (b) Filtered phase expanded signal – Point F

Figure 3.13: Phase expanded and filtered signal eyediagrams - Raised cosine pulse shaped, 5×symbol rate bandwidth system

If sufficiently high bandwidth cannot be provided in a multicarrier system, the effects of limited bandwidth on signal transitions can be significantly reduced through the application of differential phase compression, rather than simple phase compression.

Differential Phase Compression

Differential phase predistortion compresses the changes in phase between sample points, rather than the absolute sample point phase as in simple phase compression[24]. This creates a circular constellation with points that map to those of the original constellation upon phase expansion, as demonstrated in Figure 3.14. The circular nature of the differential compressed constellation will reduce spectral spreading, and so distortion, in the phase expanded constellation as it eliminates the discontinuities seen with simple phase compression, and minimizes transition path lengths.

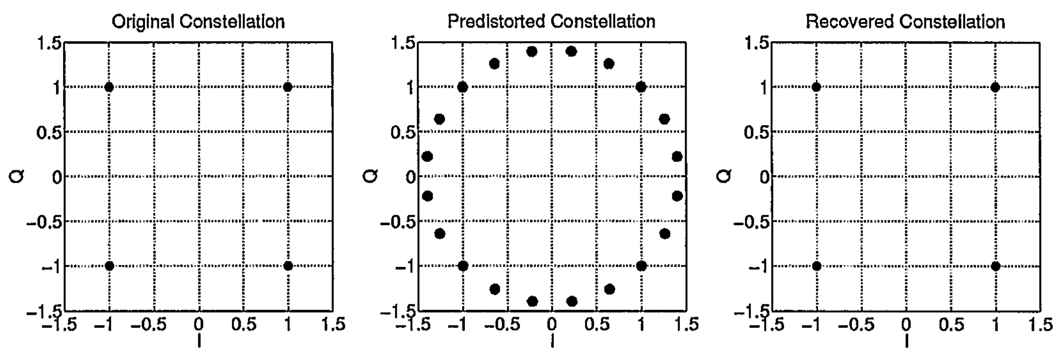

(a) QPSK constellation

(b) Differentially predistorted constellation for 5^{th} harmonic

(c) Recovered 5^{th} harmonic constellation

Figure 3.14: 5^{th} harmonic predistorted and recovered QPSK constellations

Figure 3.15 shows the signal evolution of a differentially phase compressed raised cosine pulse shaped signal through a system bandlimited at $5\times$ the information rate. The phase compressed signal constellation shown in Figure 3.15(b) no longer exhibits discontinuities and the associated signal spectrum indicates less severe spectral spreading. The system bandwidth limitation now has less of a detrimental effect, and phase expansion restores the spectrum more accurately as seen in Figure 3.15(c).

Differential phase compression is thus more resistant to the effect of limited bandwidth.

Phase expansion now produces a constellation without large circular transitions, that resembles the original constellation more closely. Although to a lesser extent, the system bandwidth limitation still produces residual high frequency components and causes small deviations around the center point. Further filtering completely removes all distortion, producing a distortion free constellation identical to the original and achieves distortionless upconversion.

Differential phase compression produces a phase expanded constellation that is nearly distortion free, with the signal low pass characteristic mostly intact. Additional filtering is now not as critical. A multicarrier system therefore would employ differential phase compression to limit spectral overlap of the subcarriers.

The signal produced at the output of the phase expansion with differential phase compression is nearly distortion free. The residual distortion stems from π-phase shifts in the signal that create diagonal transition paths that cross through the origin. These transitions are sensitive to bandwidth limitations when phase compressed. If required, loose filtering at the transmitter can easily correct the residual distortion. However, if in a bandlimited system additional filtering is not desired or possible at the receiver (such as in a multicarrier scenario), a distortion free constellation can be produced directly at the output of the phase expander (nonlinearity), by applying differential phase compression and eliminating π transitions through the use of alternate radio modulation schemes such as offset quadrature phase shift keying (OQPSK).

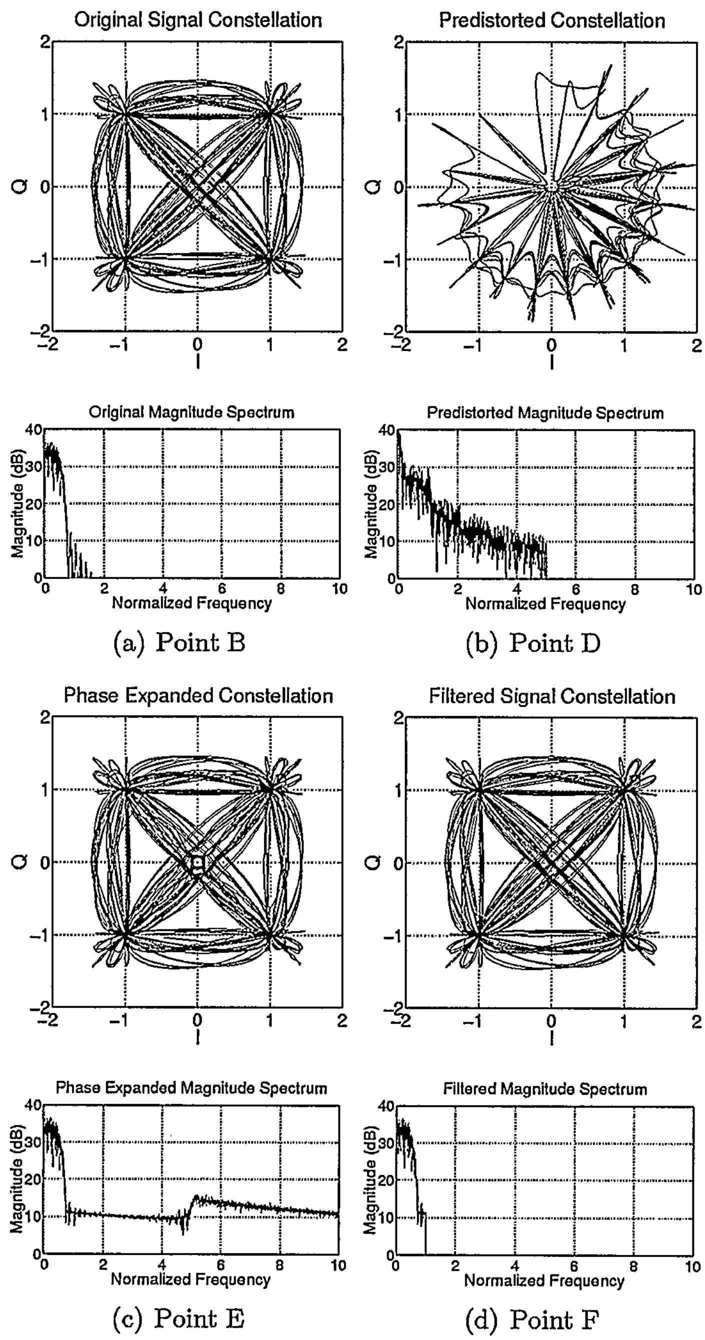

(a) Point B

(b) Point D

(c) Point E

(d) Point F

Figure 3.15: Differential phase compression and expansion – Raised cosine pulse shaping, 5×symbol rate bandwidth system

Phase Compression and Radio-on-Fiber

It is clear that the available bandwidth in the predistortion circuit significantly impacts the constellation quality of a harmonically upconverted signal.

A typical RoF system configuration employing narrowband filters in the MZM drive circuity, would lead to severe distortion in a harmonically upconverted signal. Care must therefore be taken when selecting components, specifically filters, for the MZM drive circuitry to avoid overly limiting bandwidth and incurring bandwidth related distortion.

Irrespective of what phase predistortion scheme is employed, in a single carrier system, distortion in the recovered harmonic signal can be avoided by simply maximizing excess bandwidth in the MZM drive circuitry and applying a tight harmonic selection filter.

The trade-off of wide bandwidth filters in the MZM drive circuitry is possibly increased out of band energy. This can be a concern for harmonically upconverting RoF links as the MZM must be driven with a clean spectrum to avoid intermodulation products and ensure distortionless upconversion. Fortunately, when operating with millimeter-wave and micro-wave radio carriers, harmonics originating from amplifier or mixer action are widely spaced, allowing wider bandwidth filters. If narrower bandwidth filters must be used, differential phase compression should be employed to reduce the impact of decreased bandwidth.

Fortunately, RoF systems typically transport narrowband radio signals, making the bandwidth requirements easily achievable. Consider for example a 12.5MS/s baseband differentially phase predistorted signal. The filters used in the MZM driving circuitry should be roughly at least 5×25MHz $= 125$MHz to ensure distortion free upconversion; a requirement easily met or exceeded. In deployed RoF systems, the harmonic selection filter would undoubtably be tailored to the signal bandwidth to limit out-of-band emissions in the radiated radio signal. Any residual bandwidth related distortion would then be completely removed. Therefore, if adequate bandwidth is allocated in the predistortion circuit, bandwidth effects on phase compression need not be further considered in practical RoF system design.

In multicarrier RoF systems however, the harmonic selection filter cannot be relied upon to eliminate residual distortion. To minimize distortion in the subcarriers, differential phase compression must employed and excess bandwidth in the predistortion circuit maximized.

3.4.2 Amplitude Predistortion

In Equation 3.10, the magnitude of the n^{th} harmonic is dependent on the input signal magnitude, A. This dependence is described by the harmonic response function, a_n. In RoF systems, this function is typically nonlinear, and is dependent on the link configuration, the harmonic upconversion process, the fiber chromatic dispersion transfer function, and the square-law detection process.

The harmonic response function for a specific harmonic and link configuration can be obtained from Equations 3.3, 3.4, 3.6, 3.7, 3.8, and 3.9 by extracting the coefficient of the desired harmonic term. Table 3.1 lists in exponential Fourier form (i.e. $a_n(m)e^{j2\pi n f_c t}$), the harmonic response functions, $a_n(m)$, for the various link configurations considered in this study.

Harmonic upconversion of constant envelope signals, such as phase shift keyed (PSK) modulated signals, is trivial. The input signal magnitude is treated as a

Link Configuration	$\mathbf{n^{th}}$ harmonic response function, $\mathbf{a_n(m)}$ Fourier exponential form: $\mathbf{a_n(m)e^{j2\pi n f_c t}}$
ODSB QB	$\frac{k}{2}(-1)^{\frac{n+3}{2}} J_n(2\pi m)$, n odd
ODSB QB-π	$-\frac{k}{2}(-1)^{\frac{n+3}{2}} J_n(2\pi m)$, n odd
ODSB MATB	$\frac{k}{2}(-1)^{\frac{n}{2}} J_n(2\pi m)$, n even
ODSB MITB	$-\frac{k}{2}(-1)^{\frac{n}{2}} J_n(2\pi m)$, n even
OSSB	$\frac{k}{2}(-1)^{\frac{n+3}{2}} J_n(\sqrt{2}\pi m)e^{j\frac{n\pi}{2}}$, n odd
Dispersive ODSB	$\frac{k}{2} J_n\left[2\pi m\sin(n\phi)\right]$, n even
	$\frac{k}{2}(-1)^{\frac{n+3}{2}} J_n\left[2\pi m\cos(n\phi)\right]$, n odd
Dispersive OSSB	$\frac{k}{4}\left\{J_{-n}\left[2\pi m\sin(n\phi)\right] + j^n J_n\left[2\pi m\sin(n\phi)\right]\right.$
	$\left.+je^{\frac{-n\pi}{4}}\left[J_{-n}\left(2\pi m\sin(n\phi - \frac{\pi}{4})\right) - J_{-n}\left(2\pi m\sin(n\phi + \frac{\pi}{4})\right)\right]\right\}$

Table 3.1: Harmonic Response Functions

modulation index (i.e. $v_{in} = m\cos(2\pi f_c t)$), and set so as to maximize the desired harmonic power at the receiver output, thus maximizing efficiency and signal to noise ratio (SNR).

As a simple example, consider a non-dispersive RoF link employing a 5^{th} order harmonic upconversion and ODSB-IMDD. The system response,

$$a_5(m) \propto J_5(2\pi m), \tag{3.12}$$

is shown in Figure 3.16(a). In this system, a modulation index of ~ 1.0 would be selected to maximize signal power at the receiver.

Signals containing amplitude modulation, such as quadrature amplitude modulated (QAM) signals, are more difficult to upconvert harmonically. These signals are considered as having a time varying modulation index. The harmonic response of a RoF link is nonlinear over modulation index, and would introduce severe distortion. There are however, approximately linear regions. An amplitude modulated signal

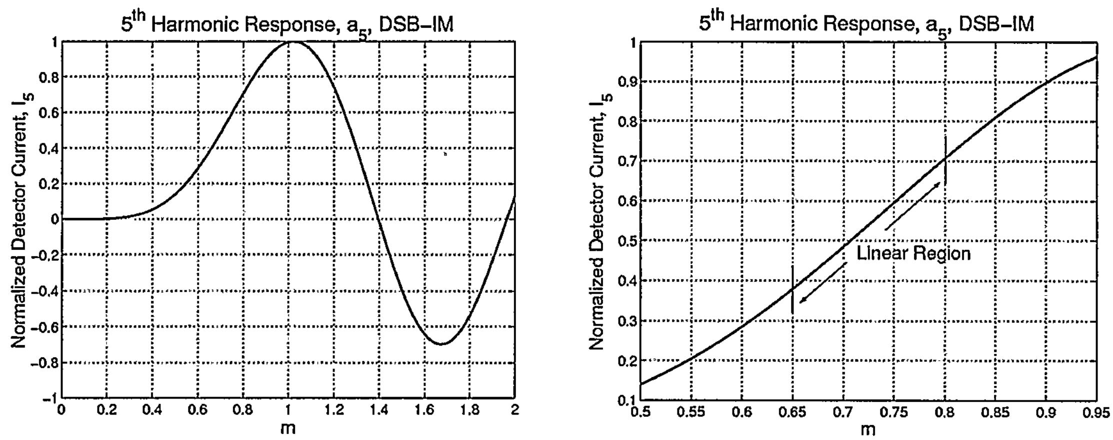

(a) $a_5(m)$ (b) $a_5(m)$, linear region

Figure 3.16: ODSB-IM 5th harmonic magnitude response

can be harmonically upconverted with minimal distortion if it is appropriately scaled and mapped into a nearly linear region of the harmonic response.

As an example, consider again the magnitude response shown in Figure 3.16(a). Although it is nonlinear over modulation index, it does contain a nearly linear region between $m = 0.65$ and $m = 0.8$, shown in detail in Figure 3.16(b). The signal magnitudes can be predistorted into the nearly linear region through the numerical map

$$m_{pred}(t) = m_{\text{lin,min}} + \frac{m_{\text{lin,max}} - m_{\text{lin,min}}}{\max[A(t)] - \min[A(t)]} \{A(t) - \min[A(t)]\} \quad (3.13)$$

$$= 0.65 + 0.225 \{A(t) - \min[A(t)]\}, \quad (3.14)$$

where m_{pred} is the predistorted amplitude (modulation index), $m_{\text{lin,min}}$ and $m_{\text{lin,max}}$ are the minimum and maximum modulation indexes of the linear region, and $A(t)$ is the input QAM signal magnitude (ranging between $\frac{1}{3}$ and 1 for 16QAM). Other monotonic sections, such as the region spanning modulation indexes 1.0 and 1.65, could also be used if a negative slope is permissible. The first monotonic region is usually the most attractive as operating at low modulation indexes reduces the drive equipment power requirements.

This form of amplitude scaling predistortion has the advantage of simplicity. However, because only the linear region of the link response is used, signal power and dynamic range are not maximized, resulting in sub-optimal efficiency and a degraded signal to noise ratio (SNR). Expanding the region of operation would increase efficiency, but at the cost of linearity, possibly altering the link error characteristics for distortion sensitive signals. Also, scaling the symbol sample points to a linear region does not preserve all symbol transitions (such as those crossing through zero). This causes spectral spreading. In single carrier scenarios, additional filtering of the upconverted signal can completely mitigate this distortion. However, in multicarrier scenarios the required filtering may not be possible, and scaling predistortion will result in uncorrectable distortion.

To overcome these issues, the harmonic response of an entire monotonic section can be linearized through precise predistortion. A signal to be harmonically upconverted would first be passed through a predistortion block as shown in Figure 3.17(a), before being applied to the RoF link. To produce an overall linear link response, the predistortion block response must be the inverse of the harmonic response of the RoF link. Figure 3.17(b) illustrates this technique, showing the response of the predistortion block, RoF link and the combined, overall response. This type of predistortion allows for maximum dynamic range and output signal power while minimizing distortion. A performance comparison of the amplitude scaling and precise linearization predistortion schemes will be performed through simulation in Chapter 4.

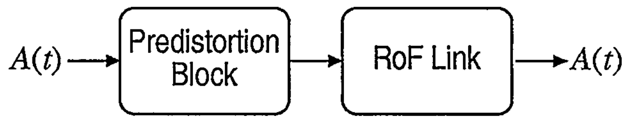

(a) Predistortion system

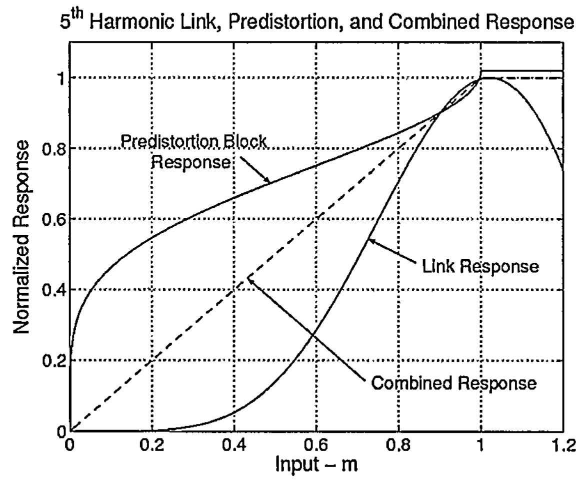

(b) 5^{th} harmonic link, predistortion block and combined response

Figure 3.17: Precise linearizing amplitude predistortion

Precise amplitude predistortion requires the predistorted signal to be precisely aligned with the link characteristic. Any misalignment would immediately cause distortion. In practice, alignment can be difficult leading to problematic implementation. Scaling predistortion, on the other hand is less sensitive to alignment.

The discussed amplitude scaling and precise linearizing predistortion schemes can be applied to the harmonic responses of all the link configurations listed in Table 3.1. The dispersive OSSB-IMDD link harmonic response however, has a modulation index dependent phase characteristic that will cause additional distortion.

Consider the theoretical 30GHz 5^{th} harmonic response of a 50.5km OSSB-IMDD

RoF link, shown in Figure 3.18 (a slice of the surface in Figure 3.5(b) for $L =$ 50.5km). The magnitude response is again nonlinear in nature and can be linearized through either scaling or precise linearizing predistortion. The phase response is non-flat, rolling off with increasing modulation index. This distortion results in a twisting of the output signal constellation. In such situations, additional precise phase predistortion tailored to the harmonic characteristic is necessary to flatten the phase response.

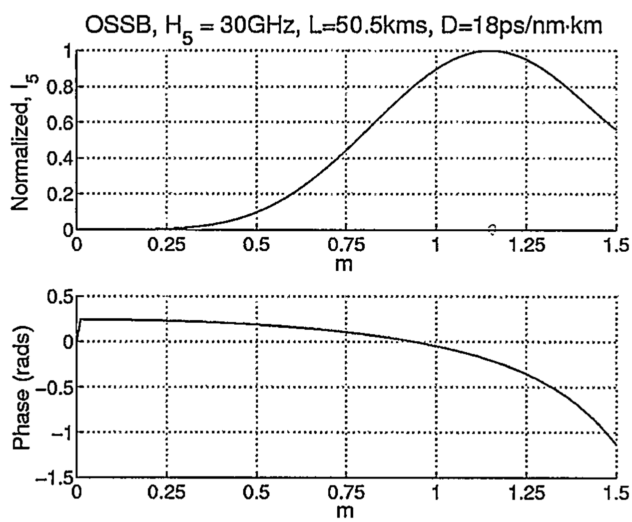

Figure 3.18: OSSB-IMDD 5^{th} harmonic magnitude and phase response

Since a precise signal alignment is required for the phase flattening predistortion to be effective, precise amplitude linearization predistortion can be performed simultaneously with no additional difficulty.

The harmonic response of dispersive RoF links depends heavily on the dispersion parameter D, fiber length L, harmonic number n and the fundamental subcarrier frequency f_c. Re-examining Figure 3.5(b), it can be seen that with OSSB-IM, every fiber length has a suitable magnitude response that can be predistorted to achieve distortionless harmonic upconversion. However, the magnitude and phase harmonic responses vary over fiber length. Consequently, every link must have a customized predistortion scheme to achieve maximum efficiency and minimal distortion.

3.5 Fiber Nonlinearity

There has been extensive research investigating the effects of fiber nonlinearity on pulse propagation in optical communications systems. As yet however, very little research has been directed towards the effects of fiber nonlinearity in analog optical systems, such as RoF.

This section serves as a preliminary investigation into the combined effects of chromatic dispersion and fiber nonlinearity on RoF link behavior and harmonic generation.

3.5.1 Self-Phase Modulation

For most applications, the refractive index of silica fiber is assumed to be independent of optical power. In actuality, at higher optical intensities silica glass exhibits a nonlinear response know as Kerr nonlinearity. This response can be characterized by the dependence of fiber refractive index n, on optical intensity as described by[30]

$$n(P_o) = n_o + n_2 \left(\frac{P_o}{A_{eff}} \right), \tag{3.15}$$

where n_o is the linear refractive index, n_2 is the nonlinear index coefficient, P_o is optical power, and A_{eff} is the effective optical area. The nonlinear index coefficient for silica glass n_2, is approximately $2.6 \times 10^{-20}\text{m}^2/\text{W}$. Even with the small effective mode area of standard single mode fiber ($\sim 85\mu m^2$), an optical power of 1mW will yield a nonlinear contribution to refractive index of only 3×10^{-13}. Although this contribution is extremely small, the accumulated effect over long lengths of fiber can be significant. Also, depending on fiber core doping, the actual nonlinear index coefficient may be much higher.

The intensity dependence of refractive index leads to an intensity dependent wave propagation constant β, as in

$$\begin{aligned} \beta' &= k_o n(P_o) \\ \beta' &= k_o n_o + k_o n_2 \left(\frac{P_o}{A_{eff}}\right) \\ \beta' &= \beta + \gamma P_o, \end{aligned} \tag{3.16}$$

where $k_o = \frac{2\pi}{\lambda}$ is the wave number, and $\gamma = \frac{k_o n_2}{Aeff}$ is the nonlinearity coefficient. An optical wave traveling a distance L, in a lossless nonlinear fiber now incurs an excess phase shift due to nonlinearity of

$$\phi_{NL} = (\beta' - \beta)L = \gamma P_o L. \tag{3.17}$$

Equation 3.17 implies that variations in optical power will result in phase modulation. In effect, this phase modulation is self-induced, and hence this phenomenon is called self-phase modulation (SPM). In multiple optical channel systems, the nonlinear phase shift for a specific channel depends on the optical power of that individual channel and also the power of the others. This phenomenon is known as cross-phase modulation (XPM).

In systems where optical power launched into the fiber is sufficiently low and fiber length sufficiently short, the effects of SPM will be negligible and need not be considered. The nonlinear length L_{NL}, provides a scale for determining the significance of nonlinearity. It is defined as[31]

$$L_{NL} = \frac{1}{\gamma P_o}. \tag{3.18}$$

The effects of nonlinearity need not be considered when the fiber length $L \ll L_{NL}$. For example, a system using a fiber with $\gamma = 3\text{W}^{-1}\text{km}^{-1}$, and input optical power of $P_o = 1\text{mW}$, will have a nonlinear length of $L_{NL} = 333\text{km}$. The system fiber length should therefore not exceed 33km if the effects of fiber nonlinearity are to be avoided.

3.5.2 Analysis

Considering fiber loss, group velocity dispersion (GVD), and the nonlinear Kerr effect, the evolution of an optical signal propagating through single mode fiber is described by the nonlinear Schrödinger equation (NLS) [31]

$$\frac{\partial A}{\partial z} + \frac{\alpha}{2}A + j\frac{\beta_2}{2}\frac{\partial^2 A}{\partial t^2} - j\gamma \left|A\right|^2 A = 0, \tag{3.19}$$

where $A = \sqrt{\eta P_o}$ is the slowly varying envelope of the optical field as in $E(z,t) = A(z,t)e^{jw_o t}$ with η the intrinsic material impedance, and w_o the optical angular frequency; z is the propagation distance along the fiber; α is the fiber loss coefficient; t is time; $\beta_2 = \frac{-\lambda_o^2 D}{2\pi c}$ is the GVD parameter, with λ_o the optical carrier wavelength, D the dispersion parameter, and c the speed of light in a vacuum; and γ is the nonlinearity coefficient.

Although Equation 3.19 does not easily lend itself to analytical solutions, there has been some success investigating fiber response with small signal analysis[33, 34]. This approach however, cannot be applied in the study of harmonic behavior in RoF systems due to the inherently large signal nature of harmonic generation. Consequently, numerical methods are required.

There are many numerical methods suitable for solving the NLS equation, all having different degrees of accuracy and speed. In this study, the symmetrized split-step Fourier (SSSF) numerical method was selected as it is simple to implement and provides excellent accuracy[31]. The details of this method are described in Appendix A.

Fiber Nonlinearity and Chromatic Dispersion in Radio-on-Fiber Systems

To understand the effects of combined fiber nonlinearity and group velocity dispersion, the SSSF method was applied in simulation. These effects are heavily dependent on the characteristics of the optical fiber in use. For the purposes of simulation, the parameters of Corning SMF-28 standard single-mode optic fiber, listed in Table 3.2, will be used. The nonlinear coefficient n_2, was unavailable for this fiber, so a value based on that of similar fibers was used.

Corning SMF-28 Standard Single-Mode Optical Fiber	
Mode-field diameter, d	10.4μm @ 1550nm
Nonlinear coefficient, n_2	4.0×10^{-20}m^2/W
Dispersion parameter, D	16.2ps/nm·km @ 1550nm
Attenuation coefficient, α	0.22dB/km @ 1550nm

Table 3.2: Fiber Parameters

Dispersion Compensation

An optical signal propagating through a length of fiber will accumulate an SPM induced phase shift and a GVD induced phase shift. The combined effect of the two phase shifts normally gives rise to nonlinear distortion. However, in standard fibers operating in the anomalous region ($\lambda_o > 1300$nm) where the GVD parameter $\beta_2 < 0$, SPM and GVD counter each other, and dispersion compensation results[35].

For mm-wave and μm-wave optical systems operating at 1550nm, fiber nonlinearity mitigates dispersion related subcarrier fading. This is demonstrated through a simulation of a 17.35GHz subcarrier RoF link employing SMF-28 fiber. The detected signal power over fiber length is shown in Figure 3.19. In the case of ODSB modulation, the effects of SPM move the fades further down the fiber, increasing the usable length. OSSB however, is shown to have degraded performance, with increased ripple and the reappearance of fades at higher optical powers. This is a result of SPM upsetting the harmonic balance required to provide sideband cancellation, and re-enabling the fading mechanism. The loss of OSSB modulation is demonstrated in Figure 3.20. As optical power increases further, the characteristics of ODSB and OSSB approach, eventually becoming near equivalents. Similar results have been demonstrated of fiber bandwidth in [36].

Despite the impairment caused by SPM, OSSB can still be useful to mitigate dispersion induced fading if optical power is limited. For example, as shown in Figure 3.19, optical power up to 15.5dBm will still prevent fades deeper than 3dB.

In Section 3.3.2, it was shown that a harmonically upconverted subcarrier exhibits fading resistance when compared to a linearly upconverted subcarrier. OSSB was also shown to mitigate fading in subcarrier harmonics, although with increased ripple. In a system exhibiting SPM however, the fading characteristics of harmonic subcarriers increases in frequency and severity for both ODSB and OSSB modulation. Figure 3.21 illustrates with a 17.35GHz subcarrier harmonic propagating down

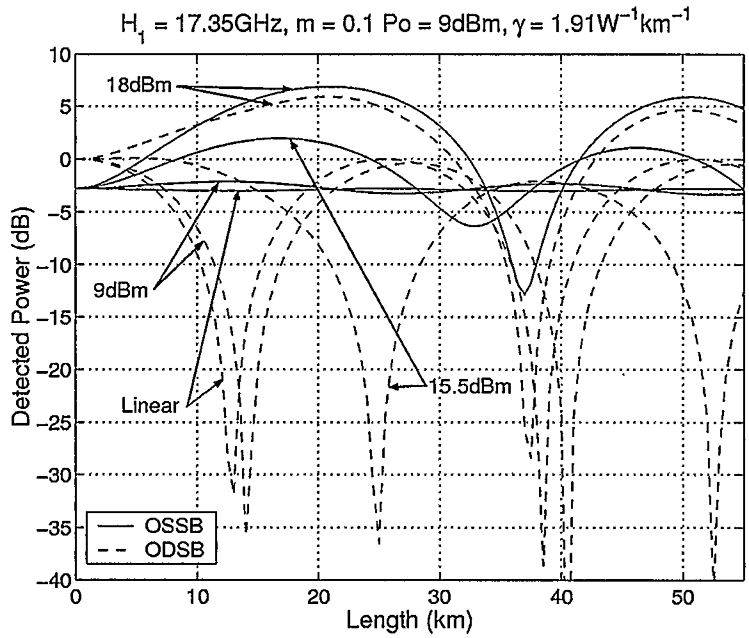

Figure 3.19: Detected 17.35GHz subcarrier power over nonlinear dispersive fiber length

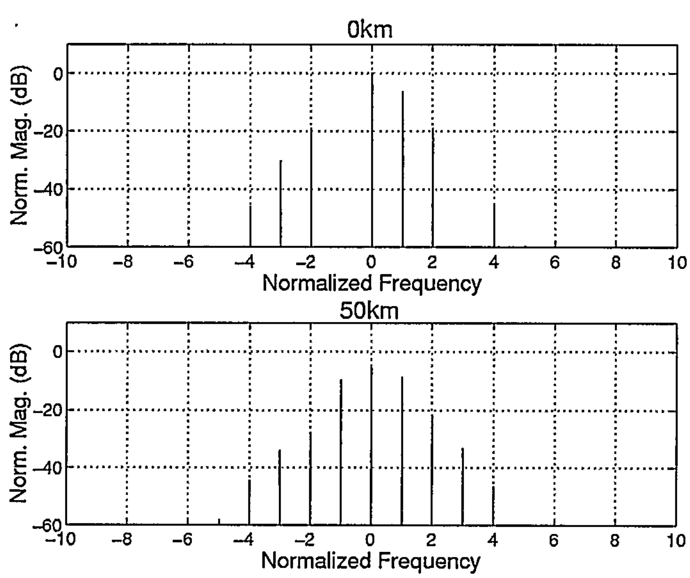

Figure 3.20: SSB optical spectrum @ 0km and 50km, $P_o = 18$dBm

a length of dispersive nonlinear fiber. Although OSSB is shown to exhibit significant fading at higher optical powers, fades never exceed -3dB for optical powers less than 16.5dBm. In this case, OSSB can still be applied to mitigate dispersion related fading in subcarrier harmonics, provided the optical power is appropriately limited.

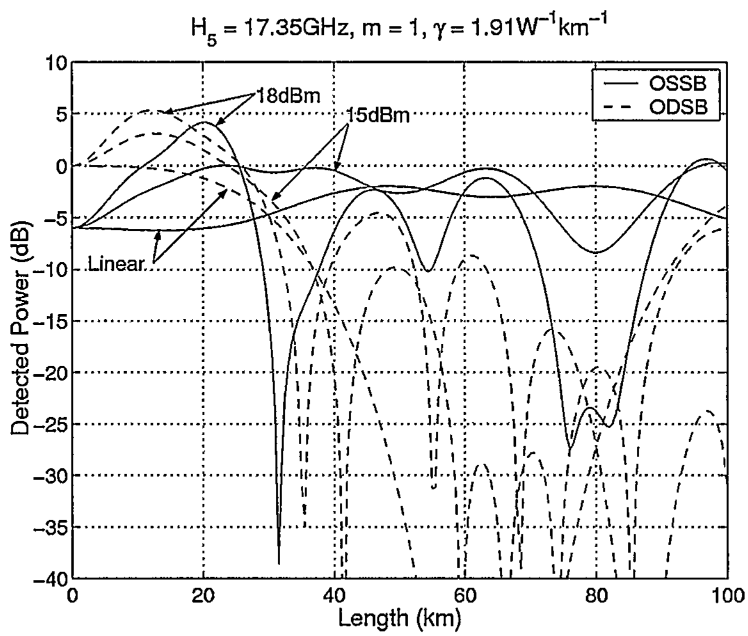

Figure 3.21: Detected 17.35 GHz 5$^{\text{th}}$ harmonic power over nonlinear dispersive fiber length

Harmonic Response

The harmonic response of a RoF system is considerably more complex when fiber nonlinearity is considered. In addition to modulation index m, subcarrier frequency f, harmonic number h, dispersion parameter D, and fiber length L, the harmonic response now also depends on input optical power P_o, nonlinearity parameter γ, and fiber attenuation α.

In an installed RoF system, the fiber parameters (D, γ, α, L) are all fixed and subcarrier frequency and the harmonic upconversion order are specified. Optical power P_o, still needs to be set. The effects of SPM need to be studied to determine whether an optimum optical power exists.

Consider again a harmonically upconverting RoF system employing 50km of SMF-28 standard fiber (see Table 3.2) and OSSB-IM. Figure 3.22 shows the 17.35GHz 5^{th} harmonic response over modulation index m, and optical input power P_o. Optical power clearly has significant impact on the harmonic response. At low optical powers, the harmonic response resembles that of a purely dispersive link. As input power increases the harmonic response steepens while shifting towards lower modulation indexes.

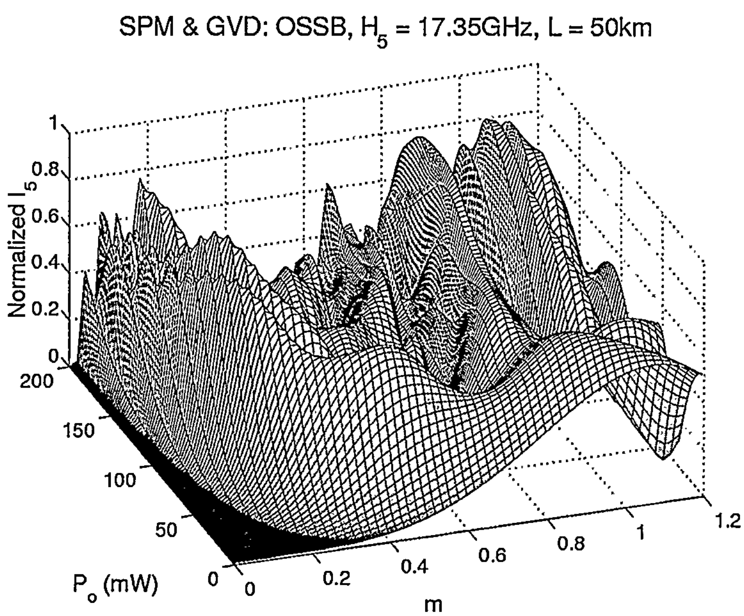

Figure 3.22: Detected OSSB 17.35GHz 5^{th} harmonic power. Loss and power normalized.

From the perspective of harmonic upconversion, the behavior depicted in Figure 3.22 is of great interest as SPM increases harmonic generation efficiency. For example, in this system an optical input power of 50mW (17dBm), yields the harmonic magnitude and phase response shown in Figure 3.23. Compared to the GVD only case (also shown in Figure 3.23), the effects of SPM have improved the magnitude characteristic significantly, allowing a higher harmonic power at a lower modulation index. In fact, the improvement constitutes an 11dB increase in link gain (assuming 50Ω system impedance, and $V_\pi = 4.5$V).

The magnitude and phase harmonic responses shown in Figure 3.23, should be amenable to harmonic upconversion with the predistortion techniques previously discussed in Section 3.4.

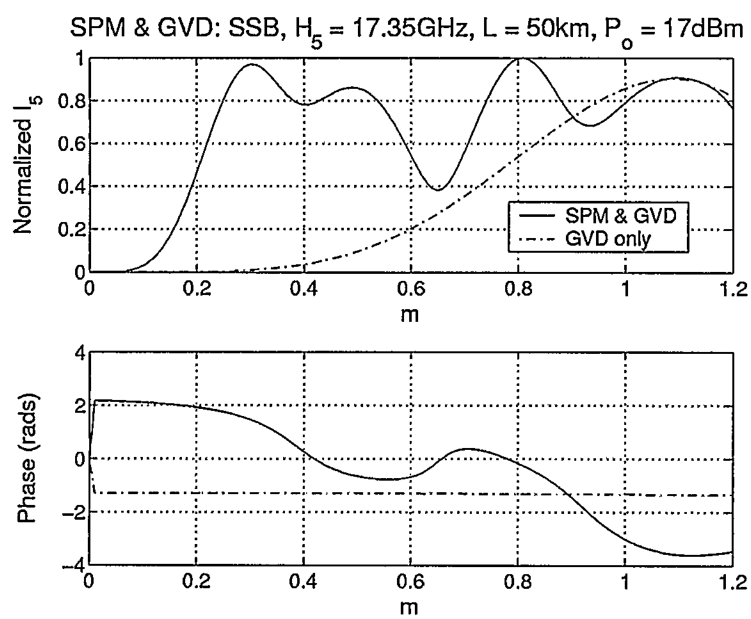

Figure 3.23: 17.35 GHz 5^{th} harmonic response, $P_o = 17$dBm

3.5.3 Discussion

In typical RoF systems, nonlinearity may be a detriment due to increased subcarrier fading. In harmonically upconverting RoF systems however, the effects of nonlinearity may be desirable as they can potentially enhance the harmonic generation of MZM/DD based RoF systems. In such a system, high optical input power would reduce link loss through SPM action, in addition to the extra gain from the increased input optical power. The increased optical power may also eliminate the need for optical amplification in the system.

The fiber used in the previous simulations was weakly nonlinear, and required high optical launch powers to demonstrate significant SPM effects. In reality, many standard single mode fibers exhibit much stronger nonlinear effects, with smaller mode-field areas and higher nonlinear coefficients. Installations using such fiber may therefore be able to take advantage of nonlinear effects with relative ease and achieve more efficient harmonic generation.

3.6 Summary

Pure harmonic upconversion translates a bandpass signal to a higher frequency through a harmonic produced by a nonlinearity. The RoF link is particularly amenable to harmonic upconversion as it inherently nonlinear and well characterized. In this chapter, the harmonic responses of nondispersive and dispersive RoF links were derived for various modes of operation. It was shown that the harmonic upconversion process inflicts severe amplitude and phase distortion in modulated signals. Predistortion was presented as an effective distortion mitigation scheme. System bandwidth effects on predistortion effectiveness were demonstrated and discussed. Fiber nonlinearity and the associated SPM phenomenon were introduced and a preliminary investigation performed on the combined effects of SPM and GVD on RoF systems and harmonic generation. It was found that SPM offers dispersion compensation, extending the usable length of fiber. SPM was also shown to enhance harmonic generation, presenting the possibility of significant link loss reduction in a harmonically upconverting system.

Chapter 4

Simulation and Experimentation

The results of computer simulations and laboratory experimentation performed in the verification and demonstration of harmonic upconversion are discussed in this chapter.

Section 4.1 describes the RoF computer simulator used to perform harmonic upconversion experiments. Simulation results are presented verifying and comparing the performance of amplitude scaling and precise linearizing predistortion schemes in both non-dispersive and dispersive fiber scenarios. A simulation demonstration of harmonic upconversion through even harmonics using the MITB and MATB points is also performed. Finally, the effects of system bandwidth on phase predistortion are verified in the context of a RoF system through simulation.

Section 4.2 contains a description of the laboratory RoF system used to perform experiments and demonstrations. The harmonic response of the laboratory system is measured and compared to theory. A demonstration of a dispersive harmonically upconverting RoF system using amplitude and phase predistortion is performed for both pulse shaped and non-pulse shaped signals.

4.1 Simulation

Accurate computer simulations are relatively easy to implement as all the major components of a RoF link are characterized by well defined mathematical models.

Harmonic upconversion and the effectiveness the proposed predistortion schemes can therefore be easily verified and demonstrated through simulation.

Figure 4.1 shows the basic block diagram of the RoF simulator used to perform harmonic upconversion experiments. A pseudo random binary sequence (PRBS) is used to generate baseband I and Q signal components. These components are pulse shaped, amplitude predistorted, phase predistorted, and phase compressed. The signals are then low pass filtered to model the finite baseband bandwidth of the transmitter before IF modulation. The modulated IF carrier is applied to a MZM model (optical baseband equivalent) with a DC bias to achieve either ODSB-IM or OSSB-IM. The fiber dispersion model is applied and followed by square-law detection. The harmonic of interest is isolated with a "brick wall" bandpass filter, and finally demodulated back into baseband I and Q components.

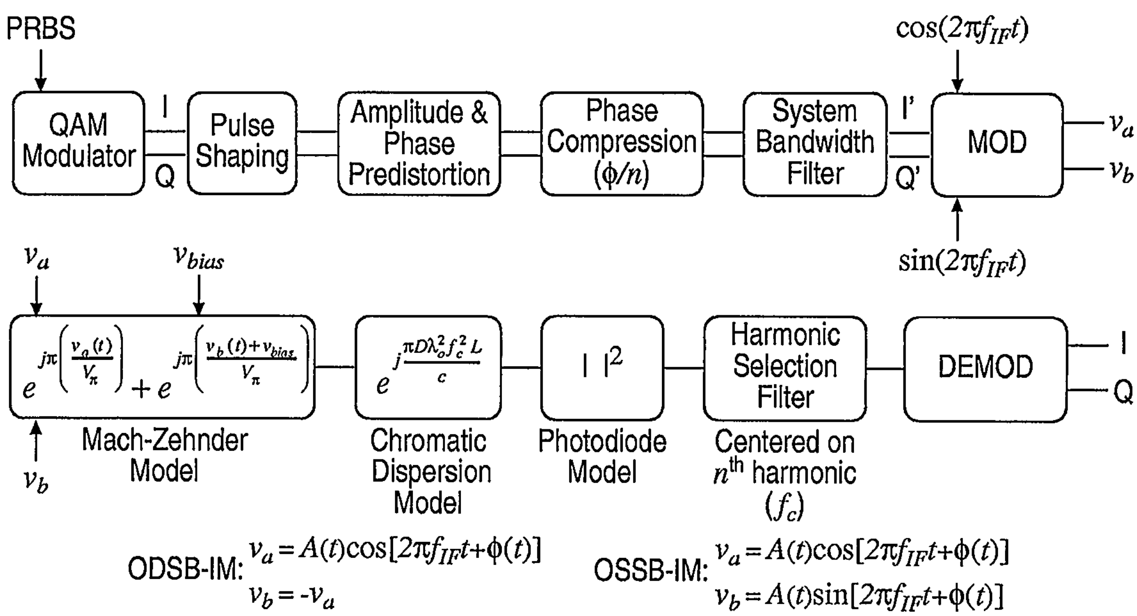

Figure 4.1: RoF harmonic upconversion simulator block diagram

4.1.1 Amplitude Predistortion Scheme Verification and Comparison

Harmonic upconversion of QAM signals such as 16QAM, requires amplitude predistortion in addition to phase compression predistortion. Two methods of amplitude predistortion were presented in Section 3.4.2: scaling and precise linearizing predistortion.

The performance of the two schemes were compared through a RoF system simulation. The simulation parameters are listed in Table 4.1

Radio Modulation	16QAM
Pulse Shape	Raised Cosine
Symbol Rate	30MS/s
Transmitter System Bandwidth	Through
Subcarrier Frequency	6GHz
Upconversion Order	5
Phase Predistortion	Simple Compression
Amplitude Predistortion	Scaling & Precise Linearization
Optical Modulation	ODSB-IM
MZM Bias	QB
Fiber Length	0km
Harmonic Selection Filter	30MHz

Table 4.1: Simulation Parameters – Amplitude Predistortion Comparison

A 16QAM raised cosine pulse shaped signal was selected as it contains both phase and amplitude information and has a sampling characteristic that easily reveals signal distortion. The system bandwidth filter was disabled and the harmonic selection filter set to the information bandwidth so as to eliminate bandwidth related distortion. Separate simulations were run for amplitude scaling predistortion and precise linearizing predistortion schemes tailored for the 5^{th} harmonic link response shown in Figure 4.2. The sampled 5^{th} harmonic constellations are shown in Figure 4.3.

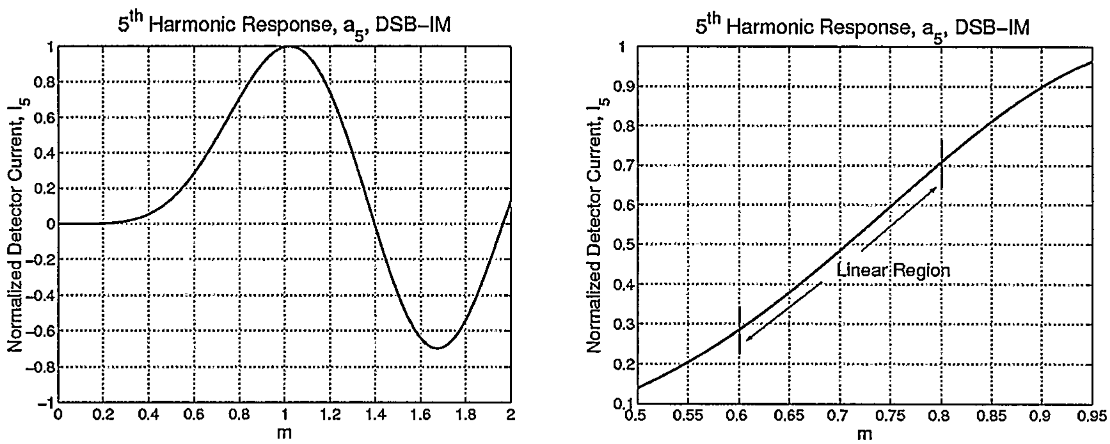

(a) $a_5(m)$ (b) $a_5(m)$, linear region

Figure 4.2: ODSB-IM 5^{th} harmonic magnitude response

The original raised cosine constellation before predistortion and harmonic up-conversion, is shown in Figure 4.3(a) to be symmetrical, with tight sample point clusters. Distortion will be visible as an enlargement of the sample clusters, and constellation asymmetry.

The input constellation was first predistorted through scaling tailored to the linear region bounded by $m = 0.55$ and $m = 0.85$. The resulting constellation is shown in Figure 4.3(b) to be of decent quality, with no errors and an average power of 105.4mW or 20.22dBm (assuming a 1Ω termination). Comparison with the original constellation shows distortion visible as an asymmetry in the constellation and enlarged sample clusters. These distortions will lead to an increased link error rate.

To reduce distortion, the scaling range was narrowed to $0.6 < m < 0.8$, as shown in Figure 4.2(b). The resulting sampled constellation, shown in Figure 4.3(c), is

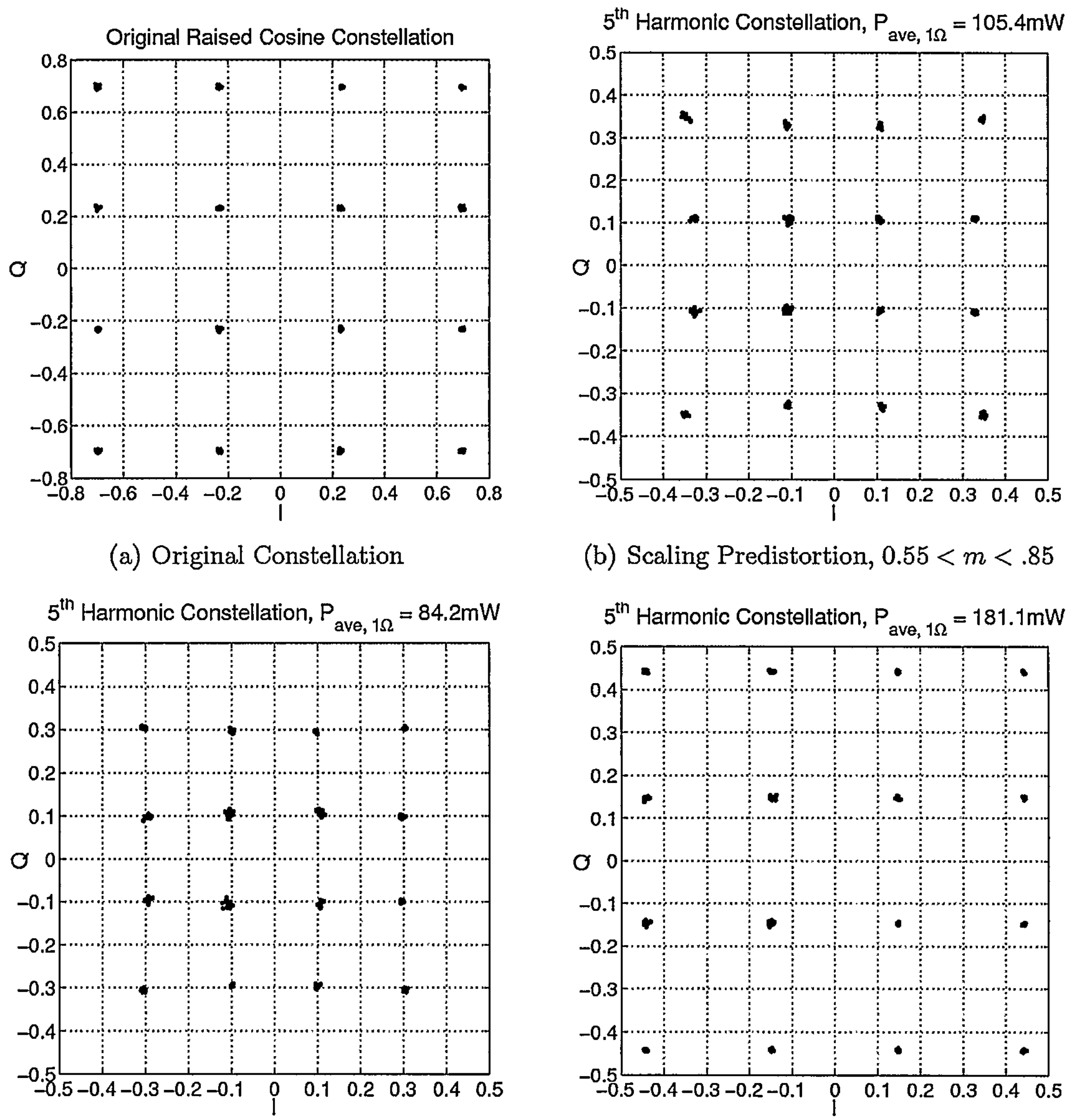

(a) Original Constellation

(b) Scaling Predistortion, $0.55 < m < .85$

(c) Scaling Predistortion, $0.6 < m < 0.8$

(d) Linearizing Predistortion

Figure 4.3: Recovered 5^{th} harmonic raised cosine 16QAM constellations - Scaling and linearizing predistortion

of much better quality, with only minimal distortion visible as a slight asymmetry and sample cluster enlargement. The average power however, has been reduced to

84.2mW, or 19.25dBm.

Next, precise linearizing predistortion was applied to the whole first monotonic section of the harmonic response shown in Figure 4.2(a). The resulting sampled constellation is shown in Figure 4.3(d) to have a symmetrical constellation with only slightly enlarged sample clusters, indicating only minimal residual distortion. The average power (1Ω termination) of the received constellation was 181.1mW or 22.58dBm.

It is clear that both predistortion schemes can provide excellent constellation quality. The precise linearizing predistortion scheme is shown to be superior, as it maximizes the available dynamic range, allowing for 3.33dB more output signal power, while incurring minimal distortion.

4.1.2 Upconversion with Even Harmonics

Simulations were performed to demonstrate harmonic upconversion with even harmonics. The simulation parameters were set to those of Table 4.1, with the exception of the upconversion order and bias point; both MITB and MATB points were used to generate a 6^{th} harmonic for upconversion. Precise linearizing amplitude predistortion was applied to maximize dynamic range. Figure 4.4 shows the resulting sampled constellation.

The constellations are again of excellent quality, demonstrating that even harmonic upconversion in a link biased at the MATB or MITB points is possible. MATB and MITB are shown to provide identical performance, except for slightly increased received signal power with MATB.

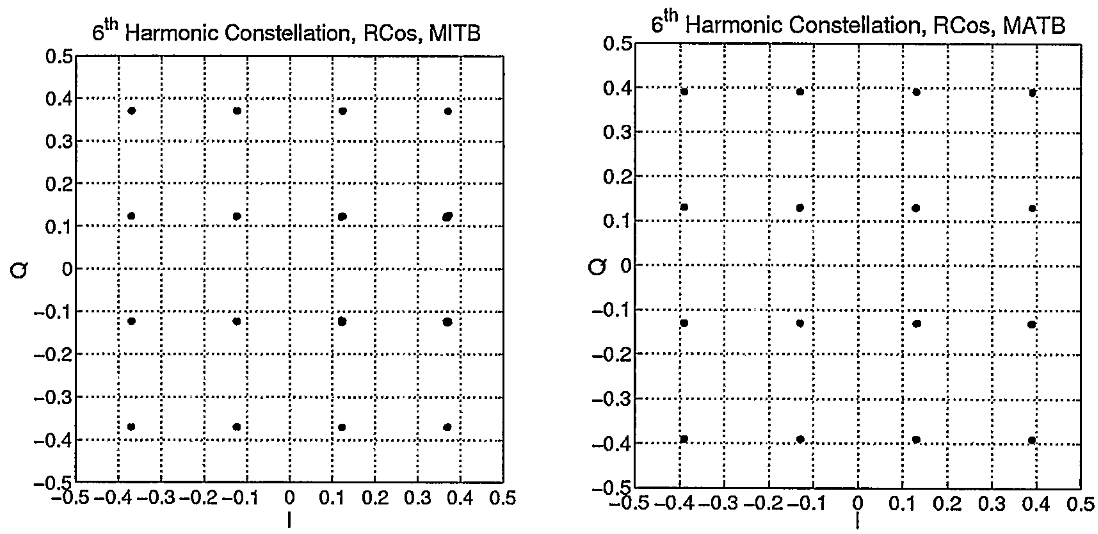

(a) MITB (b) MATB

Figure 4.4: Recovered 6^{th} harmonic sampled constellations – MITB and MATB

4.1.3 Predistortion in Dispersive Links

A simulation was performed to verify the performance of predistortion in the more realistic context of dispersive RoF links. The simulation parameters are shown in Table 4.2, and the resulting constellations in Figure 4.5. A symbol rate of 30MS/s was selected as it is sufficiently narrowband to avoid group velocity dispersion distortion.

Dispersive links will most likely employ OSSB-IM to counter chromatic dispersion induced subcarrier fading. As previously discussed in Section 3.4.2, OSSB-IM exhibits a non-flat phase response that manifests as a twisting of the signal constellation. Figure 4.5(a) demonstrates with a simulated 5^{th} harmonic constellation with no phase flattening predistortion. The constellation twisting is clearly visible. Applying additional phase flattening predistortion completely mitigates this distortion as shown in Figure 4.5(b).

Radio Modulation	16QAM
Pulse Shape	Raised Cosine
Symbol Rate	30MS/s
Transmitter System Bandwidth	Through
Subcarrier Frequency	6GHz
Upconversion Order	5
Phase Predistortion	Simple compression
Amplitude Predistortion	Precise linearization
Optical Modulation	OSSB-IM
MZM Bias	QB
Fiber Length	50.5km
Dispersion Parameter, D	18ps/nm·km
Harmonic Selection Filter	30MHz

Table 4.2: Simulation Parameters – Dispersive Link Demonstrations

The constellation shown in Figure 4.5(b) is of excellent quality being symmetrical, with small sample clusters. The lack of distortion attests to the effectiveness of

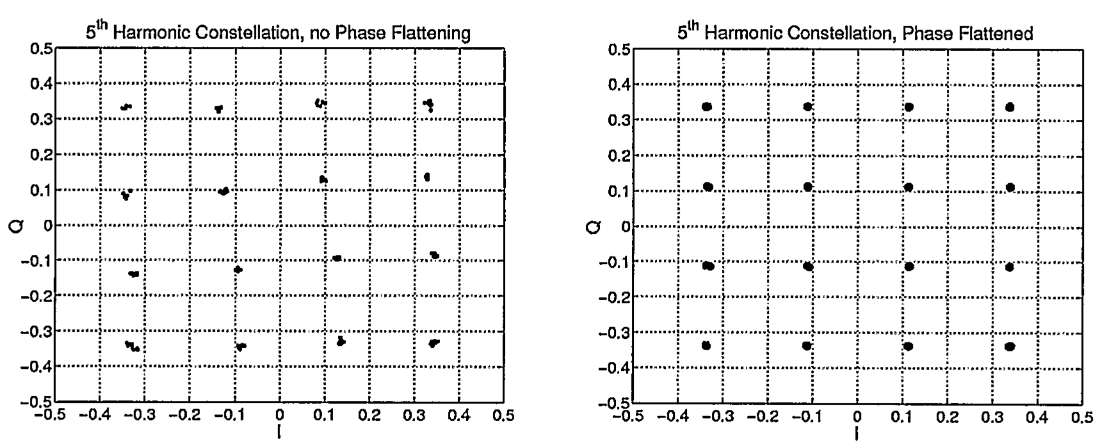

(a) No phase flattening predistortion (b) Phase flattening predistortion

Figure 4.5: Recovered 5^{th} harmonic constellations - with and without additional phase predistortion

amplitude predistortion combined with phase predistortion as a distortion mitigation scheme in a harmonically upconverting dispersive RoF system.

4.1.4 Limited Bandwidth RoF Systems

Section 3.4.1 discussed the effects of bandwidth on phase compression predistortion. The following simulations demonstrate these effects in a harmonically upconverting RoF system and verify the effectiveness of differential phase compression. The simulation parameters are listed in Table 4.3.

Radio Modulation	QPSK
Pulse Shape	Raised Cosine
Symbol Rate	30MS/s
Upconversion Order	5
Amplitude Predistortion	Precise Linearization
Optical Modulation	ODSB-IM
MZM Bias	QB
Fiber Length	0km

Table 4.3: Simulation Parameters – Limited Bandwidth Experiments

Figure 4.6 displays the result of simulation experimentation. To establish a baseline, Figure 4.6(a) shows the fundamental constellation captured at the output of the RoF link with a transmitter (Tx) bandwidth of 5$\times$ the information bandwidth (herein stated simply as 5$\times$), and a harmonic selection (Sec.) filter of bandwidth 5$\times$. There is no visible distortion.

Figure 4.6(b) shows the 5$^{\text{th}}$ harmonic constellation with the same bandwidth parameters as the fundamental case and using simple phase compression. Significant distortion is plainly visible in the form of large circular transitions and ringing effects, as previously predicted in Section 3.4.1. The presence of these effects at the 5th harmonic, and not the fundamental, demonstrates that distortion stems from phase compression predistortion followed by phase expansion in a bandlimited harmonic upconversion process.

As shown in Figure 4.6(c), reducing the harmonic selection filter to the information bandwidth (1×), removes all distortion except for the left most transitions. Note that distortion can still be reduced, but not eliminated, by further narrowing of the selection filter passband. Applying differential phase compression, completely restores the constellation, as demonstrated in Figure 4.6(d).

Relaxing the harmonic selection filter to a bandwidth of 5×, as might be required in a multicarrier system, yields the harmonic constellation shown in Figure 4.6(e). Although not completely distortion free, it is significantly improved over the constellation obtained from the same bandwidth configuration, but with simple phase compression (shown in Figure 4.6(b)). The residual distortion is minimal, and so will have a negligible effect on link error characteristics. Clearly, differential phase compression is desirable in multicarrier systems.

A final simulation was performed to verify the requirement of excess bandwidth in the transmitter circuit. As demonstrated in Figure 4.6(f), reducing the predistortion circuit bandwidth to just 2× produces uncorrectable distortion in the harmonic constellation, despite the application of differential phase compression and a 1× harmonic selection filter. This verifies the necessity of excess bandwidth in the transmitter predistortion circuit.

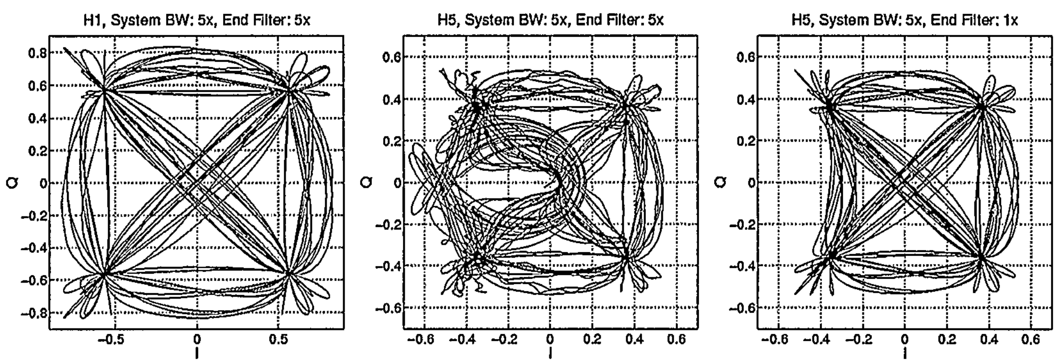

(a) H1, Tx BW: 5×, Sel. Filter: 5× (b) H5, Tx BW: 5×, Sel. Filter: 5× (c) H5, Tx BW: 5×, Sel. Filter: 1×

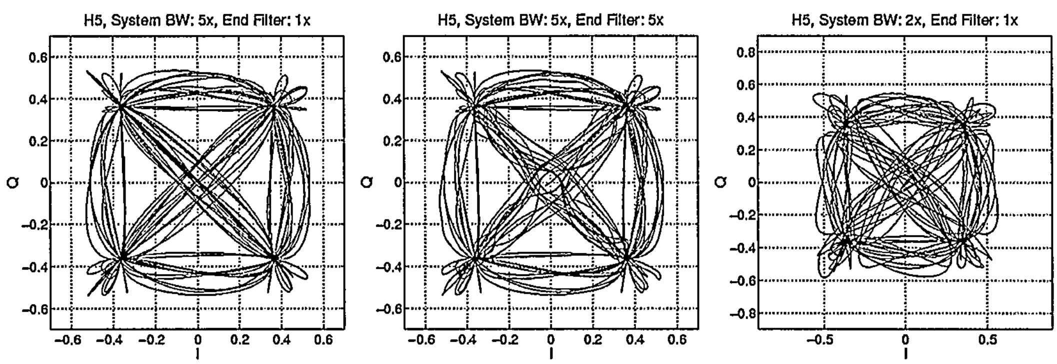

(d) H5, Diff. Comp., Tx BW: 5×, Sel. Filter: 1× (e) H5, Diff. Comp., Tx BW: 5×, Sel. Filter: 5× (f) H5, Diff. Comp., Tx BW: 2×, Sel. Filter: 1×

Figure 4.6: System bandwidth effects

4.2 Laboratory Experimentation and Demonstration

To validate the simulations and demonstrate the practical application of the theory presented in this study, a harmonically upconverting RoF system was assembled in the lab, and experiments performed.

4.2.1 Laboratory Setup

The experimental setup shown in Figure 4.7 is a harmonically upconverting RoF system using the 3^{rd} harmonic to upconvert a 3.47GHz IF carrier to a 10.41GHz RF carrier. The order and frequency selections were based on the availability and performance of laboratory equipment. Although a higher order upconversion would have been more significant, the link still provides an excellent demonstration of the application and operation of harmonic upconversion in a RoF system.

The radio transmitter portion of the lab setup is shown in Figure 4.7(a). For maximum flexibility, signal modulation and required predistortion is done in software beforehand. The resultant I and Q waveforms are downloaded to an Arbitrary Waveform Generator (AWG) and output continuously. A Vector Signal Generator (VSG) modulates the I and Q waveforms onto a 470MHz IF carrier. The modulated IF carrier is split into two paths, separately mixed with a 3.0GHz carrier wave (LO_1) and filtered to generate a pair of 3.47GHz modulated carriers. A line stretcher in one of the 3.0GHz carrier paths allows for an adjustable phase difference between the two 3.47GHz signals. These two signals are filtered with a 300MHz wide filter, amplified, filtered again to ensure a clean spectrum, and then applied to the electrodes of a dual drive MZM. A DC voltage, V_{bias}, is applied through a bias tee to one of the arms to allow for biasing. The overall bandwidth of the transmitter is hard limited to 300MHz by the passband of the filters in the upconversion chain.

The optical portion of the setup is shown in Figure 4.7(b). A 1550nm laser source, passed through a polarization rotator, is used as an unmodulated optical carrier input for the MZM. The modulated optical carrier propagates through a 50.5km length of

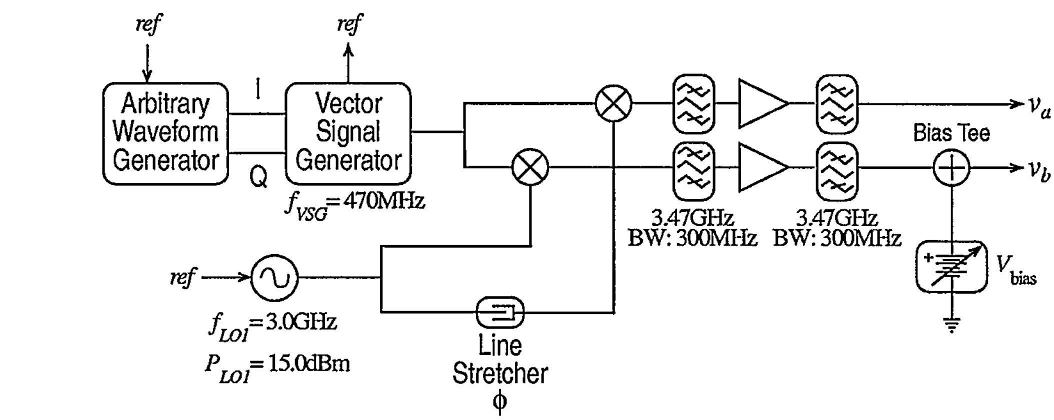

(a) Transmitter setup

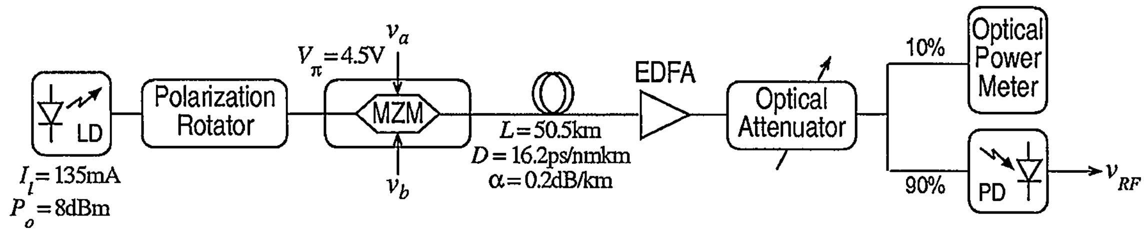

(b) Optical setup

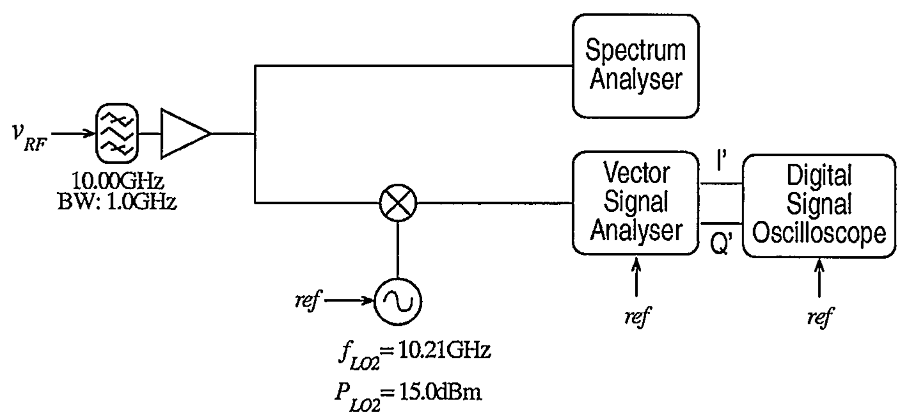

(c) Receiver setup

Figure 4.7: Experimental setup for harmonic upconversion

single mode, dispersive fiber (D = 16.2ps/nm·km), and is optically amplified with an EDFA, before being detected by a 40GHz InGaAs photoreceiver.

The receiver setup is shown in Figure 4.7(c). The signal output of the photoreceiver, v_{RF}, is filtered for the 3rd harmonic (10.41GHz), amplified and split into two. One signal is applied to a spectrum analyzer, and the other down converted to 200MHz with a mixer and a 10.21GHz carrier wave (LO_2), and finally demodulated into I and Q component waveforms by a Vector Signal Analyzer (VSA). The resultant waveforms are then captured by a digital oscilloscope and downloaded to a computer for further processing. Finally, Matlab is used to filter, sample and process the final constellation.

4.2.2 Harmonic Response Measurement

For the applied predistortion scheme to be accurate, the theoretical harmonic magnitude response function of both the ODSB-IMDD and OSSB-IMDD links must be verified.

To configure the setup for the experiment, the 50.5km fiber section and EDFA were temporarily removed, and the optical attenuator/PD section directly connected to the MZM optical output. The polarization of the MZM input optical signal was then adjusted using the polarization rotator to achieve a maximized extinction ratio of 26dB. In the process, the DC MZM V_π parameter was measured to be 4.5V. QB was set by adjusting the DC bias voltage for 3dB less than maximum optical power at the MZM optical output.

With a laser current of I_L = 135mA, and the MZM biased for maximum transmission, an optical power of 1dBm was measured at the output of the MZM. Assuming a $\gamma = 1.91\text{W}^{-1}\text{km}^{-1}$, L_{NL} is 415km. As the link length is only 50.5km, the effects of fiber nonlinearity can be neglected.

A scanning Fiber Fabry-Perot (FFP) device was then temporarily patched into the shortened link to examine the optical spectrum at the output of the MZM. A single low power tone ($m \ll 1$) was output from the VSG through the IF upconversion chain to apply a pair of 3.47GHz tone signals to the MZM electrodes. The line stretcher was then adjusted till ODSB modulation was visible, indicating a phase difference of π radians, and till OSSB modulation was visible, indicating a phase difference of $\frac{\pi}{2}$. The line stretcher positions for OSSB and ODSB were marked for later reference. Figure 4.8 shows the captured optical spectrums for OSSB and ODSB modulation.

The link configured, the FFP device was removed and the 50.5km fiber section and EDFA reinstalled. The optical attenuator was adjusted for an incident optical power of -2dBm at the photodetector. With the line stretcher set for ODSB-IM, a 3.47GHz tone was passed through the system and the peak 3$^{\text{rd}}$ harmonic (10.41GHz) output power measured with a spectrum analyzer. The harmonic response was obtained by sweeping the input tone power and measuring the resulting 3$^{\text{rd}}$ harmonic tone power. The procedure was repeated for OSSB-IM. The input signal powers applied to the MZM electrodes were translated into modulation indexes in Matlab. In the process of matching the theoretical and measured curves, it was found that a MZM $V\pi$ of 4.65V provided excellent curve matching. This value corresponds to the V_π RF voltage at a frequency of 3.47GHz, and differs from the more commonly used DC V_π.

Figure 4.9 shows the 3$^{\text{rd}}$ harmonic experimental and theoretical normalized out-

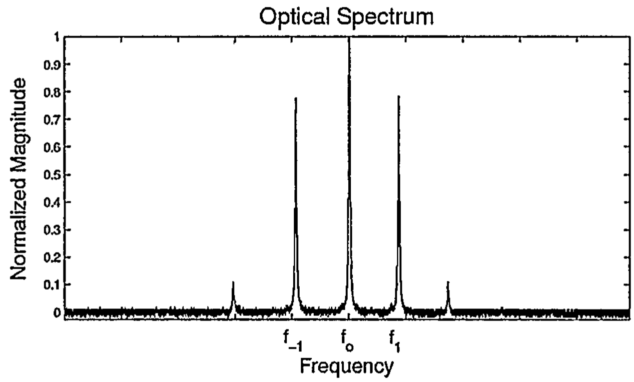

(a) ODSB-IM optical spectrum

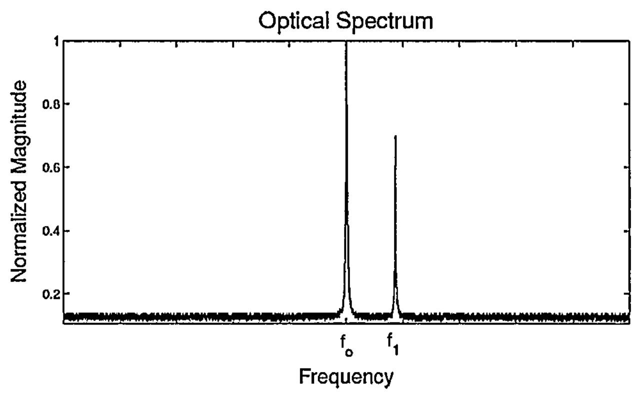

(b) OSSB-IM optical spectrum

Figure 4.8: Scanning Fabry-Perot ODSB and OSSB optical spectrums

put voltage versus modulation index for both ODSB-IM and OSSB-IM. The measured transfer characteristic is shown to match theory closely, however deviation from theory begins to occur at higher modulation indexes for both responses. This can be attributed to the MZM drive amplifiers saturating, creating distortion in the form of harmonics and intermodulation products. These added spectral components interact in the link causing the harmonic response to deviate from theory. OSSB is shown to deviate from theory at a lower modulation index than ODSB, indicating a higher sensitivity to spectral distortion. This can be attributed to the delicate spectral balance required to cancel alternating sidebands and maintain OSSB.

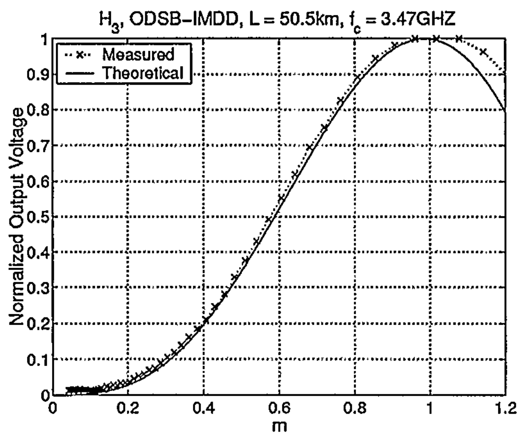

(a) ODSB-IM 3rd harmonic magnitude Response

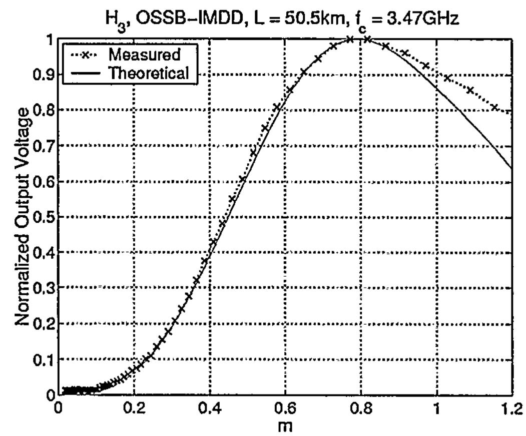

(b) OSSB-IM 3^{rd} harmonic magnitude Response

Figure 4.9: Measured ODSB and OSSB 3^{rd} harmonic magnitude responses

The collected harmonic response curves were found to be sensitive to bias point. Heating effects in the MZM caused the bias point to drift over time altering the link characteristic. To minimize error, the bias point and line stretcher were carefully set for every trial and the experiment immediately performed. This proved to be successful, as shown by the close match with theory.

4.2.3 Harmonic Upconversion Demonstration

The major goal of this thesis study is the demonstration of a practical RoF link employing harmonic upconversion. The following experiments satisfy this goal.

A pseudo random binary sequence was used to generate a 16QAM modulated signal in Matlab. QAM was selected as it consists of both phase and amplitude modulation. The 3rd harmonic theoretical ODSB and OSSB link responses for the experimental setup described in Section 4.2.1 were used to predistort the raw 16QAM constellation. These responses are shown in Figure 4.10. Provided care was taken to configure the link accurately, the use of theoretical curves was deemed acceptable as the measured link characteristic was shown to closely match theory over the desired operating range. Linearizing amplitude predistortion was done so as to maximize the dynamic range of the link, and additional phase flattening predistortion performed to compensate for the non-flat phase response. As the demonstration is of a single carrier harmonic upconversion, simple phase compression was used. The signal was oversampled at 8$\times$, and no pulse shaping was initially performed. The predistorted 16QAM constellations for ODSB-IM and OSSB-IM are shown in Figure 4.11. The additional phase flattening predistortion can be seen in the OSSB predistorted constellation. These constellations were downloaded to the AWG, and output at a rate of 100×10^6samples/s, giving a symbol rate of 12.5MS/s.

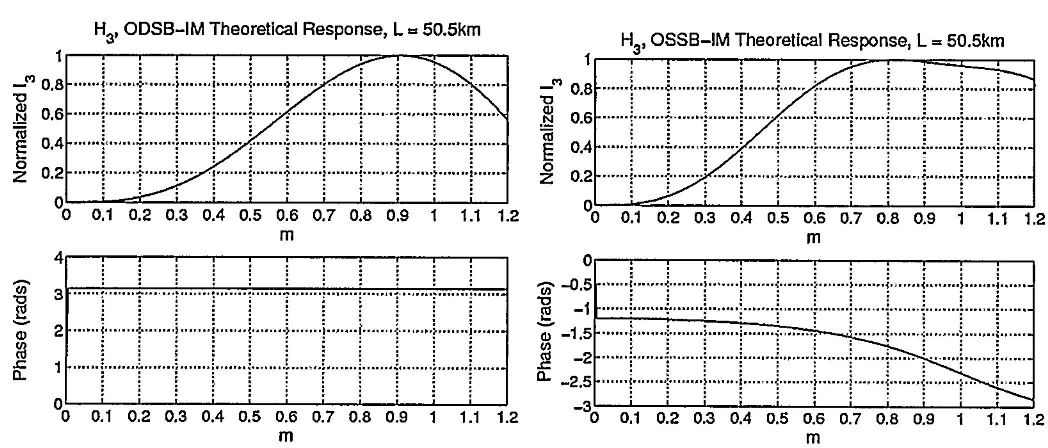

(a) ODSB-IM (b) OSSB-IM

Figure 4.10: Theoretical 3rd harmonic link response

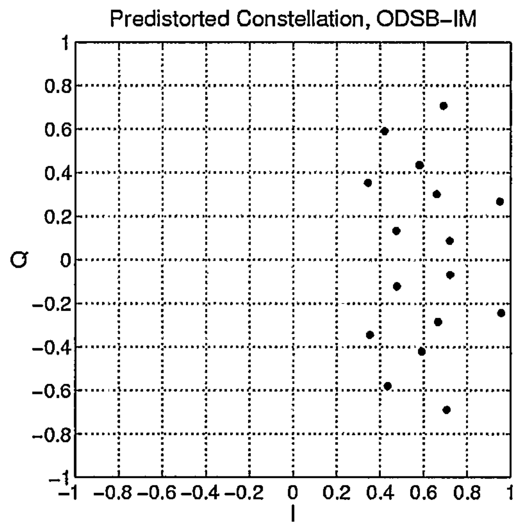

(a) ODSB-IM

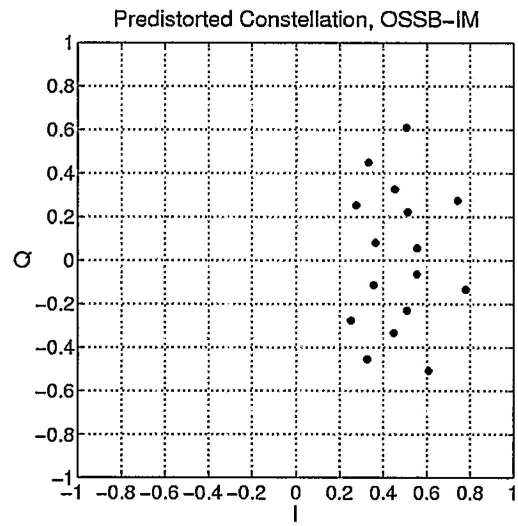

(b) OSSB-IM

Figure 4.11: 3^{rd} harmonic predistorted 16QAM constellations

With the transmitter circuit bandwidth limited to 300MHz by the IF upconversion filters, the excess bandwidth in the transmitter circuit was 12× the IF signal bandwidth; more than enough to avoid the effects of limited bandwidth and phase compression, even with simple phase compression. This was verified through simulation. The excess bandwidth also serves to demonstrate a RoF optical transmitter without tight filtering.

The link was configured in the same manner as in Section 4.2.2. Predistorted ODSB and OSSB constellations were transmitted through the link and the 3^{rd} harmonic isolated with a 10GHz bandpass (1.0GHz passband) filter. The resulting signal was then amplified, downconverted and the output constellation examined on the VSA. The input signal power to the link was slowly increased by adjusting the VSG gain until the constellation points displayed on the VSA were symmetrically spaced, indicating that the predistorted signal overlaid the correct portion of the link transfer characteristic. Once the link was properly configured, the received data was sampled by the digital oscilloscope at the same rate as the AWG (100Msamples/s), and downloaded to a computer. Matlab was then used to low pass filter the captured signals.

The received constellations and eyediagrams for ODSB and OSSB are shown in Figures 4.12 and 4.13 respectively. Both constellations are of excellent quality with good symmetry. Eyediagrams show open eyes, and indicate no bandwidth related transition distortion. There were no symbol errors. The slight asymmetries visible in both constellations indicate some residual distortion. This distortion can be attributed to a slight misalignment between the predistorted waveform and the harmonic response characteristic. Other factors include, imperfect biasing of the MZM, and spectral distortion at high modulation indexes causing deviations of the link characteristic from theory.

The next experiment demonstrates the harmonic upconversion of a pulse shaped signal. The same RoF link was used as before and configured for OSSB-IM. Matlab was used to generate an $8\times$ oversampled Butterworth low pass filtered 16QAM signal, and perform the required amplitude and phase predistortion. Precise amplitude predistortion and simple phase compression were again used. Once downloaded to the AWG, the signal was output continuously at a rate of 200Msamples/s, giving a symbol rate of 25MS/s (100Mbits/s).

The captured 3^{rd} harmonic constellation and eyediagram are shown in Figure 4.14. Again, the constellation is of excellent quality, with no symbol errors. Even with the excess bandwidth reduced to $6\times$ the signal bandwidth, there is still no bandwidth

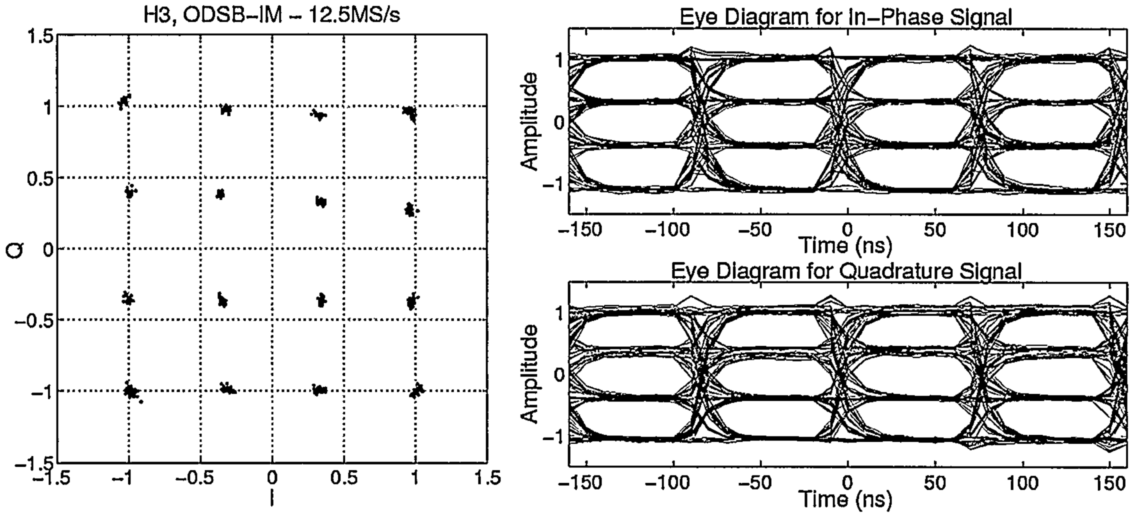

(a) Sampled constellation

(b) Eyediagram

Figure 4.12: 3rd harmonic captured constellation - ODSB-IM

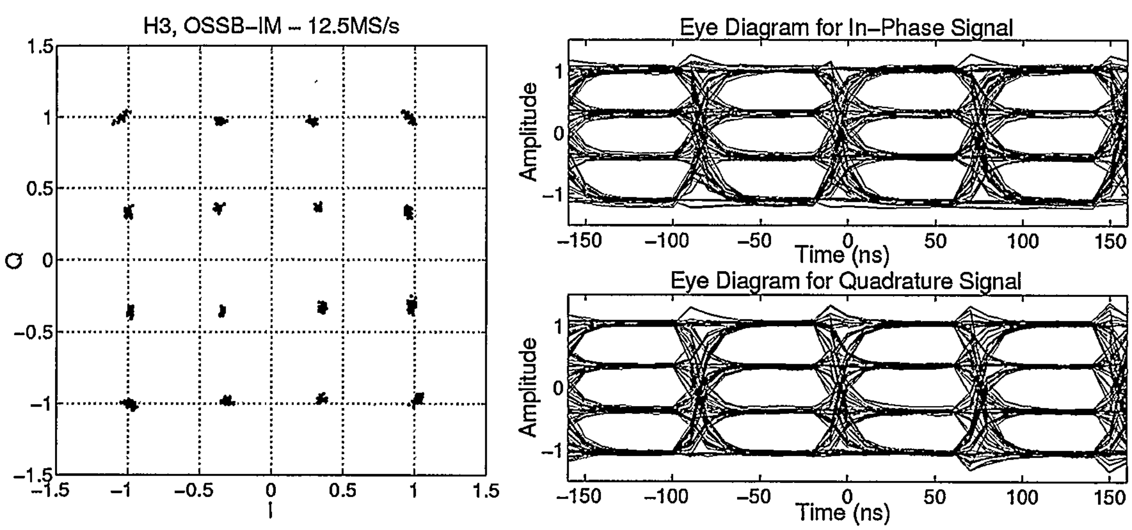

(a) Sampled constellation

(b) Eyediagram

Figure 4.13: 3rd harmonic captured constellation - OSSB-IM

related distortion visible in the eyediagrams.

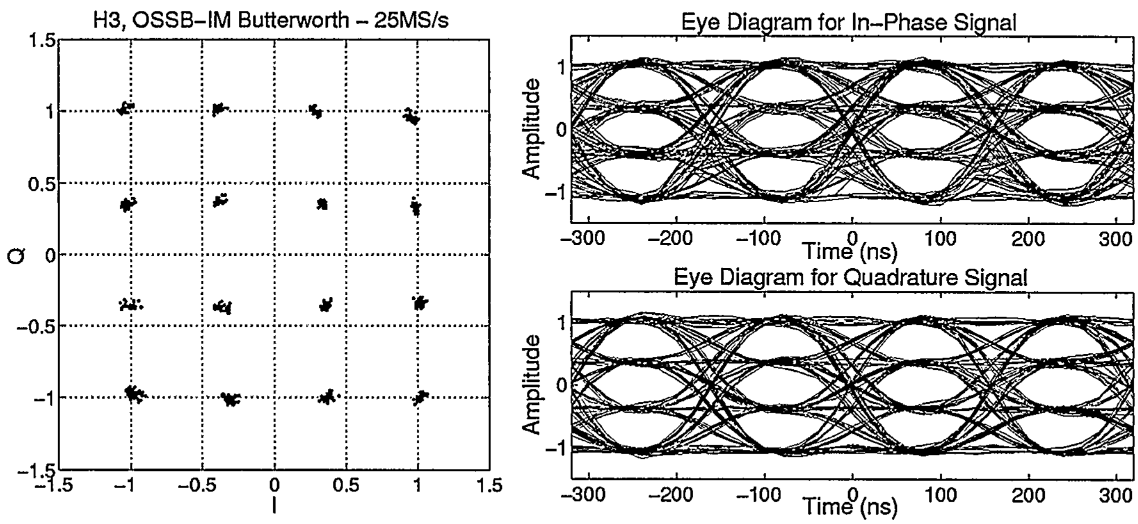

(a) Sampled constellation (b) Eyediagram

Figure 4.14: 3rd harmonic captured constellation - Butterworth filtered, OSSB-IM

4.2.4 Discussion

The previous laboratory experiments demonstrate a real world RoF fiber system employing harmonic upconversion with a significant length of dispersive fiber.

The measured 3rd harmonic responses were shown to closely match that of theory, verifying that the MZM/DD RoF link model is indeed accurate. This allowed signals to be easily predistorted in Matlab based on the theoretical link response. However, drift in the optical setup became an issue as deviations from the proper bias point alter the link response, causing improper predistortion and ultimately distortion in the received constellation. Although the results obtained were of good quality, they were achieved with extreme care to ensure the link was configured accurately. The drift in bias also precluded bit error rate testing (BER), as the optical configuration would drift before a statistically significant number of errors could be had. A practical RoF system employing harmonic upconversion, must therefore employ a feedback bias control circuit to ensure proper biasing and maintain the link response.

Another issue that became apparent over the course of experimentation was the alignment of the predistorted signal with the link characteristic; anything more than a minor misalignment resulted in distortion. In the above experiments, input signal power was adjusted till a symmetrical constellation was visible on the VSA screen, indicating a proper alignment. Assessing constellation symmetry however, was difficult at best as the VSA did not provide a clear, sampled constellation. Although the captured constellations were of good quality, it is felt that more precise alignment could offer further improvement.

The added complexity of signal alignment can be avoided by implementing the simpler scaling predistortion scheme, as it is less sensitive to variations in the harmonic response than precise linearizing predistortion. The trade off is less dynamic range and delivered signal power. Increased signal gain at the remote basestation may be required to compensate.

The sensitivity associated with linearizing predistortion can also be avoided by using a constant envelope radio modulation scheme such as QPSK. In such a scenario, no amplitude predistortion is required; the signal modulation index need only be set to optimize received signal power. Further predistortion to flatten the phase response, is also not required. The trade off in this case is decreased spectral efficiency.

While distortionless harmonic upconversion is highly desirable, it need not be distortionless in practice. As RoF systems transport signals that are destined for the radio channel, complex error correction schemes must be employed to ensure satisfactory error rates at the end user. The quality of the delivered signal need only be sufficient to achieve the desired error rate; in practice a certain level of distortion is admissible. Residual distortion from the harmonic upconversion process will likely be tolerable.

The RoF system demonstrated was configured to minimize bandwidth related distortion by allowing excess bandwidth in the MZM drive circuitry and application of a narrow final stage filter in Matlab. No bandwidth effects were visible in the eyediagram transitions with the excess bandwidth reduced to 6× the signal bandwidth. This demonstrates how in practice, bandwidth distortion can be completely mitigated. However, the large bandwidth filters were carefully selected to avoid undesirable components originating from mixer artifacts, LO feed through, harmonics and intermodulation products. In any RoF system design, care must be taken when implementing wider filters to ensure a clean spectrum in the MZM drive signals.

Overall the performed experiments clearly demonstrate the application of harmonic upconversion in a practical RoF system.

4.3 Summary

The operation of a harmonically upconverting RoF system was studied and demonstrated in this chapter through both computer simulation and laboratory experimentation.

A RoF computer simulation model was presented and used to perform verification and comparison of scaling and precise linearizing amplitude predistortion schemes. Both schemes were shown to effectively mitigate distortion. Precise linearizing predistortion however, provided superior dynamic range with increased received signal power.

Harmonic upconversion using even harmonics in a RoF system was performed successfully through simulation. Even harmonic generation through both the MITB and MATB bias points was shown to perform identically.

A harmonically upconverting dispersive RoF system implementing OSSB-IM was also simulated. The constellation twisting distortion resulting from a non-flat phase response was demonstrated. Additional phase predistortion was shown to successfully mitigate this distortion. This simulation also served to demonstrate the ability of the proposed predistortion schemes to completely mitigate all distortion in a RoF link exhibiting chromatic dispersion.

Simulations were also performed verifying the impact of available bandwidth on phase compression predistortion in a harmonically upconverting RoF system. The impacts were shown to be an issue in a 5$\times$ bandwidth predistortion circuit. A harmonic selection filter tailored to the signal bandwidth corrected most distortion, with differential phase compression completely mitigating all distortion. The requirement for excess bandwidth in the predistortion circuit, despite a tight harmonic selection filter and differential phase compression, was demonstrated. Differential phase compression was also shown to provide quality constellations without a tight harmonic selection filter, demonstrating its potential for multicarrier scenarios.

Laboratory experiments were performed to demonstrate the operation of a practical RoF system employing harmonic upconversion, and highlight implementation issues. A demonstrative 3rd order harmonically upconverting RoF system is described in detail. The harmonic response of the system was measured and shown to closely match that predicted by theory, verifying the theoretical models used to derive link harmonic response. Amplifier saturation proved to be a problem, causing the measured harmonic response to deviate from theory at higher modulation indexes. Increasing amplifier power handling or decreasing the MZM V_π voltage would alleviate this problem. Drift in the DC bias circuit was identified as an issue, causing the link characteristic to shift over time. It was proposed that a bias control circuit would be required in a practical system.

The harmonic upconversion of a 12.5MS/s (50Mb/s) 16QAM signal was demonstrated using simple phase compression and precise linearizing predistortion, with excellent quality received constellations. Residual distortion was attributed to misalignment between the predistorted waveform and the link characteristic. Finally, a 25MS/s (100Mb/s) Butterworth pulse shaped 16QAM signal was harmonically upconverted with excellent results.

Chapter 5

Conclusion

Pure harmonic upconversion is a new idea for frequency translation. Although easy in concept, application is not. As yet, little research has been directed toward pure harmonic upconversion, leaving application still infeasible. This work has advanced the current state of literature by accomplishing several objectives, first outlined in Section 1.3, and in so doing, has brought pure harmonic upconversion closer to the ultimate goal of application.

The first objective was to formalize the concept of pure harmonic upconversion, with emphasis on RoF application. Chapter 3 satisfied this goal with an in depth discussion of pure harmonic upconversion in RoF systems. As part of this discussion, analysis of the RoF link harmonic response and associated theory was performed. Distortion mechanisms stemming from both the harmonic upconversion process and the RoF link itself were identified and characterized. These included phase multiplication, nonlinear amplitude response and a non-flat phase response. Predistortion was presented as means of distortion mitigation. Specifically simple phase compression and differential phase compression were proposed to counter phase multiplication and scaling and precise amplitude predistortion to counter amplitude distortion. The effectiveness of the proposed predistortion schemes were later verified through simulation in Chapter 4. Chapter 3 also investigated the impact of available bandwidth on phase compression.

The second objective was to account for the effects of fiber chromatic dispersion through predistortion. The effects of fiber chromatic dispersion on the harmonic response of a RoF link were analyzed in Chapter 3. Although chromatic dispersion was shown to alter the harmonic amplitude and phase characteristic, it was found that if OSSB-IM was used to counter dispersion related fading, a harmonic response suitable for harmonic upconversion existed at all fiber lengths. The applied predistortion schemes need only be tailored to specific harmonic response of the dispersive RoF link in question. In Chapter 4, the theoretical model for harmonic response in a dispersive RoF link was verified through laboratory experimentation.

The third objective was to demonstrate the use of precise amplitude predistortion. The concept of precise amplitude predistortion was presented in Chapter 3, and demonstrated through both simulation and laboratory experiments in Chapter 4. Precise amplitude predistortion was shown to maximize signal dynamic range and power at the remote unit, and provided superior distortion mitigation. The same technique was also applied to counter the non-flat harmonic phase response of dispersive fiber links employing OSSB-IM, with excellent results.

The fourth objective was the demonstration of a practical RoF system. In Chapter 4, a prototype RoF system employing 50.5km of dispersive fiber, and implementing a 3^{rd} order harmonic upconversion scheme translating a 3.47GHz IF signal to 10.41GHz was described. The OSSB-IM and ODSB-IM link harmonic responses were measured, and found to match theory closely. Experiments were performed harmonically upconverting a 12.5MS/s (50Mb/s) 16QAM signal using precise amplitude predistortion and simple phase compression. Received constellations were shown to be of excellent quality with little residual distortion. A second experiment harmonically upconverting a 25MS/s (100Mb/s) Butterworth pulse shaped 16QAM signal was performed and also provided excellent results. These experiments demonstrated the application of harmonic upconversion in a representative RoF system.

The final objective was to investigate the effects of fiber nonlinearity on RoF systems. In the later portion of Chapter 3, the concept of fiber nonlinearity and the associated SPM phenomenon were presented and studied through simulation. It was found that SPM can significantly affect a RoF system. Specifically, SPM was found to counter chromatic dispersion, reducing fading frequency in ODSB-IM links, and extending usable fiber length. OSSB however, was shown to lose fading immunity at high optical powers. SPM was also shown to enhance the harmonic generation ability of a RoF system, allowing a harmonic to be maximized at lower modulation indexes, potentially reducing link loss significantly.

5.1 Future Work

There is yet much work to be done before harmonic upconversion can be implemented in a RoF system.

The issue of link stability must be addressed if precise predistortion is to be viable. Theory has shown to accurately model the response of a MZM/DD RoF link allowing precise predistortion based on theory to be applied. However, optical drift alters the link characteristic over time, resulting in incorrect predistortion, and precluding BER testing. It is believed that optical drift is caused by heating effects altering the electro-optic properties of the MZM and shifting the bias point. If the heating effects cannot be stabilized through environmental control, a method of bias control will need to be developed to ensure accurate biasing of the MZM at all times.

Link stability would be greatly improved with bias control, allowing for more reliable predistortion, and BER testing.

Alignment of the predistorted waveform and the link response proved to troublesome during experimentation. If harmonic upconversion is to be applied practically, an automated method must be developed to reliably perform this alignment. If the link response proves to be unreliable, even with bias control, a feedback system will be also be required to ensure proper alignment.

Research to ascertain the permissible level of distortion in the harmonic constellation would be a valuable contribution. This knowledge would determine the required precision of the predistortion scheme. It is possible that slightly misaligned predistorted waveforms may in fact be permissible, allowing for simpler predistortion schemes to be applied and relaxed control circuitry.

A deployed RoF system would likely be required to transport multiple radio carriers. The harmonic upconversion of multicarrier signals should be investigated to determine feasibility. Wideband radio schemes such as OFDM (orthogonal frequency division multiplexing) and CDMA (code division multiple access) are prime candidates for future RoF based LMCS/LMDS systems and should be investigated for harmonic upconversion also.

The effects of fiber nonlinearity have only been briefly investigated in this study and preliminary simulation results have been promising. Further work is required to experimentally verify the results of simulation. The stability of an SPM enhanced link should be investigated to determine its suitability for predistortion and harmonic upconversion purposes. Ultimately, harmonic upconversion of a modulated signal using predistortion needs to be investigated through simulation and laboratory experimentation.

Harmonic upconversion in this study has been presented in the context of RoF systems. In actuality, the concept of harmonic upconversion may find application in other areas. Work should done exploring other applications.

5.2 Conclusion

This thesis has advanced the current state of literature in the area of pure harmonic upconversion. In this work, the concept has been formalized, and application in RoF systems discussed in depth. Pure harmonic upconversion was demonstrated in a practical RoF system employing dispersive fiber through both computer simulation and laboratory experimentation. Excellent results were presented demonstrating pure harmonic upconversion as a viable means of frequency translation.

Bibliography

[1] J.M. Cioffi, "Asymmetric digital subscriber lines," *The Communications Handbook*, J.D. Gibson, Ed., ch. 34, pp. 450–479. CRC Press, Boca Raton, Florida, 1997.

[2] DSL Forum, "DSL anywhere," White paper, DSL Forum, www.dslforum.org/about_dsl/dsl_anywhere.doc, May 2001.

[3] B.M. Testa, "U.S. phone companies set stage for fiber to the curb," *IEEE Spectrum Mag.*, pp. 14–15, Sept. 2003.

[4] "Most commonly asked cable modem and xDSL questions," www.cablemodeminfo.com, Nov. 1999.

[5] D. Wake, I.C. Smith, N.G. Walker, I.D. Henning, and R.D. Carver, "Video transmission over a 40ghz radio-fibre link," *Electronics Letters*, vol. 28, no. 21, pp 2024-2025, October 1992.

[6] S.M. Cherry, "The wireless last mile," *IEEE Spectrum Mag.*, pp. 18–22, Sept. 2003.

[7] Industry Canada website, "Local Multipoint Communication Systems in the 28GHz range: policy, authorization procedures and evaluation criteria," http://strategis.ic.gc.ca/epic/internet/insmt-gst.nsf/vwGeneratedInterE/sf01817e.html.

[8] FCC website, "FCC auction 17:Local Multipoint Distribution System (LMDS)," http://wireless.fcc.gov/auctions/17/, April 2002.

[9] S. M. Cherry, "Telcos in trouble," *IEEE Spectrum Mag.*, pp. 21, Sept. 2003.

[10] N.G. Walker, D. Wake, and I.C. Smith, "Efficient millimeter-wave signal generation through FM-IM conversion in dispersive optical fibre links," *Electronics Letters*, vol. 28, no. 21, pp 2027-2028, October 1992.

[11] R.P. Braun, G. Grosskopf, R. Meschenmoser, D. Rohde, F. Schmidt, and G. Villino, "Optical harmonic upconversion for microwave generation in bidirectional broadband mobile communications system," *Electronic Letters*, vol. 33, no. 22, pp. 1884–1886, January 1997.

[12] T. Young and J. Conradi, "Generation and transmission of FM and pi/4 DQPSK signals at microwave frequencies using harmonic generation and optoelectronic mixing in mach-zehnder modulators," *IEEE Trans. On Micr. Theory and Tech.*, vol. 44, no. 3, March 1996.

[13] H. Ogawa and Y. Kamiya. "Fiber optic microwave transmission using harmonic modulation and optoelectronic mixing/optically pumped mixing," *IEEE MTT-S Dig.*, pp 593–596, 1991.

[14] J.J. OReilly, P.M. Lane, R. Heidemann, and R. Hofstetter, "Optical generation of very narrow linewidth millimeter wave signals," *Electronics Letters*, vol. 28, no. 25, pp. 2309–2311, 1992.

[15] M. Tsuchiya, and T. Hoshida, "Nonlinear photodetection scheme and its system

applications to fiber-optic millimeter-wave wireless down-link," *IEEE Trans. on Micr. Theory and Tech.*, vol. 47, no. 7, July 1999.

[16] R.J. Davies, *Optical Single sideband for Broadband and Subcarrier Systems.* Ph.D. thesis, University of Alberta, 1999.

[17] J. Park, A.F. Elrefaie, K.Y. Lau, "Fiber chromatic dispersion effects on multichannel digital millimeter-wave transmission," *IEEE Photonics Tech. Letters*, vol. 8, no. 12, pp. 1716–1817, Dec. 1996.

[18] G. Keiser, *Optical Fiber Communications*, McGraw-Hill, Inc., 2000.

[19] H. Schmuck, "Comparison of optical millimeter-wave system concepts with regard to chromatic dispersion," *Electronics Letters*, vol. 31, no. 21, pp. 1848–1849, Oct. 1995.

[20] P.A Morton, R.A. Logan, T. Tanbun-Ek, P.F. Sciotino, Jr, A.M. Sergent, R.K. Montgomery, and B.T. Lee, "25 GHz bandwidth 1.55um GaInAsP p-doped strained multiquantum well lasers," *Electonics Letters*, vol. 28, pp. 2156–2157, 1992.

[21] G.L. Li, and P.K. Yu, "Optical intensity modulators for digital and analog applications," *Journal of Lightwave Tech.*, 2003.

[22] G.H. Smith, D. Novak, Z. Ahmed, "Technique for optical SSB generation to overcome dispersion penalties in fibre-radio systems," *Electronics Letters*, vol. 34, no. 17, pp. 1674–1675, August 1998.

[23] B.P. Lathi, *Linear Systems and Signals*, Berkeley-Cambridge Press, 1992.

[24] B.D. Davis, *Design Considerations for radio-on-fiber systems*, M.Sc. thesis, University of Calgary, 2002.

[25] K. Noguchi, O. Mitomi, and H. Miyazawa, "Millimieter-wave Ti:$LiNbO_3$ Optical Modulators," *Journal of Lightwave Tech.*, vol. 16, no. 4, April 1998.

[26] S. Lee, S.M. Garner, V. Chuyanov, H. Zhang, W.H. Steier, F. Wang, L.R. Dalton, A.H. Udupa, and H.R. Fetterman, "Optical intensity modulator based on a novel electrooptic polymer incorporating a high $\mu\beta$ chromophore," *IEEE Journal of Quantum Elec.*, vol. 36, no. 5, May 2000.

[27] G.K. Gopalakrishnan, and W.K. Burns, "Performance and modeling of resonantly enhanced $LiNbO_3$ modulators for low-loss analog fiber-optic links," *IEEE Trans. on Micr. Theory and Tech.*, vol. 42, no. 12, Dec. 1994.

[28] S.V. Hum, *Electro-optic modulators for radio-on-fiber applications*, M.Sc. thesis, University of Calgary, 2001.

[29] M.A.J. Weldon, R.J. Davies, S.V. Hum and M. Okoniewski, "Enhancement of electro-optic modulator using traveling-wave resonators," in *Proceedings of SPIE*, vol. 5247, 2003, pp. 373–381.

[30] G.P. Agrawal, *Fiber-optic Communication Systems*, Wiley-InterScience, 2002.

[31] G.P. Agrawal, *Nonlinear Fiber Optics, Third Edition*, Academic Press, 2001.

[32] B. Davis, *MZM Harmonic Upconversion*, TRLabs Internal Report, Calgary, Alberta, 1999.

[33] J. Wang, and K. Petermann, "Small signal analysis for dispersive optical fiber communication systems," *IEEE Journal of Lightwave Tech.*, vol. 10, no. 1, Jan. 1992.

[34] A.V.T. Cartaxo, B. Wedding, "Influence of fiber nonlinearity on the fiber transfer function: theoretical and experimental analysis," *IEEE Journal of Lighwave Tech.*, vol. 17, no. 10, Oct. 1999.

[35] F. Ramos, J. Marti, V. Polo, and J.M. Fuster, "On the use of fiber-induced self-phase modulation to reduce chromatic dispersion effects in microwave/millimeter-wave optical systems," *IEEE Photonics Tech. Letters*, vol. 10, no. 10, Oct. 1998.

[36] P.Laurêncio, and M.C.R. Medeiros, "Dynamic range of optical links employing optical single side-band modulation," *IEEE Photonics Tech. Letters*, vol. 15, no. 5, May 2003.

[37] O.V. Sinkin, R. Holzlöhner, J. Zweck, and C.R. Menyuk, "Optimization of the split-step fourier method in modeling optical-fiber communications systems," *Journal of Lightwave Tech.*, vol. 21, no. 1, Jan. 2003.

Appendix A

The Split-Step Fourier Numerical Method

An optical signal propagating through a fiber will experience the effects of nonlinearity and dispersion concurrently. The split-step Fourier (SSF) method assumes that nonlinearity and dispersion can be considered as acting independently over a short propagation distance, h. An approximate solution to the nonlinear Schrödinger equation can then be obtained by applying the effects of dispersion and nonlinearity independently over a series of small segments, until the propagation distance of interest is reached.

To demonstrate the SSF method mathematically, consider the nonlinear Schrödinger equation,

$$\frac{\partial A}{\partial z} + \frac{\alpha}{2}A + j\frac{\beta_2}{2}\frac{\partial^2 A}{\partial t^2} - j\gamma\left|A\right|^2 A = 0, \tag{A.1}$$

but written in the form[31]

$$\frac{\partial A}{\partial z} = \left(\hat{D} + \hat{N}\right) A, \tag{A.2}$$

where $\hat{D}$ is a differential operator that accounts for fiber dispersion and absorption, and $\hat{N}$ is a nonlinear operator that accounts for the effects of fiber nonlinearity. These operators are given as

$$\hat{D} = -j\frac{\beta_2}{2}\frac{\partial^2}{\partial t^2} - \frac{\alpha}{2}, \tag{A.3}$$

$$\hat{N} = j\gamma\frac{\left|A\right|^2}{\eta}. \tag{A.4}$$

Applying the SSF method, the optical signal envelope after propagating through a segment of length h, with group velocity v_g, is

$$A(z+h, t+h/v_g) \approx \exp(h\hat{D})\exp(h\hat{N})A(z,t) \tag{A.5}$$

The accuracy of Equation A.5 can be further improved by lumping the effect of non-linearity over the entire segment at the half way point of the segment. This improved version is called the symmetrized split-step Fourier method, and is described by

$$A(z+h, t+h/v_g) \approx \exp(\frac{h}{2}\hat{D})\exp(h\hat{N})\exp(\frac{h}{2}\hat{D})A(z,t) \tag{A.6}$$

Implementation of the symmetrized SSF method is straight forward. An optical signal $A(z=0,t)$, is launched into a fiber that has been divided into a large number of segments, not necessarily equal. The optical signal is propagated from segment to segment through consecutive application of Equation A.6 until the full length of fiber has been traversed, and the final solution obtained.

The accuracy and speed of the SSF method is directly related to step size distribution and application. For the purposes of modeling fiber nonlinearity in a RoF system, a constant step size is sufficient[37]. It was found that step sizes smaller than 1000 meters provided no discernible change in simulation results. To ensure accuracy, all simulations performed in this study use a constant step size of 500 meters.